



Ricardo Infante Gomes

Licenciado em Ciências da Engenharia Civil

Assessment of hygrothermal characteristics of earthen materials

Dissertação para obtenção do Grau de Mestre em
Engenharia Civil – Perfil de Construção

Orientador: Fionn McGregor, Researcher, École Nationale des
Travaux Publics de l'État

Co-orientador: Paulina Faria, Professora Associada, Faculdade de Ciências e
Tecnologia da Universidade Nova de Lisboa

Júri:

Presidente: Professor Doutor Daniel Aelenei
Arguente: Professor Doutor Luís Baltazar
Vogais: Doutor Fionn McGregor



FACULDADE DE
CIÊNCIAS E TECNOLOGIA
UNIVERSIDADE NOVA DE LISBOA

Dezembro 2019

© Copyright Ricardo Infante Gomes, da FCT/UNL e da UNL

A Faculdade de Ciências e Tecnologia e a Universidade Nova de Lisboa têm o direito, perpétuo e sem limites geográficos, de arquivar e publicar esta dissertação através de exemplares impressos reproduzidos em papel ou de forma digital, ou por qualquer outro meio conhecido ou que venha a ser inventado, e de a divulgar através de repositórios científicos e de admitir a sua cópia e distribuição com objetivos educacionais ou de investigação, não comerciais, desde que seja dado crédito ao autor e editor.

To my mother, Sara Infante

Acknowledgements

Firstly, I would like to express my sincere gratitude to Professor Paulina Faria. For the confidence in giving me this great opportunity and for the support and help always shown, despite the distance. Also, for all the motivation throughout the work, but also during the period of the Civil Engineering courses in which her commitment made me gain interest for research.

I would also like to express my acknowledgments to my supervisors Fionn McGregor and Antonin Fabbri for accepting me for this internship and for all their support and help during my months at ENTPE. Additionally, by the manner they received me and the good times, both scientific and personal. I am also grateful to ENTPE for the financial support and help of all the staff.

To all the colleagues I met and friends I made during my stay in France. In special to Rudy Bui, for all the scientific support, but specially for all the good times we spent at the school and outside it, and for his lasting friendship. A special thanks, to Yasmina Mahmoudi, a great friend I made and without who I could not have had the same good time I spent in Lyon and for her lasting friendship. Also, in special, to Paola Martinez, my officemate that brightened the office every day with a smile, and my adventure companion. To Noha Al Fahar for all the help given and for the laughs.

Despite the distance, my friends from home were always with me. I want to thank specially to Andreia Pereira, for the unconditional friendship and constant motivation, not only during this time but always. To Barbara Teixeira and Inês Fernandes, for their lasting friendship. To my friends from FCT who made these years of hard work easier.

To one of the most important persons, Ivo Guerreiro, for the unconditional support and patient. A particular thanks to Teresa Loureiro, my friend forever, for her true friendship and unlimited support and motivation.

Finally, the greatest thanks to my family. To my dear aunt Ana Infante, for her unconditional love and for always keeping me happy and to my sister by heart Beatriz Pedroso. Especially dedicated to my mother Sara Infante, the most important person, who made everything possible and for all the support, patient and love always shown.

Dissemination

The author was invited to present orally the research performed in this thesis at a meeting of the RILEM TC 274 that was held in Université de Pau et Pays de l'Adour at Anglet, France, in October 2019.

Gomes, R. (2019). *Assessment of hygrothermal characteristics of earthen materials. RILEM TC 274 meeting.*

Abstract

One of the biggest challenges currently faced by society is the fight against climatic change. The building sector is an important part of the total emissions of carbon dioxide. Hence, there has been a rising interest on the building sector to reduce its impact on the environment.

Earth is used as a construction material since ancient times and its known for its sustainability, hygroscopic and thermal behaviour, making it a natural moisture buffer, helping in the regulation and control of the indoor air quality, maintaining the levels of relative humidity inside the buildings, providing a healthier environment for their occupants.

Despite being an ancient building material, its use is not disseminated across the world, mainly due to the lack of appropriate and specified standards for assessing its characteristics. Therefore, studies must be performed with the aim to establishing technical guides and standards for earthen building materials.

The aim of this dissertation is to elaborate accurate, repeatable and reproducible test protocols in order to measure the dry mass and the water vapour permeability for earthen materials. Furthermore, there is the need to confirm the reliability of the different methods assessed, mainly through round robin tests performed in different laboratories.

Samples manufactured with a chosen reference earth at two laboratories are tested at both laboratories. Firstly, it is evaluated the similarity of samples fabricated at different laboratories with the same protocol, and finally, the assessment of the hygrothermal characteristics is studied.

Results show that samples manufactured with the same earth at different laboratories with the same protocol can be considered similar regarding their apparent and dry densities and thermal conductivity, however with slightly differences. Samples manufactured at ENTPE present lower apparent and dry densities as well as lower thermal conductivity values than the ones manufactured at NOVA. Therefore, the assessment of the water vapour permeability is studied based on three different methods, showing similar results by the experimental data collected. The wet cup test performed through the gloves box obtained the lowest variations of the water vapour resistance factor. Several drying-methods were studied mainly through sorption isotherms and cycles of drying-wetting, with one outcoming drying-method. Oven-drying at 105°C prove to be an accurate and repeatable dry-method and able to allow the material to return to its initial state from a hygroscopic point of view.

Keywords: Earthen material; Hygrothermal behaviour; Round robin test; Drying-method; Water vapour permeability

Resumo

O maior desafio actualmente enfrentado pela sociedade é o combate às alterações climáticas. O sector da construção é responsável por grande parte das emissões de dióxido de carbono. Assim, tem surgido, um crescente interesse no sector da construção com vista à redução do seu impacto no ambiente.

A terra é utilizada na construção desde a antiguidade, sendo conhecida a sua sustentabilidade, o seu comportamento higroscópico e térmico, que a tornam um material capaz de contribuir para regular e controlar a qualidade do ar interior, equilibrando os níveis de humidade relativa dentro dos edifícios e contribuindo para um ambiente mais saudável para os seus ocupantes.

Apesar do seu uso histórico na construção, a sua utilização não se encontra disseminada pelo mundo. Tal deve-se à inexistência de normas específicas e apropriadas para a avaliação das propriedades dos produtos da construção com terra. Desta forma, devem ser realizados estudos com vista à sua elaboração.

O objectivo da presente dissertação é a elaboração de protocolos de ensaio precisos, repetíveis e reprodutíveis de forma a medir a massa seca e a permeabilidade ao vapor de água de materiais com base em terra. Existe a necessidade de confirmar a confiança nestes métodos, nomeadamente através de ensaios realizados em diferentes laboratórios utilizando os mesmos procedimentos.

São produzidos provetes realizados em dois laboratórios com a mesma terra de referência e seguindo o mesmo protocolo, comparada a sua semelhança e depois avaliadas as suas características higrotérmicas.

Os resultados mostram que os provetes realizados nos dois laboratórios podem ser considerados idênticos, em termos de massas volúmicas aparente e seca, e de condutibilidade térmica, embora com ligeiras diferenças. Os provetes produzidos na ENTPE apresentam valores inferiores àqueles produzidos na NOVA. A análise de três métodos para a determinação da permeabilidade ao vapor de água mostra que os resultados são semelhantes, embora com algumas variações dependendo do método utilizado. O ensaio de difusão ao vapor de água realizado pelo método da caixa com luvas apresenta menores variações de fator de resistência ao vapor que os restantes. Diferentes métodos de secagem foram estudados, nomeadamente através da adsorção de vapor de água e de ciclos de secagem e molhagem. O método de secagem a 105°C prova ser um método preciso e repetível, permitindo ao material voltar ao seu estado inicial em termos higroscópicos.

Palavras-chave: Material à base de terra; Comportamento higrotérmico; Ensaio interlaboratorial; Método de secagem; Permeabilidade ao vapor de água

Notations and symbols

A	Area [m ²]
A	Water absorption coefficient [kg/(m ² .s ^{1/2})]
c _p	Specific heat capacity at constant pressure [J/(kg.K)]
d	Thickness [m]
d _a	Thickness of the air layer [m]
D _L	Permeability coefficient [kg/(Pa.m.s)]
e	Voids index [-]
f	Gravity acceleration [m/s ²]
G	Water vapour flow rate [kg/s]
g	Water vapour flux [kg/m ² or kg/s]
g _L	Liquid flux density vector [kg/(m ² .s)]
g _v	Vapour flux density vector [kg/(m ² .s)]
g _v ^a	Vapour flux density vector [kg/(m ² .s)]
h _c	Convective surface film coefficient [W/(m ² .K)]
i	Volume of liquid absorbed per surface unit [m or m ³ /m ²]
m	Mass of moist sample [g]
m ₀	Mass of dried sample [g]
p _o	Atmospheric pressure [Pa]
p _v	Water vapour partial pressure [Pa]
p _{v,sat}	Saturation water vapour pressure [Pa]
q	Heat flux [W/m ²]
q'	Internal heat generation [W/m ²]
q _{conv}	Heat flux by convection [W/m ²]
Q	Amount of heat energy [W]
RH	Relative humidity [%]
r	Pore radius [m]
S	Sorptivity [m/s ^{1/2}]

s	Exposed surface area [m ²]
S _d	Water vapour diffusion equivalent air layer thickness [m]
S _i	Intrinsic sorptivity [m ^{1/2}]
S _r	Saturation ratio [-]
T	Temperature [K]
t	Time [s]
u	Water content [kg/kg]
v	Water vapour concentration [kg/m ³]
v _s	Saturation limit [kg/m ³]
w	Water content [%]
W	Water vapour permeance [kg/(m ² .s.Pa)]
Z ^s	Surface vapour transfer resistance [(m ² .s.Pa)/kg]
β	Apparent vapour surface transfer coefficient [kg/(m ² .s.Pa)]
δ _p	Water vapour permeability [kg/(Pa.m.s)]
δ _a	Water vapour permeability of air [kg/(Pa.m.s)]
δ _p ^{ISO}	Air gap corrected water vapour permeability [kg/(Pa.m.s)]
δ _p ^{ap}	Apparent water vapour permeability (kg/(Pa.m.s))
δ _p ^β	Skin factor corrected water vapour permeability [kg/(Pa.m.s)]
Δp	Capillary pressure gradient [Pa]
Δp _v	Water vapour pressure gradient [Pa]
η	Liquid dynamic viscosity [kg/(m.s)]
θ	Wetting contact angle [°]
λ	Thermal conductivity [W/(m.K)]
μ	Water vapour resistance factor [-]
μ ^{ISO}	Air gap corrected water vapour resistance factor [-]
μ ^{ap}	Apparent water vapour resistance factor [-]
μ ^β	Skin factor corrected water vapour resistance factor [-]
ξ	Moisture storage capacity [kg/m ³]

ρ	Apparent density [kg/m ³]
ρ_d	Apparent dry density [kg/m ³]
ρ_L	Liquid density [kg/m ³]
σ	Surface tension [N/m]
ϕ	Porosity [-]
ϕ_G	Porosity filled by the gas phase [-]
ϕ_L	Porosity filled by the liquid phase [-]
φ	Relative humidity [-]
Ω	Volume of the material [m ³]
Ω_G	Volume of the gas [m ³]
Ω_L	Volume of the liquid [m ³]
Ω_S	Volume of the solid [m ³]
Ω_v	Volume of voids [m ³]

Contents

Acknowledgements	I
Abstract	III
Resumo	V
Notations and symbols	VII
Contents	XI
List of Figures	XIII
List of Tables	XV
1. Introduction	1
1.1. Context.....	1
1.2. Objective and methodology.....	2
1.3. Dissertation structure.....	2
2. Earthen materials and their hygrothermal behaviour	3
2.1. Earth as a construction building material and porous media.....	3
2.1.1. Earth.....	3
2.1.2. Three-phase system.....	3
2.1.3. Types of porous.....	5
2.2. Heat transfer.....	5
2.2.1. Conduction.....	6
2.2.2. Convection.....	7
2.3. Moisture storage.....	7
2.4. Moisture transport.....	11
2.4.1. Water vapour diffusion.....	11
2.4.2. Liquid water transport.....	12
3. Materials and methods	15
3.1. Materials.....	15
3.2. Tests procedure.....	17
3.2.1. Apparent density.....	17
3.2.2. Dry density.....	17
3.2.3. Thermal conductivity.....	17
3.2.4. Water vapour permeability.....	19
3.2.5. Sorption isotherms.....	22
3.2.6. Cycles of drying-wetting.....	23
4. Sample repeatability experiments	25
4.1. Density.....	25
4.1.1. Apparent density.....	25
4.1.2. Dry density.....	28
4.1.3. Comparison between densities.....	30

4.2.	Thermal conductivity.....	31
4.2.1.	Contact probe.....	31
4.2.2.	Hot wire.....	34
4.3.	Discussion	35
5.	Assessment of the hygrothermal characteristics.....	39
5.1.	Water vapour permeability	39
5.1.1.	Plastic boxes	39
5.1.2.	Climatic chamber.....	44
5.1.3.	Gloves box.....	48
5.1.4.	Comparison between the three procedures	49
5.2.	Drying experiments	54
5.2.1.	Sorption isotherms.....	54
5.2.2.	Cycles of drying-wetting	56
5.3.	Discussion	58
6.	Conclusions	59
6.1.	Summary	59
6.2.	Future work	59
	References	61
	Appendix	A.1
I.	Sample repeatability experiments.....	A.1
II.	Water vapour diffusion test.....	A.5
III.	Drying experiments.....	A.10

List of Figures

Figure 2.1 - Schematic representation of the three-phase system of the soil.....	4
Figure 2.2 – Schematic cross-section of a porous solid.....	5
Figure 2.3 – Psychrometric diagram.....	8
Figure 2.4 – Types of the sorption isotherms curves.....	9
Figure 2.5 – Sorption isotherms for different building materials	10
Figure 2.6 – Sorption isotherms and moisture storage regimes.....	11
Figure 2.7 – Contact angle.....	13
Figure 2.8 – Capillary suction within a pore	14
Figure 3.1- Granulometric curve of Dagneux earth.....	15
Figure 3.2 – Example of the measurement of sample thickness with a digital calliper.....	17
Figure 3.3- Thermal conductivity test using the contact probe method	18
Figure 3.4- Measurement of thermal conductivity with the hot wire method	18
Figure 3.5- Example of sample design with saturated salt solution for wet cup test.....	19
Figure 3.6- Wet cup test setup performed in a plastic box	20
Figure 3.7- Wet cup test setup performed in climatic chamber.....	20
Figure 3.8- Wet cup test setup performed in gloves box	20
Figure 3.9- Example of samples used for the sorption isotherms determination	22
Figure 3.10- Example of samples placed in plastic box for the determination of sorption isotherms.....	22
Figure 3.11 – Dynamic Vapour Sorption equipment (Intrinsic 2, SMS®).....	23
Figure 3.12- Experimental steps used for the drying/wetting cycles.....	24
Figure 3.13- Samples placed in plastic box with dry air flow for drying at 0%	24
Figure 4.1 – Apparent density of NOVA samples.....	25
Figure 4.2 – Apparent density of ENTPE samples.....	26
Figure 4.3 - Apparent density of NOVA and ENTPE samples	27
Figure 4.4 - Apparent density determined with the assumed volume of NOVA and ENTPE samples.....	27
Figure 4.5 - Dry density of NOVA samples	28
Figure 4.6 – Dry density of ENTPE samples	29
Figure 4.7 – Dry density of NOVA and ENTPE samples	30
Figure 4.8 – Comparison between the apparent density and dry density of NOVA and ENTPE samples	30
Figure 4.9 - Thermal conductivity measured by the contact probe method of NOVA samples.....	31
Figure 4.10 - Thermal conductivity measured by the contact probe method of ENTPE samples.....	32
Figure 4.11 – Thermal conductivity measured by the contact probe of NOVA and ENTPE samples.....	33
Figure 4.12 – Comparison between the thermal conductivity measured by the contact probe and the apparent density	33
Figure 4.13 - Thermal conductivity measured by the hot-wire method of NOVA and ENTPE samples... ..	35
Figure 4.14 – Comparison between the thermal conductivity measured by the hot wire and the apparent density	35
Figure 4.15 - Comparison between the thermal conductivity, obtained by the contact probe method, and dry density of NOVA and ENTPE samples.....	37
Figure 5.1 – Mass variation during the wet cup test performed in plastic boxes for NOVA samples	39
Figure 5.2 – Mass variation during the wet cup test performed in plastic boxes for ENTPE samples.....	40
Figure 5.3 – Layout of the process during the wet cup test (McGregor et al., 2017).....	42
Figure 5.4 – $d/\delta p_{ISO}$ as a function for the wet cup test performed in plastic boxes of NOVA and ENTPE samples	42
Figure 5.5 – Comparison between the water vapour resistance factor results obtained by the wet cup test performed in plastic boxes for NOVA and ENTPE samples	43
Figure 5.6 – Mass variation during the wet cup test performed in the climatic chamber at ENTPE for NOVA and ENTPE samples.....	44
Figure 5.7 – Comparison between the water vapour resistance factor results obtained by the wet cup test performed in the climatic chamber at ENTPE for NOVA and ENTPE samples	45

Figure 5.8 – Mass variation during the wet cup test performed in the climatic chamber at NOVA for NOVA and ENTPE samples	46
Figure 5.9 – Comparison between the water vapour resistance factor results obtained by the wet cup test performed in the climatic chamber at NOVA for NOVA and ENTPE samples	47
Figure 5.10 – Mass variation during the wet cup test performed in the gloves box for NOVA and ENTPE samples	48
Figure 5.11 – Comparison between the water vapour resistance factor results obtained by the wet cup test performed in the gloves box for NOVA and ENTPE samples.....	49
Figure 5.12 – Comparison between the water vapour resistance factor results obtained by the three procedures of the wet cup test performed at ENTPE after the ISO correction.....	50
Figure 5.13 – Comparison between the water vapour resistance factor results obtained by the three procedures of the wet cup performed at ENTPE after the β correction.....	50
Figure 5.14 – Vapour surface transfer coefficient determined according to the method proposed by McGregor et al. (2017) for the three procedures of the wet cup test.....	51
Figure 5.15 – Comparison between the water vapour resistance factor obtained by the climatic chamber procedure carried out at ENTPE and NOVA after ISO and β correction.....	51
Figure 5.16 – Comparison between the water vapour resistance factor results obtained by the three procedures of the wet cup test, with the climatic chamber procedure performed at NOVA after the ISO correction.....	52
Figure 5.17 – Comparison between the water vapour resistance factor results obtained by the three procedures of the wet cup test, with the climatic chamber procedure performed at NOVA after the β correction.....	52
Figure 5.18 – Vapour surface transfer coefficient determined according to the method proposed by McGregor et al. (2017) for the three procedures of the wet cup test the three procedures of the wet cup test, with the climatic chamber procedure performed at NOVA.....	53
Figure 5.19 – Oven-drying temperature influence on the sorption isotherms	54
Figure 5.20 – Oven-drying temperatures and pre-conditioning influence on the sorption isotherms	55
Figure 5.21 – Comparison between the sorption isotherms obtained by the desiccator method for the three oven-drying temperatures and by the DVS method	55
Figure 5.22 – Water content in dry and wet mass during the drying-wetting cycles	56
Figure 5.23 – Dry mass in each cycle for the different drying-methods	57
Figure 5.24 – Wet mass in each cycle for the different drying-methods.....	57
Figure A.1 – Layout of the process during the wet cup test.....	A.5
Figure A.2 – $d/\delta p_{ISO}$ as a function for the wet cup test performed in plastic boxes	A.6
Figure A.3 – $d/\delta p_{ISO}$ as a function for the wet cup test performed in the climatic chamber at ENTPE.....	A.7
Figure A.4 – $d/\delta p_{ISO}$ as a function for the wet cup test performed in the climatic chamber at NOVA	A.8
Figure A.5 – $d/\delta p_{ISO}$ as a function for the wet cup test performed in the gloves box.....	A.9

List of Tables

Table 2.1 – Thermal conductivity values for earthen materials found in the literature	7
Table 3.1 – Dagneux earth properties	15
Table 3.2 – List of samples under study and tests performed.....	16
Table 3.3 – Salt solutions substances and respective RH at 20°C	23
Table 4.1 – Apparent density of NOVA samples by thickness	26
Table 4.2 – Apparent density of ENTPE samples by thickness	26
Table 4.3 – Dry density by thickness of NOVA samples	29
Table 4.4 – Dry density by thickness of ENTPE samples	29
Table 4.5 – Thermal conductivity by thickness measured by the contact probe of NOVA samples.....	32
Table 4.6 – Thermal conductivity by thickness measured by the contact probe of ENTPE samples.....	32
Table 4.7 – Thermal conductivity measured by the hot wire of NOVA samples.....	34
Table 4.8 – Thermal conductivity measured by the hot wire of ENTPE samples	34
Table 4.9 – Variation within the sample repeatability experiments	36
Table 5.1 – Average values of water vapour permeability and water vapour resistance factor for NOVA and ENTPE samples obtained by the wet cup test performed in plastic boxes.....	40
Table 5.2 – Average values of water vapour permeability and water vapour resistance factor for NOVA and ENTPE samples obtained by the wet cup test performed in plastic boxes after the ISO correction.....	41
Table 5.3 – Surface vapour transfer resistance and apparent vapour surface transfer coefficient obtained according to the method proposed by McGregor et al. (2017) for the wet cup test performed in plastic boxes.....	42
Table 5.4 – Average values of water vapour permeability and water vapour resistance factor for NOVA and ENTPE samples obtained by the wet cup test performed in plastic boxes after the beta correction.....	43
Table 5.5 – Average values of water vapour permeability and water vapour resistance factor for NOVA and ENTPE samples obtained by the wet cup test performed in the climatic chamber at ENTPE.....	44
Table 5.6 – Average values of water vapour permeability and water vapour resistance factor for NOVA and ENTPE samples obtained by the wet cup test performed in the climatic chamber at ENTPE after the ISO correction.....	45
Table 5.7 – Surface vapour transfer resistance and apparent vapour surface transfer coefficient obtained according to the method proposed by McGregor et al. (2017) for the wet cup test performed in the climatic chamber at ENTPE.....	45
Table 5.8 – Average values of water vapour permeability and water vapour resistance factor for NOVA and ENTPE samples obtained by the wet cup test performed in the climatic chamber at NOVA.....	46
Table 5.9 – Average values of water vapour permeability and water vapour resistance factor for NOVA and ENTPE samples obtained by the wet cup test performed in the climatic chamber at NOVA after the ISO correction.....	47
Table 5.10 – Surface vapour transfer resistance and apparent vapour surface transfer coefficient obtained according to the method proposed by McGregor et al. (2017) for the wet cup test performed in the climatic chamber at NOVA.....	47
Table 5.11 – Average values of water vapour permeability and water vapour resistance factor for NOVA and ENTPE samples obtained by the wet cup test performed in the gloves box	48
Table 5.12 – Average values of water vapour permeability and water vapour resistance factor for NOVA and ENTPE samples obtained by the wet cup test performed in the gloves box after the ISO correction..	48
Table 5.13 – Surface vapour transfer resistance and apparent vapour surface transfer coefficient obtained according to the method proposed by McGregor et al. (2017) for the wet cup test performed in the gloves box	49
Table 5.14 – Average values of the water vapour resistance factor obtained by the wet cup test performed with the three procedures after the β correction and its variation	53

Table A.1 – Samples mass and dimensions used for the determination of apparent density	A.1
Table A.2 – Apparent density of NOVA and ENTPE samples	A.2
Table A.3 – Dimensions of NOVA samples measured through a digital calliper for the dry density determination.....	A.2
Table A.4 – Dimensions of ENTPE samples measured through a digital calliper for the dry density determination.....	A.3
Table A.5 – Dry density of NOVA and ENTPE samples.....	A.3
Table A.6 – Thermal conductivity obtained by the contact probe method.....	A.4
Table A.7 – Average values of thermal conductivity obtained by the contact probe method	A.4
Table A.8 – Thermal conductivity obtained by the hot wire method	A.5
Table A.9 – Values of water vapour permeability and water vapour resistance factor obtained by the wet cup test performed in plastic boxes	A.6
Table A.10 – Values of δ^{β} and μ^{β} obtained by the wet cup test performed in plastic boxes.....	A.6
Table A.11 – Values of water vapour permeability and water vapour resistance factor obtained by the wet cup test performed in the climatic chamber at ENTPE	A.7
Table A.12 – Values of δ^{β} and μ^{β} obtained by the wet cup test performed in climatic chamber at ENTPE.....	A.7
Table A.13 – Values of water vapour permeability and water vapour resistance factor obtained by the wet cup test performed in the climatic chamber at NOVA	A.8
Table A.14 – Values of δ^{β} and μ^{β} obtained by the wet cup test performed in climatic chamber at NOVA	A.8
Table A.15 – Values of water vapour permeability and water vapour resistance factor obtained by the wet cup test performed in the gloves box.....	A.9
Table A.16 – Values of δ^{β} and μ^{β} obtained by the wet cup test performed in the gloves box	A.9
Table A.17 – Water contents obtained through the sorption for the first cycle of RH levels.....	A.10
Table A.18 – Water contents obtained through the desorption for the first cycle of RH levels	A.11
Table A.19 – Water contents obtained through the sorption for the second cycle of RH levels	A.12
Table A.20 – Water contents obtained through the desorption for the second cycle of RH levels	A.13
Table A.21 – Water content in dry and wet mass during the drying-wetting cycles for the cycle dried at 23%	A.14
Table A.22 – Dry mass in each cycle for the different drying-methods for the cycle dried at 23%.....	A.14
Table A.23 – Water content in dry and wet mass during the drying-wetting cycles for the cycle dried at 0%.....	A.15
Table A.24 – Dry mass in each cycle for the different drying-methods for the cycle dried at 0%.....	A.15
Table A.25 – Water content in dry and wet mass during the drying-wetting cycles for the cycle dried at 105°C	A.16
Table A.26 – Dry mass in each cycle for the different drying-methods for the cycle dried at 105°C	A.16
Table A.27 – Water content in dry and wet mass during the drying-wetting cycles for the cycle dried at 70°C	A.17
Table A.28 – Dry mass in each cycle for the different drying-methods for the cycle dried at 70°C	A.17

1. Introduction

1.1. Context

One of the biggest challenges currently faced by society is the fight against climate change, which includes the mitigation of carbon dioxide emissions. Each year, about 48% of global energy is consumed by buildings, in their construction, design service life and deconstruction (Dixit et al., 2017). There is thus a need to reduce the impact of the building sector on the environment (Cellura et al., 2014; Fgaier et al., 2015; Saidi., 2018).

Embodied energy can be defined as the energy used in the constructive processes and to produce construction building materials (Dixit, 2019; Habert et al., 2012). In this context, every material used in building construction must be considered in order to reduce the energy impact of the building sector (Chastas et al., 2018). In addition, operating energy, energy used in heating and cooling systems, as well as in lightning and ventilation appliances, have a significant impact on the amount of global energy consumed by buildings (Anderson et al., 2015; Dixit et al., 2010; Praseeda et al., 2016). As such, these energies must be optimized in a combined form, to minimize the carbon dioxide emissions of buildings (Labat et al., 2016; Monteiro et al., 2016; Stephan et al., 2012).

Approximately 90% of people's time is spent indoors (Klepeis et al., 2001; Rupp et al., 2015). Consequently, the quality of indoor air is very important, seeing as it has a significant impact on the health of occupants of buildings (Al horr et al., 2016; Arundel et al., 1986; Tham, 2016), as are the energy demands of buildings (Antunes et al., 2019; Feng & Janssen, 2016). With the increasing focus on environmental concerns and the indoor comfort of users, new solutions, such as passive solutions (e.g. construction materials with high hygroscopic properties or with high moisture buffering capacity), are gaining ground against mechanical solutions. This kind of materials, such as unfired earth, can help influence the stabilization and maintenance of buildings' indoor air quality, while also having a low impact on the environment (Allinson & Hall, 2010; Cagnon et al., 2014; Kwiatkowski et al., 2009; McGregor et al., 2014; Medjelekh et al., 2016).

Over the past decades, upon the emergence of new materials, such as aluminium and concrete, these environmental concerns were not relevant. However, low embodied energy materials, like earthen materials, are now gaining a new interest and numerous studies are being conducted with a view to replace or minimize the use of modern materials, which consume a more significant amount of energy (Chabriac et al., 2014; Fabbri et al., 2018; Habert et al., 2012; McGregor et al., 2016; Melià et al., 2014; Morel et al., 2001; Remki et al., 2017; Santos et al., 2018).

Earth has been used as a construction material since ancient times, especially since it can be found in several places across the world in great natural abundance. Earthen materials are recognized as having many advantages when applied in the building sector. The fact that earth is an abundant and recyclable material (when not stabilized), with a low embodied energy, makes it an eco-friendly and sustainable asset for current construction concerns. Earth's hygroscopic and thermal behaviour, which makes it a natural moisture buffer, helps maintain the RH levels inside buildings, thus controlling indoor air quality and providing a healthier environment for their occupants (Bui et al., 2014; Gomes et al., 2018; Laborel-Préneron et al., 2018; Santos et al., 2019). This moisture storage capacity is explained by the porous microstructure of earth-based materials and by the phenomena of single and multi-layer adsorption, as well as capillary condensation (Dubois et al., 2014; Hall & Allinson, 2009; Soudani et al., 2016; Zhang et al., 2018).

Despite the use of earth as a construction material since ancient times, its use is not disseminated across the world. One of the reasons for this is the absence of appropriate specified standards for assessing the properties of earthen materials, namely those properties related to earth's sustainability and hygrothermal behaviour (Champiré et al., 2016; Fabbri et al., 2019; Medjelekh et al., 2016; Moevus et al., 2012). Studies must thus be performed to support future establishment of technical guides and standards for the characterization of earthen construction products.

To assess hygrothermal properties, it is necessary to understand heat transfer, moisture transport and storage capacity. These properties can be evaluated based on thermal conductivity, water vapour permeability and the isothermal sorption-desorption curves. There have been numerous studies on these properties; however, they have focused on other porous building materials, rather than earthen materials. In certain of these studies, round robin tests were performed to assess its reproducibility and repeatability. Also, several of these studies have been conducted at ENTPE focusing the hygrothermal properties of bio-based and raw earth materials, mainly that carried out by Costa (2017) which focused on cycles of drying-wetting. Nevertheless, these cycles need more investigation, namely by enlarging the experimental data and its repeatability. According to Roels et al. (2010), these tests carry a significant variance between the results when performed in different laboratories. Consequently, for earthen materials, which are highly hygroscopic and porous materials, there emerges a need to validate the reproducibility and repeatability of the tests carried out to assess their hygrothermal characteristics, with the aim of elaborating precise and appropriate test procedures.

This dissertation takes place within the framework of the *RILEM TC 274 - TCE*: Testing and characterisation of earth-based building materials and elements, which aims to define dedicated testing procedures for stabilized and unstabilized earth as a building construction material.

1.2. Objective and methodology

The scope of this dissertation is to assess the hygrothermal characteristics of earthen materials, with the main objective to elaborate precise and appropriate test protocols for this assessment. Despite the ancestral use of earth as a building material, standards for this material are still inexistent or not specified.

To this end, one reference earth was chosen and samples of three different thicknesses were made at NOVA and at ENTPE, applying the same formulation and procedure. First, the samples were validated based on apparent density, dry density and thermal conductivity to evaluate the similarity of the samples manufactured in different laboratories. Following this validation, water vapour permeability was evaluated using three different methods, implemented in both laboratories, and the various dry methods, mainly through cycles of drying and wetting, as well as sorption isotherms. Finally, a study was conducted to evaluate which method is the most accurate, reproducible and repeatable, for the assessment of water vapour permeability and for the drying method.

1.3. Dissertation structure

Chapter Two is dedicated to a literature review on earthen materials and their hygrothermal behaviour. It is well known that earth-based materials are highly hygroscopic, with the ability to adsorb moisture. Proper knowledge on the heat transfer, moisture transport and storage of these materials is thus fundamental.

Chapter Three presents a description of the earth studied and of how the samples were prepared. It also explains the experimental procedures used to assess the hygrothermal characteristics under study; namely, thermal conductivity, water vapour permeability, the sorption isotherms and the cycles of drying and wetting.

The validation of the samples tested in both laboratories is presented in Chapter Four. This validation consists of a comparison of the apparent density, dry density and thermal conductivity of the different samples fabricated at NOVA and at ENTPE. Chapter Five is devoted to an analysis and evaluation of the assessment of hygrothermal characteristics and, finally, Chapter Six outlines the conclusions of this dissertation and suggestions of future paths of study.

2. Earthen materials and their hygrothermal behaviour

2.1. Earth as a construction building material and porous media

2.1.1. Earth

Earth, also designated as soil when mentioned as a raw material, is a product resultant from rocks' deterioration, by mechanical, chemical or biological processes. It is a non-homogenous material, composed mainly by mineral solid material, water and air. Within the solid material it is possible to find clays, silts, sands, gravels and fibres.

Soil can be divided in different layers: the top layer known as humus, the fraction of organic matter; the topsoil, a mixture between organic material and mineral particles; the subsoil composed only by mineral material; the deepest layer, a layer of rock named bedrock.

For construction proposes the earth used must be extracted from the subsoil layer, due to its lack of organic matter. Therefore, in the present work, earth is referred to the material extracted from the subsoil and used as a building material.

Earth is used as a construction material, either stabilised or unstabilized, in several construction techniques, mainly adobe or compressed earth bricks (CEB) masonry, cob and rammed earth monolithic walls (Fabbri et al., 2018; Parracha et al., 2019). For adobe and CEB masonry, adobe and CEB are previously produced. Adobe consists in the manufacture of bricks by filling moulds with fresh earth mortars, without compaction, which are dried naturally air-dried. Alternatively, CEB consists in compressing, either by manual or mechanic means, moistened earth (not a plastic mortar) within a mould. By contrast, cob and rammed earth techniques monolithic constructions have no pre-fabrication and are totally produced on site. Cob technique involves the use of a fresh earthen mortar with natural fibres which portion are manually piled to form a wall whereas, for rammed earth, it is used a moistened earth which is compacted (i.e. rammed) in consecutive layers within temporary formworks, both forming monolithic walls. Additionally, earth is used in the fabrication of mortars mortars, either for layering adobe and CEB on masonry (Duriez et al., 2020), for repair of earth walls (Gomes et al., 2019) and for plasters (Lima et al., 2020) and renders of earthen or other walls (Santos et al., 2019).

2.1.2. Three-phase system

The connections between the earth's solid components are not perfect, and therefore, there are some voids known as porous, that can be filled by water or air. These porous forms a network, called porous network that make earth a porous media.

Consequently, it is possible to describe it as a three-phase system, composed by the solid phase, the liquid water phase and the gas phase, as shown in Figure 2.1. If the voids are completely empty, meaning without water, the soil is in a dry state, opposing the saturated state, when all the pores are filled with water. Otherwise, if simultaneously water and air are contained in the voids, the soil is in the unsaturated state.

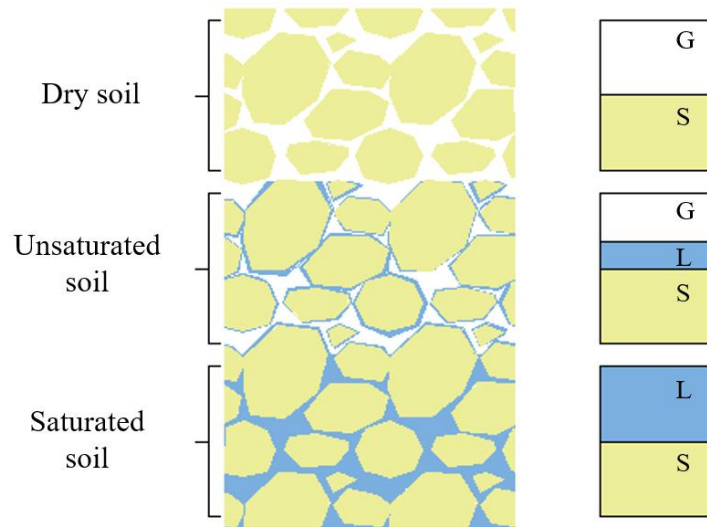


Figure 2.1 - Schematic representation of the three-phase system of the soil

The morphology of the porous materials three-phase system can be described in terms of volume and mass ratios. The total volume (Ω) combines the volume of the solid part (Ω_S) with the volume of liquid water (Ω_L) and the volume of gas (Ω_G), following eq. 1 to 3:

$$\Omega_S = (1 - \phi)\Omega \quad (1)$$

$$\Omega_L = \phi_L \Omega = S_r \phi \Omega \quad (2)$$

$$\Omega_G = \phi_G \Omega = (1 - S_r)\phi \Omega \quad (3)$$

where ϕ , ϕ_L and ϕ_G note the material porosity, the porosity when filled by the liquid phase and the gas phase, respectively. The saturation ratio, noted by S_r , express the ratio between the current volume of liquid and the current volume of the porous network.

The porosity of the material (ϕ) is described by eq. 4. The voids index (e) is obtained by the ratio of the pore volume (Ω_v), being the sum of the volume of the liquid water with the volume of gas, following eq. 5:

$$\phi = \frac{\Omega_v}{\Omega} = \frac{e}{1 + e} \quad (4)$$

$$e = \frac{\Omega_v}{\Omega_S} \quad (5)$$

It is possible to express the amount of water present in the material using the gravimetric water content, denoted by w , defined as the ration between the weight of the water (W_w) and the weight of the solid particles (W_S), given by equation 6.

$$w = \frac{W_w}{W_S} \quad (6)$$

It is assumed that W_S is the weight of the solid particles within the dry state opposing the mass of the wet soil, W_w .

2.1.3. Types of porous

Pores can be defined as voids, cavities, channels or interstices, or simply as spaces between particles. While the definition of pores is easily understandable, their geometry is often difficult to define or represent due to their large variability of shapes and sizes. Rouquerol et al. (1994) proposed a hypothetical schematic representation of the different types of pores – see Figure 2.2.

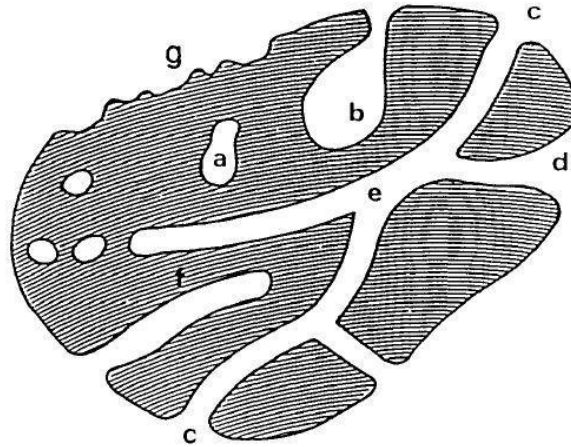


Figure 2.2 – Schematic cross-section of a porous solid (Rouquerol et al., 1994)

Briefly, pores can be divided in two categories in function to their accessibility to water: open and closed. The open pores, which have communication with the external surface, can be open at one end (b), described as blind, or open in both sides (e), described as through pores. Contrarily, the totally isolated pores are designated as closed pores (a). This type of pores, opposing the open pores, are not responsible concerning the mass transfer characteristics, but do have an influence on properties such as density, mechanical strength and thermal conductivity (Rouquerol et al., 1994).

2.2. Heat transfer

According to thermodynamics, there are several forms of energy. When, between two surfaces there is a gradient, a transfer of energy takes place until equilibrium is reached. In the case of a temperature gradient, this energy occurs in the form of heat and its transfer is called heat transfer, always from the higher temperature to the lower.

Heat transfers can be quantified by the amount of heat, Q [W], or by the heat flux, q [W/m²]. The heat flux, can be determined as the ratio of the amount of heat transferred per unit area, in which the transfer occurs, A [m²] – see equation 7.

$$q = \frac{Q}{A} \quad (7)$$

Three different heat transfer phenomena can be distinguished:

- Conduction;
- Convection;
- Radiation.

Unlike conduction and convection, modes of heat transfer where direct contact between the different surfaces is required, radiation does not need such contact to the heat to be transferred. Briefly, heat transfers by conduction occur inside the material, while convection and radiation occur at its surface (Henriques, 2016).

2.2.1. Conduction

Conduction phenomenon can be described as the heat transfer mode between the physical contact of surfaces at different temperatures. It can occur not only in solids, but also in fluids, whether liquid or gas. The energy is transferred between adjacent molecules, from the most agitated – higher temperature – to the less agitated – lower temperatures – until equilibrium is reached.

The analysis of heat transfer under real conditions takes into account the resulting variations over time, being referred to as a variable regime, and is described by the general equation of heat diffusion – see equation 8.

$$\frac{\partial}{\partial x} \left(\lambda \frac{\partial T}{\partial x} \right) + \frac{\partial}{\partial y} \left(\lambda \frac{\partial T}{\partial y} \right) + \frac{\partial}{\partial z} \left(\lambda \frac{\partial T}{\partial z} \right) + q' = \rho c_p \frac{\partial T}{\partial t} \quad (8)$$

Thus, the heat transfer is dependent of the dry density, ρ [kg/m³], specific heat capacity, c_p [J/(kg.K)], thermal conductivity, λ [W/(m.K)] and as explained on the temperature and time; q' represents the internal heat generation.

Specific heat capacity can be defined as the amount of energy demanded to increase a unit of temperature of a material to its unit of mass, being expressed in J/(kg.K). In a study conducted by Cagnon et al. (2014), unfired earth bricks recorded values from a range of 900 to 960 J/(kg.K). According to Moevus et al (2012), earthen materials present a heat capacity that varies from 600 to 1000 J/(kg.K) with a mean value of 800 J/(kg.K).

On a steady-state regime, this analysis is performed independently of time, i.e. the stored energy is not considered – the incoming energy is the outgoing energy. Equation 9 describes the steady – state heat diffusion equation, when there is no internal heat generation:

$$\frac{\partial}{\partial x} \left(\lambda \frac{\partial T}{\partial x} \right) + \frac{\partial}{\partial y} \left(\lambda \frac{\partial T}{\partial y} \right) + \frac{\partial}{\partial z} \left(\lambda \frac{\partial T}{\partial z} \right) + q' = 0 \quad (9)$$

If it is assumed that there is no internal heat generation, this equation takes the form following equation 10:

$$\frac{\partial}{\partial x} \left(\lambda \frac{\partial T}{\partial x} \right) + \frac{\partial}{\partial y} \left(\lambda \frac{\partial T}{\partial y} \right) + \frac{\partial}{\partial z} \left(\lambda \frac{\partial T}{\partial z} \right) = 0 \quad (10)$$

The majority of the analysis related to heat transfer in civil engineering is done on a steady-state and unidirectional basis, ensuring a simplified analysis. Therefore, in a steady-state and unidirectional regime the equation of heat diffusion is the following:

$$\frac{\partial}{\partial x} \left(\lambda \frac{\partial T}{\partial x} \right) = 0 \quad (11)$$

Hence, and according to Fourier's law, the heat flux density in a certain direction is proportional to the temperature gradient in that same direction, described by equation 12:

$$q_x = -\lambda \frac{dT}{dx} \quad (12)$$

where λ [W/(m.K)] is the thermal conductivity, meaning the amount of heat passing per unit of surface area per unit of thickness of the material when there is a temperature difference.

Therefore, the thermal conductivity defines the materials' ability to transfer thermal energy by conduction. Materials with a low thermal conductivity are good thermal insulations opposing the ones with high values that are good heat conductors. Table 2.1 shows several thermal conductivity values found in the literature for earthen materials.

Table 2.1 – Thermal conductivity values for earthen materials found in the literature

Material	λ [W/(m.K)]
Compacted earth	0.50 – 1.70 (Moevus et al., 2012)
Compressed earth bricks	0.52 – 0.93 (Zhang et al., 2018)
Compressed stabilized earth bricks	0.66 – 0.85 (Touré et al., 2017)
Fibred earth	0.10 – 0.30 (Moevus et al., 2012)
Unfired earth bricks	0.77 - 0.95 (Medjelekh et al., 2017)
Unfired clay bricks	0.90 (Fgaier et al., 2015)

Thermal conductivity of porous materials can be highly influenced by its water content; water has a value of λ twenty-four times higher than the air (Henriques, 2016). Therefore, porous materials with higher water contents have a greater value of λ than, for example, dried materials.

2.2.2. Convection

When submitted to temperature variations, the molecules change their relative position and consequently its density. Thus, originating the typical convection currents. Higher temperatures increase the agitation level of the molecules, leading to a decrease of density and, therefore, to an elevation of the hotter fluid. On the opposite side, lower temperatures cause increased density of the molecules, leading the cold air to come down. As explained, in order for convection to occur it is necessary a variation of the molecules' volume, which is not possible in solids. Thus, convection only happen in fluids, being its principal mechanism of heat transfer.

Considering a surface at a temperature T_1 and the ambience temperature T_2 , the flux by convection occurring between them can be described by Newton's law of cooling – see equation 13.

$$q_{conv} = h_c(T_1 - T_2) \quad (13)$$

where h_c is the convective surface transfer coefficient [W/(m².K)], which is variable according to the geometry of the surface, the fluid nature and the movement type.

Convection can be divided in two types, according to the type of movement existent: natural or forced. Natural convection is the result of the air currents due to temperature variations that lead to changes of the fluid density. In contrast, when the movement of the fluid is created by an exterior source, such as example a fan, the convection is named forced.

2.3. Moisture storage

As referred in chapter 1, people spend approximately 90% of their time inside buildings (Rupp et al., 2015) thus, indoor air quality has a fundamental role in the occupants' health. The maintenance of a clean indoor air is therefore seeking by the occupants and owners of the spaces but also by the building industry. Several factors can influence the control of the air quality, paying special attention to the indoor air pollution. This pollution is mainly due to dampness (i.e. excessive levels of moisture), mould (i.e. microscopic fungi), chemicals and other biological agents (WHO, 2009).

Most of indoor pollution problems stem from dampness, leading to the proliferation of biological organisms. According to WHO (2009), several conditions increase the risk of dampness to happen: dissipation of energy due to insufficient insulation or a deficient ventilation; the building involving area; extreme weather conditions and the adequacy of the building materials and construction techniques used. Hence, buildings materials can influence the indoor air pollution, counteracting or mitigating their causes.

It is important to know the mechanisms associated with the transport and storage of moisture as well as its quantification. Relative humidity (ϕ) is defined as the ratio between the amount of water vapour (v [kg/m³]) by its limit of saturation at the same temperature (v_s [kg/m³]) – see equation 14.

$$\phi = \frac{v}{v_s} = \frac{p_v}{p_{v,sat}} \quad (14)$$

Also, is possible to define it as the ratio between the partial vapour pressure (p_v [Pa]) and the saturated vapour pressure ($p_{v,sat}$ [Pa]) (eq. 14). The saturated vapour pressure, $p_{v,sat}$, is the pressure resultant when the maximum amount of water vapour is present in the air at a certain temperature. Thus, RH is dependent of temperature, since $p_{v,sat}$ is a function of temperature; RH increases with the decreasing of the temperature and decreases with its increment. The relationship between the temperature, the partial vapour pressure and the relative humidity is expressed on the psychrometric diagram (Figure 2.3). With the temperature in the abscissa, the partial vapour pressure in ordinate and several curves of RH, this diagram is a practical support.

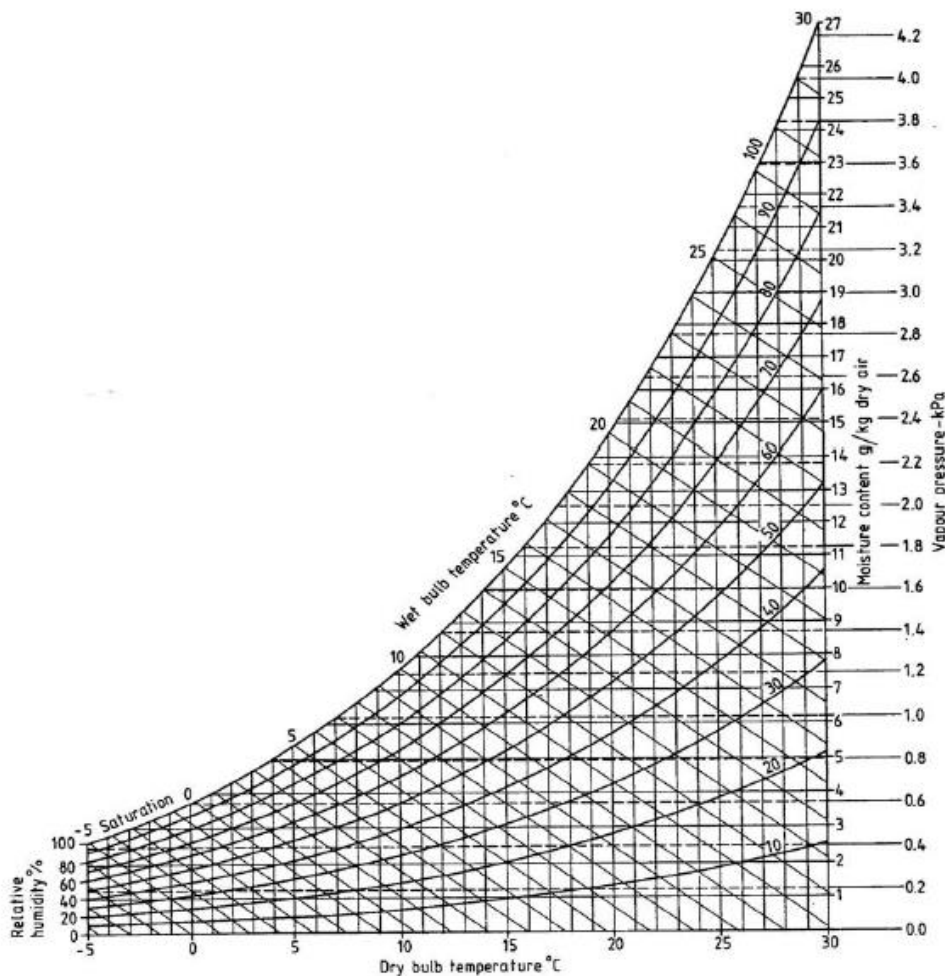


Figure 2.3 – Psychrometric diagram (BSI 1989)

It can be understood that a relative humidity corresponding to 1 or 100% means that the air contains the maximum possible water vapour content at a given temperature (i.e. the partial vapour pressure is equal to the saturated vapour pressure). In these conditions, where the humidity level reaches 100%, occurs the phase change of the water vapour to liquid water (i.e. condensation).

Sorption isotherms

When submitted to contact with moist air, a porous material will retain some water, either in the form of liquid water or water vapour, whether the conditions of relative humidity and temperature.

The water molecules will adhere to the material's porous media until its water content is equilibrated with the moist air of the ambient. This phenomenon (i.e. adhesion of water molecules to the surface of the pores) is called sorption.

Therefore, a porous material can have moisture in liquid or vaporous form; some can be physically fixed to its pores but other part as free water. According to the EN ISO 12751:2013 (CEN 2013), it is possible to express this amount of water present in the material, denoted by u , or w , defined by equation 15.

$$u = \frac{m - m_0}{m_0} \quad (15)$$

where m is the mass of the material (i.e. wet material) and m_0 the material's dry mass.

Moisture storage of porous materials can be evaluated by the hygroscopic sorption properties, expressed in curves denoted as sorption isotherms. These curves relate the water content adsorbed with the relative humidity at a given constant temperature. Generally, it is possible to distinguish and classify these curves into six types as shown in Figure 2.4. Earthen building materials present a sorption curve like the type II isotherm, with a "S" shape.

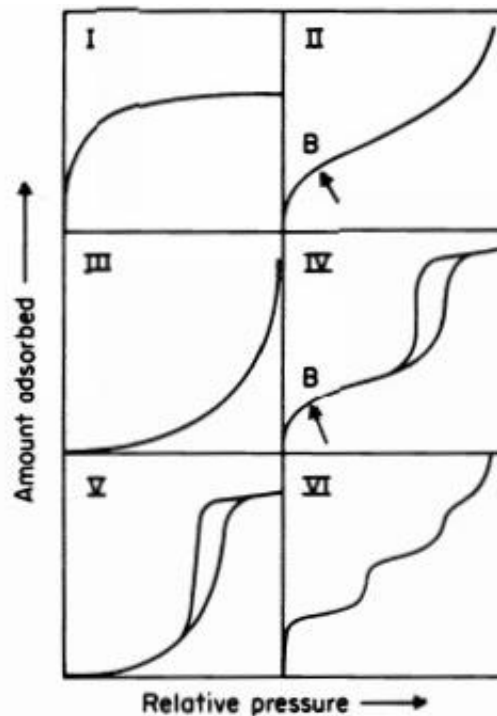


Figure 2.4 – Types of the sorption isotherms curves (Sing, 1985)

Sorption phenomena are complemented by inverse water loss phenomena, occurring when the ambient relative humidity decreases, called desorption. In most materials, this desorption is much slower than the adsorption. Thus, in addition to the adsorption curve, the desorption curve is also important for the definition of the sorption isotherms – see Figure 2.5. The different behaviour between these two hygroscopic curves is named hysteresis. It is particularly dependent on the shape of the pores (Henriques, 2016) and often occurs at high levels of RH within the capillary condensation (McGregor et al., 2014).

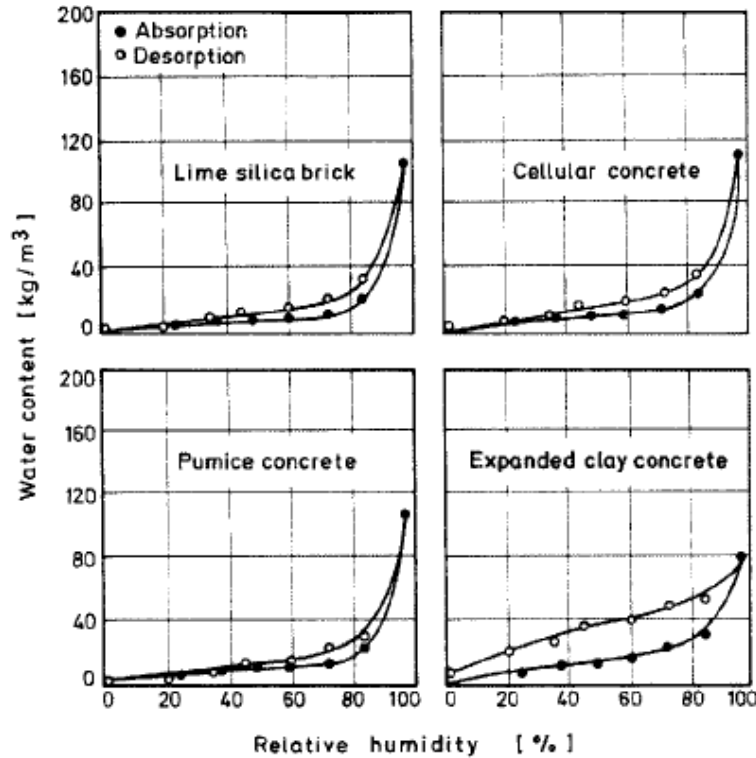


Figure 2.5 – Sorption isotherms for different building materials (Künzel, 1995)

Like most building materials, earth building materials have a progressively higher sorption as relative humidity increases, with a convex area in the range of 0% to 40% RH and a concave area between 40% and 98% and a linear area above the 98%. Therefore, it is possible to define three moisture storage domains as shown in Figure 2.6, the hygroscopic regime, followed by the capillary domain and finally the saturation domain.

The hygroscopic regime corresponding to the range of RH between 0% and 95% can be understood as the junction of three distinct phases. Firstly, the single-layer of adsorbed molecules, usually up to 15% of RH, thereafter, the multiple layers of adsorbed molecules occurring between the range of relative humidities of 15% and 50%. These two phases of molecular adsorption are followed by capillary condensation, occurring when the adsorbed water layers start to interact to each other forming water meniscus, due to the arrangement of the water molecules to a more stable position. With the end of the hygroscopic regime, the capillary domain begins corresponding to the range of relative humidities above the critical moisture content, between 95% and 98%. A sharp rise of the sorption curves occurs within the capillary domain (Krus & Kiej, 1998). Lastly, above the 98% of relative humidity, in the supersaturated region it is no longer possible to achieve the fully saturation of the pores by means of capillary saturation. Thus, in order to reach it, it is needed to remove the entrapped air within the pores (i.e. vacuum system).

The hygroscopic behaviour of a material can be evaluated by its moisture storage capacity, ξ [kg/m³], defined as the amount of moisture that a certain material adsorbs or releases per unit of mass and relative humidity, obtained from the sorption isotherms following equation 16.

$$\xi = \rho_d \frac{\partial u}{\partial \varphi} \quad (16)$$

where ρ_d [kg/m³] is the dry density of the material and $\frac{\partial u}{\partial \varphi}$ is the average slope of the isotherm, within the linear section of the isotherm and the hygroscopic domain (Hall & Allinson, 2009; McGregor et al., 2014).

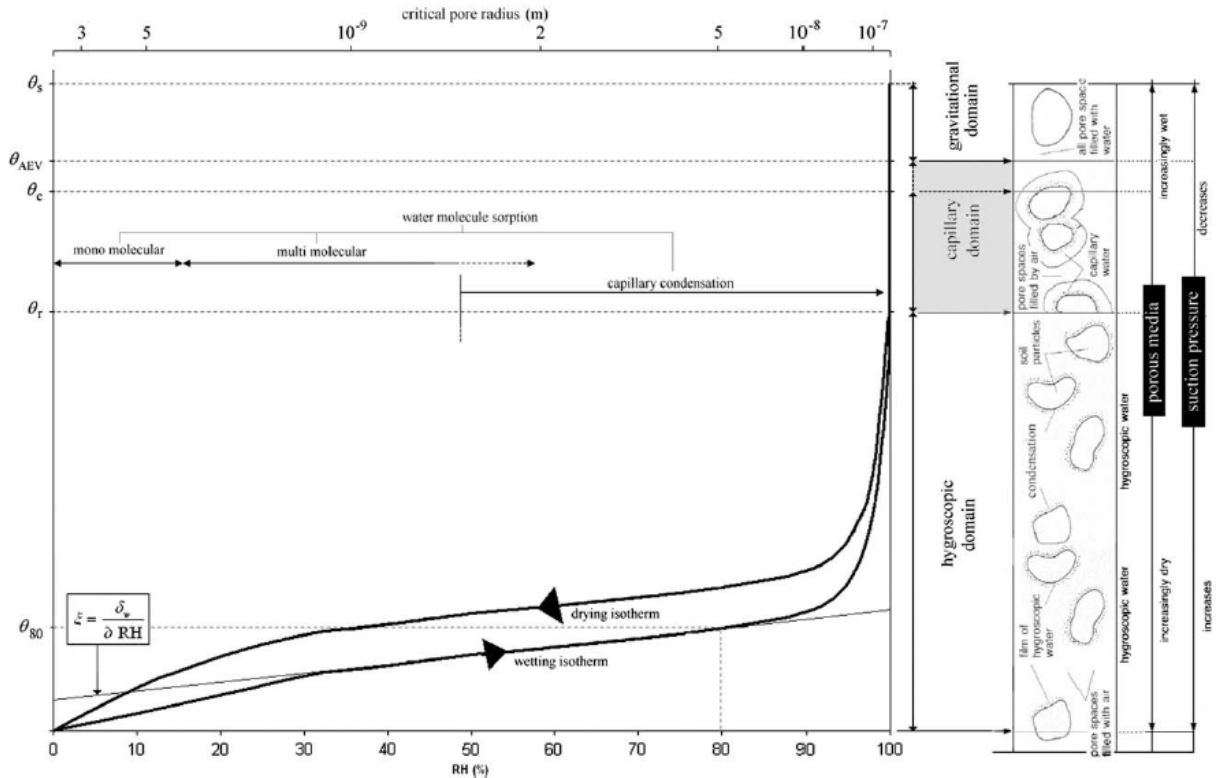


Figure 2.6 – Sorption isotherms and moisture storage regimes (Hall & Allinson, 2009)

2.4. Moisture transport

Moisture transport, unlike the heat transmission phenomena, fits into the mass transfer phenomena, such as, gas or liquid migration. In order for this transport to occur, a porous medium and a potential difference is required (Henriques, 2016).

Regarding mass transfers occurring in buildings, it is given particular attention to moisture transport, being divided in water vapour diffusion and liquid water transport (Hall & Allinson, 2009; Henriques, 2016; Künzle, 1995; Soudani et al., 2016; Whitaker, 1977).

2.4.1. Water vapour diffusion

Within the porous medium, the existing pores do not present a uniform distribution of water vapour. Therefore, it will occur a transfer of water vapour due to the different pressure values resulting from a gas concentration gradient or a temperature and pore radius variations. Molecular movements are thus generated until the equilibrium is reached, to the direction of the lower concentrations. (Hall & Allinson, 2009; Henriques, 2016; Hens, 2012; Künzle, 1995).

For a certain porous material, such as earthen materials, the water vapour permeability, denoted as δ_p [kg/(s.m.Pa)], is defined as the amount of water vapour that flows by time through the material's thickness, divided by the water vapour pressure gradient between its two faces (Henriques, 2016; McGregor, 2014).

Commonly, for convenience, in the literature, for the characterization and quantification of the water vapour permeability is used the water vapour resistance factor, μ , being the ratio between the water vapour permeability of air, δ_a , and the water vapour permeability of the material, δ_p – see equation 17. This factor is characteristic value of the material.

$$\mu = \frac{\delta_a}{\delta_p} \quad (17)$$

The diffusion of water vapour is described by Fick's law, under the assumption of perfect gases, and presented in equation 18:

$$\mathbf{g}_v^a = -\delta_a \mathbf{grad}(p_v) \quad (18)$$

where \mathbf{g}_v^a [kg/(m².s)] is the water vapour flux density vector, δ_a is the water vapour diffusion coefficient of air and $\mathbf{grad}(p_v)$ is the vapour pressure gradient.

Flick's law can be written taking into account the interactions happening within the porous medium, between the fluid and the pores walls, introducing the water vapour resistance factor, following equation 19:

$$\mathbf{g}_v = -\frac{\delta_a}{\mu} \mathbf{grad}(p_v) = -\delta_p \mathbf{grad}(p_v) \quad (19)$$

where \mathbf{g}_v is the vapour diffusion flux density vector within the porous medium.

2.4.2. Liquid water transport

Liquid water transport mechanisms can occur in different ways, either by the action of gravity, or by forces contrary to it (i.e. capillarity), or through horizontal or vertical migration.

Similarly, to the water vapour flow, it is possible to describe the flow of liquid water, in turn through the generalized Darcy's law, presented in equation 20:

$$\mathbf{g}_L = -D_L(\mathbf{grad}(p_L) - \rho_L \mathbf{f}) \quad (20)$$

where \mathbf{g}_L [kg/(m².s)] is the liquid flux density vector, D_L (s) the permeability coefficient, $\mathbf{grad}(p_L)$ the liquid pressure gradient, ρ_L the liquid density and \mathbf{f} [m/s²] is the gravity acceleration.

The transport of liquid water within porous media often occurs by actions that counteract the action of gravity, known as capillarity. These phenomena are defined as the occurrence of suction forces thus enabling the movement of liquid water opposing the force of gravity and depend on the pores size, surface tension and the contact angle (Henriques, 2016).

Interactions within a liquid such as water are distinct from those arising from the liquid contact with air. In parallel, it should be noticed that water molecules have attractive intermolecular forces resulting in the attraction of each other. Therefore, within the liquid, the molecules are surrounded by others, nullifying the forces of attraction, as opposed to those on the surface, where part of these forces is not compensated. As a result, a perpendicular force to the surface is generated into the water mass, creating an unequal distribution of the attraction forces of the molecules. Thus, producing a tension on the fluid surface designated as surface tension, denoted as σ [N/m].

During the rearrangement of water molecules, forces of attraction between the liquid and the pore walls may occur. This attraction is determined by the contact angle, θ [°], defined as the inclination of the tangent that a drop of liquid forms with the surface – see Figure 2.7.

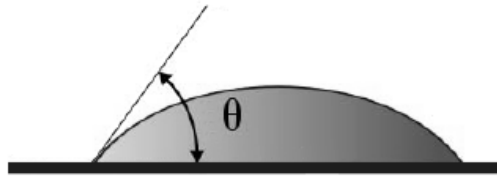


Figure 2.7 – Contact angle (Henriques, 2016)

When the attraction between water and pore walls is greater than the attraction of water and air, the contact angle is smaller than 90° , forming a concave meniscus. On the other hand, when the attraction between water and air is stronger, the meniscus forms a convex shape with a contact angle bigger than 90° . In the first case, the pore walls have a hydrophilic behaviour, contrasting to a hydrophobic behaviour in the second case.

The capillary pressure gradient (Δp) and the surface tension (σ) are related by Young-Laplace equation – see equation 21.

$$\Delta p = 2\sigma C \quad (21)$$

where C is the meniscus medium curvature, which is the inverse of the meniscus radius in two orthogonal directions.

Considering a circular tube with radius r , equal in both orthogonal directions, with its curvature $R = r/\cos(\theta)$, the equation can be written as follows (equation 22):

$$\Delta p = \frac{2\sigma \cos(\theta)}{r} \quad (22)$$

It is possible to notice that the capillary pressure increases with the decreasing of the pore radius. Therefore, the absorption of water by capillarity of a porous material is determined based on the diameter of its pores.

Within the hydrostatic equilibrium, the capillarity pressure is compensated by a certain liquid height h , which is the maximum theoretical height that the liquid can reach in a circular tube with radius r , and it is given by equation 23:

$$h = \frac{2\sigma \cos \theta}{r \rho g} \quad (23)$$

where ρ [kg/m^3] is the liquid density and g the gravity acceleration.

It can be understood by Figure 2.8, which presents a scheme with the geometric relations, the influence of the contact angle and the pore size on the capillary rise of the liquid.

The amount of water absorbed by capillarity can be quantify by the water absorption coefficient, denoted as A [$\text{kg}/(\text{m}^2 \cdot \text{s}^{1/2})$]. The higher this coefficient, the greater is the amount of water absorbed by capillarity per the surface in contact with water in less time. The A -value is a characteristic of the material and it is, commonly, the preferred parameter to measure the liquid water permeability of earthen materials, although with a significant variability of experimental results (Fabbri et al., 2018).

In addition to the A -value, it should be noted the parameter sorptivity, S [$\text{m}/\text{s}^{1/2}$] to quantify the absorption of liquid water for a porous material. It can be described by the product of the volume of water absorbed per unit cross-section, i [kg/m^2], with the length of time (t), in seconds, that absorption takes place, presented in equation 24:

$$i = S \cdot \sqrt{t} \quad (24)$$

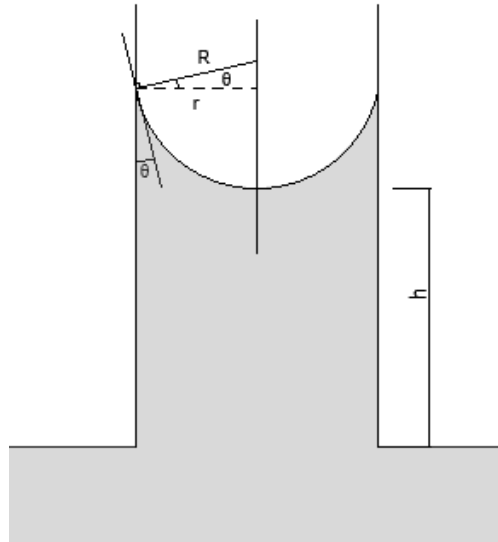


Figure 2.8 – Capillary suction within a pore

Sorptivity is not characteristic of the porous medium since it depends partly on the properties of the liquid and temperature (Gummerson et al., 1980; Henriques, 2016). This is why, it is of fundamental importance to define an intrinsic sorptivity, S_i , relating the sorptivity to its constraining factors, following equation 25:

$$S = S_i \left(\frac{\sigma \cos \theta}{\eta} \right)^{1/2} \quad (25)$$

where η is the liquid dynamic viscosity [kg/(m.s)].

3. Materials and methods

The present chapter describes the materials tested, as well as the methods used to assess the hygrothermal characteristics of earthen materials. The aim of these experiments is to define precise protocols for earth-based materials. As such, the exact same protocols must be applied and executed in the two laboratories. Only after validation of the materials used for the round robin tests, is it possible to study the different experimental protocols.

3.1. Materials

For the assessment of the hygrothermal properties of earthen materials, and since this study includes a series of round robin tests, one reference type of earth was chosen. The reference earth specimen was extracted from an existing rammed earth construction located in Dagneux, a town near Lyon, in France. This material is therefore referenced as “Dagneux”.

According to its granulometric curve (Figure 3.1), obtained by the wet sieve method, this earth specimen has a high clay and silt content, of around 85%, and quite a low sand and gravel content, of 15%, which makes it a fine earth, as shown in table 3.1.

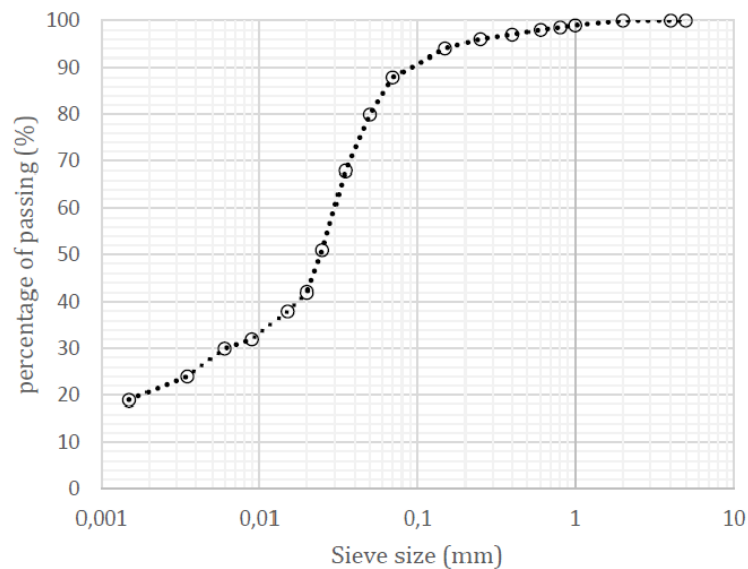


Figure 3.1- Granulometric curve of Dagneux earth (Al Haffar, 2017)

Table 3.1 – Dagneux earth properties (Al Haffar, 2017)

Methylene Blue Value			1.8
Clay activity index			4.05
Main mineral content	Quartz		80%
	Albite		10%
	Illite		10%
Particle grading	Clay	(<2 μ m)	20%
	Silt	(50 μ m-2 μ m)	65%
	sand & fine gravel	(2mm-5mm)	15%

The earth samples were produced in the two laboratories where the experiments were carried out, namely, at ENTPE in Lyon (France) and at FCT NOVA (NOVA) in Caparica (Portugal) in 2018, following the exact same procedure described by Al Haffar (2017). The samples made at each laboratory were sent to the other in order to test both types of samples at the two laboratories and cross-check the results.

To briefly describe the production process, the samples were prepared by compacting the earth at its optimum water content of 14% and optimum dry density of 1.85 g/cm³. This procedure consists of three main steps. Firstly, the soil is sieved at 5 mm and then mixed with the aim of homogenising it. This preparation is followed by the moulding step, where the earthen material is placed into moulds, in one sole layer, with a diameter of 100 mm and three different thicknesses, namely, 20, 30 and 40 mm. The earthen material is then compacted by the hydraulic press, with a compressive axial stress of 3.77 MPa; once the compaction step is completed, the samples are demoulded. Their weights and dimensions are confirmed, and the samples are then labelled with a soft permanent marker.

Regarding the laboratory where the samples were produced, they were classified as type E or N, depending on whether they had been produced at ENTPE or at NOVA laboratories. When identifying samples, it is important to establish easily understandable designations. As such, the samples were identified as follows: C because the samples are cylindrical; thickness of the sample (2, 3 or 4 cm); E or N, depending on the laboratory where the sample was manufactured (ENTPE or NOVA, respectively); and the number of the sample (1, 2, ...) – see Table 3.2. For example, sample C4N1 is a cylindrical sample with 4 cm thickness, made at NOVA, and is the sample number 1 of that type.

Table 3.2 – List of samples under study and tests performed

Manufacture laboratory	Group	Thickness [cm]	Sample identification	Sample number	Tests performed
NOVA	C2N	2	C2N1	1	ρ and ρ_d ; λ contact probe and hot wire; μ ENTPE and NOVA
			C2N2	2	
			C2N3	3	
	C3N	3	C3N1	1	ρ ; λ contact probe; sorption isotherms
			C3N3	3	
			C3N7	7	
			C3N2	2	ρ and ρ_d ; λ contact probe; drying-wetting cycles
			C3N5	5	
			C3N4	4	ρ and ρ_d ; λ contact probe; drying-wetting cycles
			C3N6	6	
	C3N8	8	ρ and ρ_d ; λ contact probe and hot wire; μ ENTPE		
	C3N9	9			
	C4N	4	C4N1	1	ρ and ρ_d ; λ contact probe; drying-wetting cycles
			C4N2	2	
			C4N3	3	ρ and ρ_d ; λ contact probe and hot wire; drying-wetting cycles
			C4N4	4	
ENTPE	C2E	2	C2E1	1	ρ and ρ_d ; λ contact probe; μ NOVA
			C2E2	2	
			C2E3	3	
			C2E4	4	
			C2E5	5	
	C3E	3	C3E1	1	ρ and ρ_d ; λ contact probe
			C3E2	2	
			C3E3	3	
			C3E4	4	μ NOVA
			C3E5	5	λ hot wire
			C3E6	6	
			C3E7	7	
	C4E	4	C4E1	1	ρ and ρ_d
			C4E2	2	
			C4E3	3	ρ and ρ_d ; λ contact probe; μ NOVA
			C4E4	4	
			C4E5	5	λ hot wire; μ ENTPE
			C4E6	6	λ hot wire; μ NOVA

3.2. Tests procedure

Samples manufactured at different laboratories were tested within the sample repeatability experiments and afterwards for the assessment of the hygrothermal characteristics of earthen materials; the tests performed for each sample are presented in Table 3.2.

3.2.1. Apparent density

In the standard DIN 18945 (NABau, 2012) it is defined the procedure for the determination of the apparent density of earth blocks. This procedure consists in placing the test samples in a conditioning room with environment conditions of $23\pm 5^{\circ}\text{C}$ temperature and $50\pm 15\%$ relative humidity until constant mass is reached. The constant mass is obtained when the result of two successive weightings do not differ more than 0.2% within an interval of 24h. In order to obtain the volume of the samples, its dimensions (i.e. diameter and thickness) are measured through a digital calliper – see Figure 3.2. Thus, the apparent density is determined by the ratio of the obtained mass by the volume of the sample.

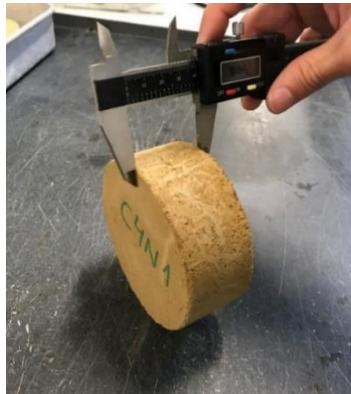


Figure 3.2 – Example of the measurement of sample thickness with a digital calliper

3.2.2. Dry density

The dry density is defined as the ratio between the dry mass (m_0) with the volume of the specimen (V). To obtain the dry mass, the specimens were dried in a ventilated oven at a temperature of 105°C , until the constant mass is reached. The dimensions of the samples were measured through a digital calliper, in order to obtain the volume.

3.2.3. Thermal conductivity

There are numerous test protocols to measure the thermal conductivity of the materials and, therefore, there is a large variability on the equipment and test protocol in different laboratories. Due to that, in the current work, the test methods used of the two laboratories is different. In the NOVA laboratory, the test method used is the contact probe, while at the ENTPE laboratory is used the hot wire method. Both methods are dynamic methods to assess the thermal conductivity.

3.2.3.1. Contact probe

The measurement of the thermal conductivity at NOVA was performed with the ISOMET 2104 Heat Transfer Analyser equipment and a contact probe AP 210412 of 6 cm diameter. The test protocol consists on placing the contact probe on the surface of the material in order to apply several heat flow impulses, in order to assess the material's response and, then give the value of the thermal conductivity measured – see Figure 3.3.



Figure 3.3- Thermal conductivity test using the contact probe method

Previously the test, the samples were stored in a conditioning room until the equilibrium was reached with the environment conditions of 20 ± 3 °C temperature and 50 ± 5 % relative humidity. To assure homogeneous boundary conditions, the samples were placed on extruded polystyrene boards preventing the heat flow dissipation. For each sample three measurements in the centre of the surface were performed.

3.2.3.2. Hot wire

At ENTPE the test method used for the measurements of the thermal conductivity was the hot wire performed with the NeoTIM FP2C equipment. This method is based on the measurement of the temperature rise defined from a linear heat source – the hot wire (Davis, 1978). The hot wire is placed between two samples, it is defined the duration and the source of the heat and the thermal conductivity is measured – see Figure 3.4.



Figure 3.4- Measurement of thermal conductivity with the hot wire method

Three measurements were performed for each pair of samples with the same thickness. Before the measurements took place, the samples were stored in a room, with the environment conditions of 20 ± 2 °C temperature and 40 ± 10 % relative humidity, until equilibrium was reached. The samples tested were the samples fabricated at NOVA and sent to ENTPE, as well the samples from ENTPE not sent to NOVA.

3.2.4. Water vapour permeability

Water vapour permeability is one of the main hygrothermal properties that quantifies the water vapour flow through a porous material, under a vapour pressure gradient once the steady state is reached (Rahim et al., 2015). The procedure was performed according to the standard EN ISO 12572 (CEN 2001), which describe the experimental protocol and the associated calculations.

The experimental procedure is divided in dry cup or wet cup, either a desiccant or an aqueous saturated solution is used. The wet cup method was chosen in the experimental set up of the current work. The aim is to obtain a constant value of relative humidity inside the cup of 75%. In order to obtain such value a salt solution of Sodium Chloride (NaCl) was placed inside the cup. This condition was monitored by placing a sensor inside the plastic cup through an existent hole.

Following the cup design by McGregor et al. (2014), the samples are sealed to the top of the plastic cup with a thin layer of silicon. To assure the one direction water vapour flow through the top of the sample, a vapour-tight aluminium taped was used, sealing the sides of the sample to the cup – see Figure 3.5.

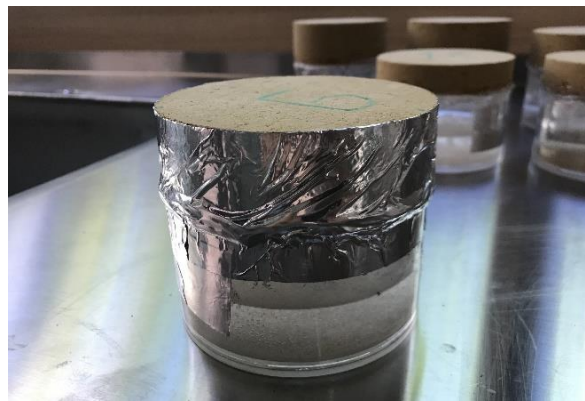


Figure 3.5- Example of sample design with saturated salt solution for wet cup test

Samples manufactured at NOVA and at ENTPE were tested, of which two samples were tested for each thickness. Measurements of the total mass, composed by the plastic cup, salt solution and sample were done periodically, on a scale with an accuracy of 0.01g until a linear function between time and variation of mass was reached.

Given the aim to assess the most accurate method to measure the vapour permeability of earthen materials, three different methods were performed concerning the maintenance of the environmental conditions at 43% relative humidity and 20°C temperature: plastic boxes, Ineltec climatic chamber at ENTPE, Fitoclima climatic chamber from Aralab at NOVA and laboratory-made gloves box. The first method, which uses plastic boxes as desiccators, maintains the pretend conditions by using a saturated salt solution of Potassium Carbonate (K_2CO_3) (Figure 3.6). Most frequent, samples are stored in a climatic chamber, which constantly controls the conditions inputted by the operator (Figure 3.7). Both methods described face a disadvantage; very often, the scale is placed outside the plastic boxes and the climatic chamber and then, in order to measure the mass, it is necessary to open them, thus creating a disruption on the environmental conditions. To counter it, a hermetic box with incorporated gloves was created; the RH level and temperature pretended are maintained with Potassium Carbonate (K_2CO_3) saturated salt solution placed on the bottom of the box and a scale is placed inside, hence the measurements are performed without opening the box – see Figure 3.8.

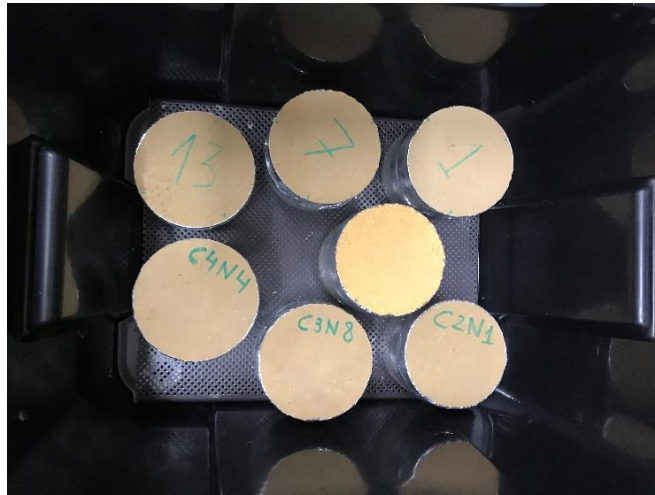


Figure 3.6- Wet cup test setup performed in a plastic box



Figure 3.7- Wet cup test setup performed in climatic chamber



Figure 3.8- Wet cup test setup performed in gloves box

Three phases happen within the mass variation. First, the initial non-linear equilibrium stage, in which the water vapour flow produced by the aqueous salt solution is adsorbed by the sample and a part is dissipated through evaporation; the permanent state, occurring when the water vapour flow reaches a constant rate; the last phase, not often during the test period, take place when the salt solution is insufficient.

Results analysis was performed according to the standard EN ISO 12575 (CEN 2001) and McGregor et al. (2017), to take into account the skin factor of the three different thicknesses. Once the linear relation between mass variation and time is reached, the vapour flux, G [kg/s], being the slope of the regression line, can be determined. The water vapour permeance, W [kg/(m².s.Pa)], in the permanent state, is given by eq. 26:

$$W = \frac{G}{A \cdot \Delta p_v} \quad (26)$$

where A [m²] is the exposed area of the specimen and Δp_v [Pa] the water vapour pressure difference across the sample. The water vapour permeability, δ_p [kg/(s.m.Pa)] can be deduced through Fick's law of diffusion following eq. 27 or, simply has the product between the water vapour permeance with the sample thickness, d [m]:

$$\delta_p = \frac{G}{A \cdot \Delta p_v} = W \cdot d \quad (27)$$

Usually, for convenience, the water vapour resistance factor is used to quantify the water vapour permeability. It is given by the ratio between the water vapour permeability of air, δ_a , and the water vapour permeability – see equation 17 of Chapter 2.

The water vapor permeability of air, δ_a , can be estimated from the relation given by Künzel (1995) (eq. 28):

$$\delta_a = 2 \times 10^{-7} \cdot \frac{T^{0.81}}{p_0} \quad (28)$$

where T is the ambient air temperature [K] and p_0 is the atmospheric pressure [Pa]. Hence the tests were performed at 20°C and at atmospheric pressure of 101325 Pa, the water vapour permeability of air takes a value of $\delta_a=1.97 \times 10^{-10}$ kg/(m s Pa).

The standard EN ISO 12752 (CEN 2001) proposes a correction for the resistance of the air layer between the sample and the salt solution. It takes into account that the air layer promotes a resistance to the water vapour flow from the salt solution through the sample and assumes that the vapour flow only occurs by diffusion. It is recommended when the water vapour diffusion equivalent air layer thickness, s_a , given by eq. 29, is lower than 0.2m:

$$s_a = \mu \cdot d_a \quad (29)$$

This correction leads to eq. 30 and 31, where d_a [m] is the thickness of the air layer between the sample and the salt solution inside the cup:

$$\delta_p^{ISO} = \frac{G \cdot d}{A \cdot \Delta P_V - G \frac{d_a}{\delta_a}} \quad (30)$$

$$\mu^{ISO} = \frac{\delta_a}{\delta_p^{ISO}} \quad (31)$$

3.2.5. Sorption isotherms

The sorption isotherms determination was performed following the standard EN ISO 12571 (CEN 2000). According to it, two methods can be used: the “Desiccator method” or the “Climatic chamber method”. The first method maintains the relative humidity by using aqueous saturated salt solutions while, in the other the chamber controls the temperature and relative humidity. Despite the method used, a sorption-desorption curve for earthen materials can be made approximately in four months. Conversely, other method using the Dynamic Vapour Sorption (DVS) equipment, which is more precise as it works at microscale in a controlled environment (i.e. the entire process is made inside the equipment), allows to obtain a sorption-desorption curve in 1-2 weeks. However, for the DVS method, only one sample can be tested at the time and the small size of the sample can limit representativeness of heterogenous construction materials.

3.2.5.1. Salt solutions

In the current work, the “Desiccator method” was chosen. Three samples, manufactured at NOVA, were each one cut in six smaller samples, placed in plastic and aluminium containers to prevent any material lost and, then tested – see Figure 3.9.



Figure 3.9- Example of samples used for the sorption isotherms determination

Firstly, the samples were dried in order to obtain the dry mass, m_0 , at three temperatures: 50°C, 70°C and 105°C. They were then placed at different increasing levels of relative humidity: 23, 43, 59, 75, 85 and 97%, at 20°C. For each level of RH, a plastic box was used acting as a desiccator – see Figure 3.10. Salt solutions were prepared according to Annex B in the standard EN ISO12571 (CEN 2000); the salts and correspondent RH are presented in Table 3.3. The conditions of RH inside the plastic boxes were monitored by a portable sensor.

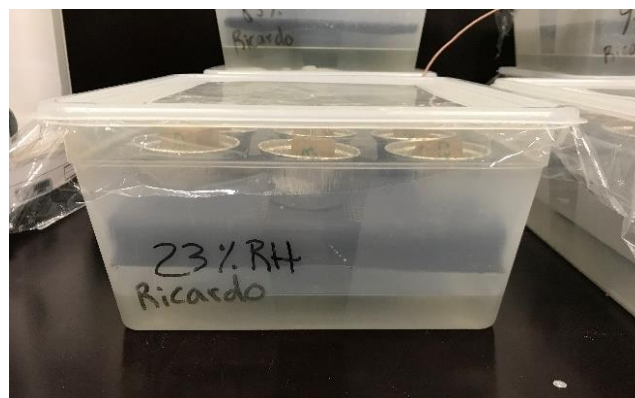


Figure 3.10- Example of samples placed in plastic box for the determination of sorption isotherms

Table 3.3 – Salt solutions substances and respective RH at 20°C

RH [%]	Substance
23	Potassium acetate (KC ₂ H ₃ O ₂)
43	Potassium carbonate (K ₂ CO ₃)
59	Sodium bromide (NaBr)
75	Sodium chloride (NaCl)
85	Potassium chloride (KCl)
97	Potassium sulphate (K ₂ SO ₄)

Samples were weighted periodically, approximately 3 in 3 days, to avoid opening the boxes daily disturbing the inside conditions, with a scale of an accuracy of 0.001g. When the equilibrium moisture content was reached, the mass variation between three consecutive measurements was less than 0.1%, the samples were placed in the next level of RH.

The results of the sorption isotherms are plotted into curves of water content over RH; ascending order for the sorption curve and descending order for the desorption curve. The equilibrium water content was determined following equation 15 of Chapter 2.

3.2.5.2. Dynamic Vapour Sorption

The sorption isotherms obtained by the DVS equipment (see Figure 3.11) was performed according to McGregor et al. (2014). The equipment measures gain and moisture losses by the insertion of a gas at a specific relative humidity through a small sample, with a mass inferior than 1 g, which is suspended in a microbalance with an ultra-sensitive mass record.

**Figure 3.11** – Dynamic Vapour Sorption equipment (Intrinsic 2, SMS®)

However, being a fast and reliable method for the determination of the sorption isotherms, for certain materials the sample may not be representative of the material. Overall, concerning the earthen material under study, it is considered to be representative since it is virtually a homogeneous material because it has no coarse aggregates (the coarser is sand).

3.2.6. Cycles of drying-wetting

Four types of cycles were tested to study the effect of drying methods on the microstructure of the porous network and its repeatability and reproducibility. Three temperatures at oven-drying were chosen: 50°C, 70°C and 105°C and two relative humidities: 0% and 23%.

Samples of three thicknesses, 2cm, 3cm and 4cm were tested for each cycle, except for the cycle of dry temperature at 70°C, accounting five samples for each cycle of drying and wetting. The samples were dried at each drying temperature and then placed at 85% for the wetting cycle – see Figure 3.12. They were weighed periodically with a scale of an accuracy of 0.01g. The duration of drying and wetting was fifteen days for the different cycles.

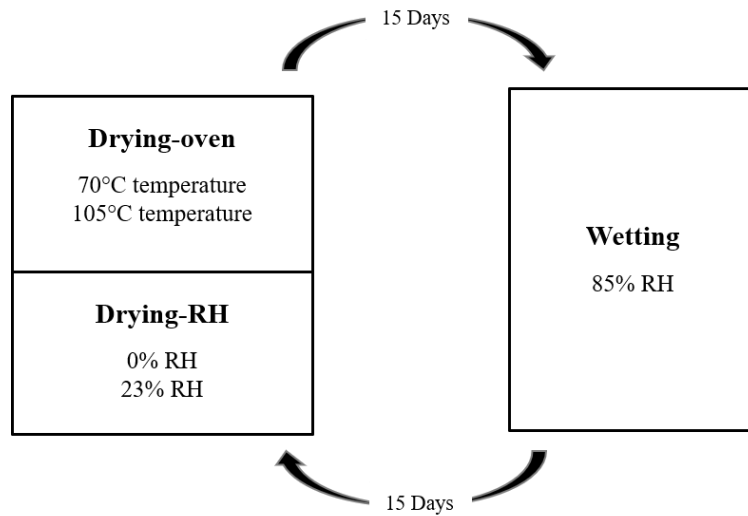


Figure 3.12- Experimental steps used for the drying/wetting cycles

Drying oven methods were performed on ventilated ovens - For the drying method of 0% RH, a box with constant flow of dry air and silica gel on the bottom was used; two holes on two opposite sides of the box were done, for the dry air entrance and exhaustion. The box was sealed to the top with vapour-tight aluminium taped – see Figure 3.13.



Figure 3.13- Samples placed in plastic box with dry air flow for drying at 0%

Salt solutions were used to reach and maintain the RH levels of 23% for drying and 85% for wetting the samples, following the same procedure as described in section 3.2.4.

4. Sample repeatability experiments

With the aim to achieve the best procedure to assess the hygrothermal characteristics of earthen materials, samples made at different laboratories were tested. Firstly, there is the need to ensure if these samples are similar. For that purpose, preliminary tests were conducted, such as apparent density, dry density and thermal conductivity, which are fast and reliable methods.

Previously to the comparison between the samples from NOVA and ENTPE, it is important to guarantee that the samples made at the same laboratory present the same characteristics.

This pre-study took place at the materials laboratory of the Civil Engineering Department at NOVA in the beginning of the present work, and at the Tribology and System Dynamics Laboratory (LTDS) at ENTPE.

4.1. Density

4.1.1. Apparent density

The first procedure used to check the similarity and repeatability of samples manufactured at different laboratories was their apparent density. As explained in Chapter 3, the samples were stabilised in a conditioning room at 20 ± 3 °C temperature and 50 ± 5 % relative humidity until two consecutive measurements of mass differ less than 0.2%, within a 24h interval. After which, the samples' dimensions were measured with a digital calliper.

The results obtained for the NOVA samples were plotted in Figure 4.1. The samples showed a great heterogeneity of values, not only between the three different thicknesses but also the samples within the same thickness. Samples of 4 cm thickness are the samples with the lowest variation of apparent density values – see Table 4.1. A remark must be made concerning the sample C2N3, since it has a substantially higher apparent density than the others, possibly due to the fabrication process.

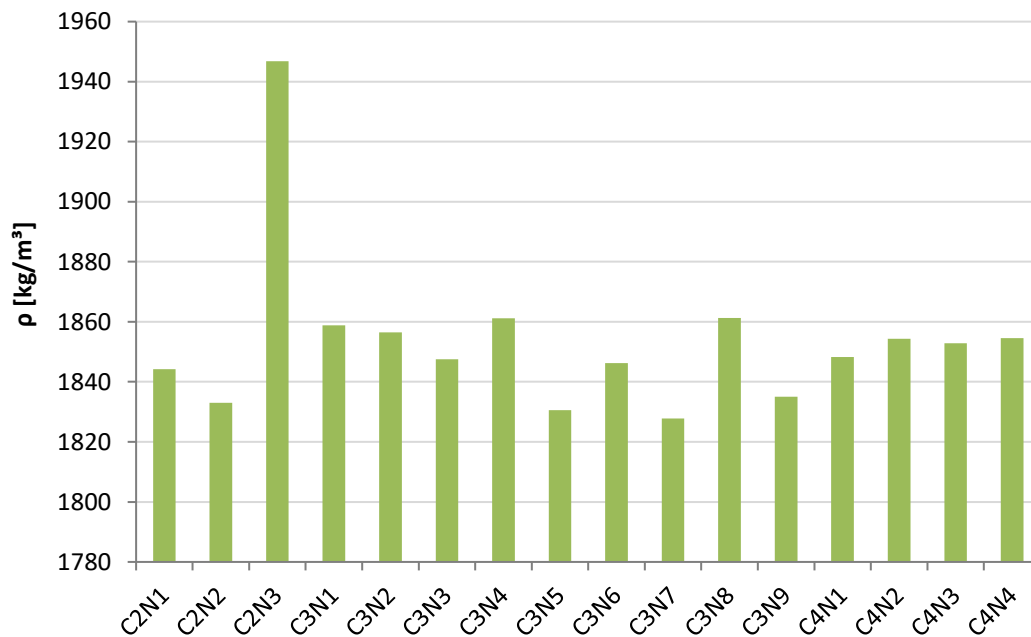


Figure 4.1 – Apparent density of NOVA samples

Table 4.1 – Apparent density of NOVA samples by thickness

Thickness [cm]	ρ [kg/m ³]	
	Average	Standard deviation
2	1874.66	62.68
3	1847.19	13.31
4	1852.49	2.95

Regarding the samples manufactured at ENTPE, the results of the apparent density also performed at NOVA are shown in Figure 4.2. With small variations within the same thickness, the samples made at ENTPE present a difference of the apparent density of the three thicknesses – see Table 4.2.

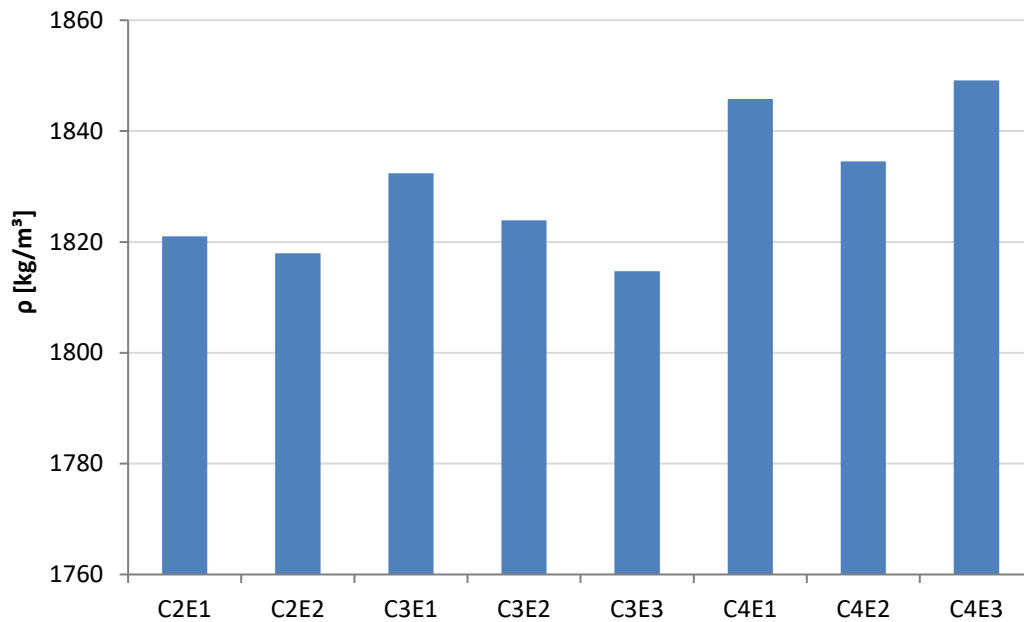


Figure 4.2 – Apparent density of ENTPE samples

Table 4.2 – Apparent density of ENTPE samples by thickness

Thickness [cm]	ρ [kg/m ³]	
	Average	Standard deviation
2	1819.47	2.17
3	1823.67	8.85
4	1843.16	7.65

Despite some significant variations within samples manufactured in the same laboratory, it can be concluded that these samples show a similar behaviour concerning their apparent density. NOVA samples present a difference of around 27 kg/m³, taking into account all the samples tested, whereas ENTPE samples have a difference of about 13 kg/m³.

Provided that the comparison of the apparent density between samples made at the same laboratory is accepted, the comparison between samples made at both laboratories is done. The average values of the apparent density for each thickness for both types of samples are present in Figure 4.3.

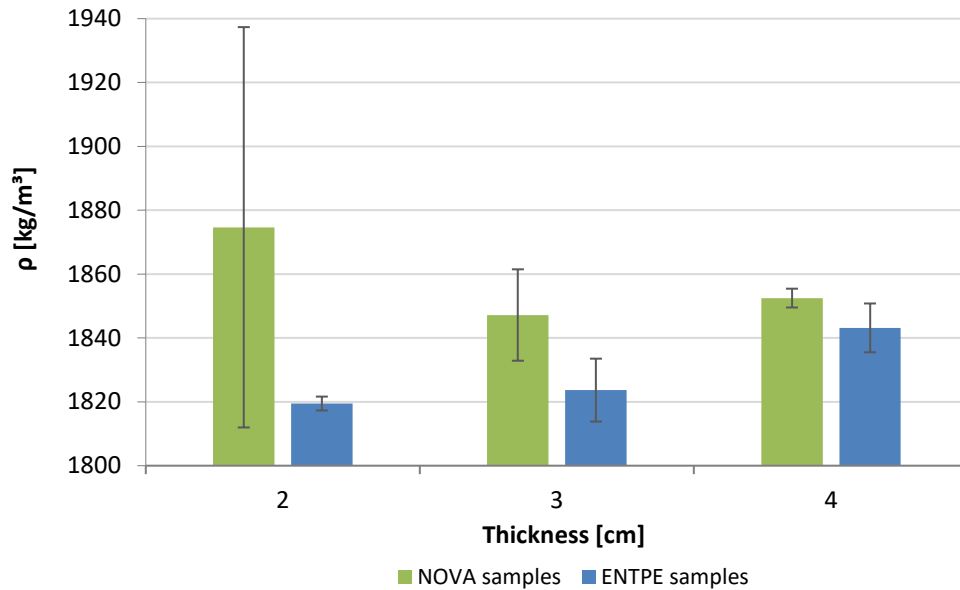


Figure 4.3 - Apparent density of NOVA and ENTPE samples

Samples from NOVA present a higher apparent density than the samples made at ENTPE. This difference is more noticeable for the samples of 2 cm thickness, while the samples of 4 cm thickness show a lower variation.

For the calculation of the volume, samples dimensions were measured with a digital calliper. Three measures of diameter and thickness were done for each sample. Although a significative number of measurements were done, the volume calculated is not accurate; a wide number of samples do not have completely regular surfaces and perfect edges. Hence, results of the apparent density were plotted in Figure 4.4, with the assumed volume of the samples. This volume being $1,57E-04$, $2,36E-04$ and $3,14E-04$ m³ for the samples of 2, 3 and 4 cm thickness, respectively.

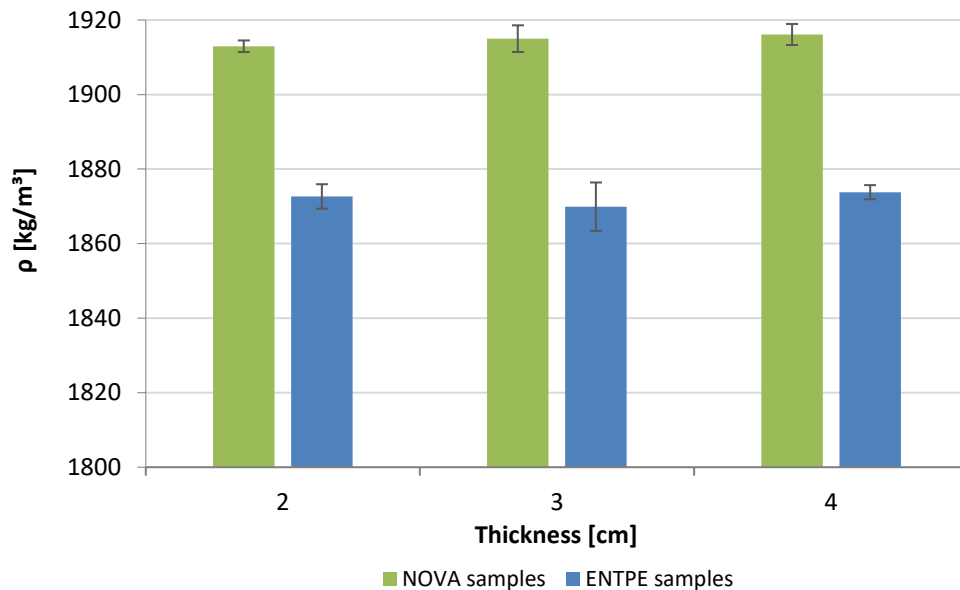


Figure 4.4 - Apparent density determined with the assumed volume of NOVA and ENTPE samples

When the assumed volume is used for the determination of the apparent density, its variation between samples of different thickness becomes drastically reduced, both for NOVA and ENTPE samples. Nevertheless, samples manufactured at different laboratories present a higher variation. Therefore, to obtain the exact volume of the samples, the hydrostatic method should be used.

4.1.2. Dry density

The second procedure used for the comparison and validation of samples manufactured at both laboratories following the same procedure was the dry density. The dry density of the compacted earth samples was obtained using the dry mass of the circular samples, either from NOVA and ENTPE. This dry mass stemmed from drying the samples in a ventilated oven at 105°C temperature until constant mass was reached, as previously explained in Chapter 3. Following the same procedure used for the apparent density, the volume of the samples was determined by the measurements of its dimensions with a digital calliper. In order to obtain a more realistic and accurate volume, although with some limitations, more measurements were done; five measurements for each dimension (i.e. diameter and thickness) opposing the three measurements used for the apparent density. Owing to the limited number of samples available for the experimental campaign, not every samples used for the apparent density and thermal conductivity were tested, since oven drying earthen materials at 105°C can interfere with their microstructure. Furthermore, three samples of 3 and 4 cm thickness were tested and two samples of 2 cm thickness were tested, making a total of eight tested samples of each laboratory.

Figure 4.5 gives the dry density for NOVA samples. The results stemmed from the ratio between the dry mass and the volume of the samples, being this volume determined with the average of the five measurements for each dimension of the samples. The dry density presents a rather good consistency, yet the samples of 2 cm thickness show slightly lower values. Also, the sample C4N3 presents a higher value than the samples with the same thickness.

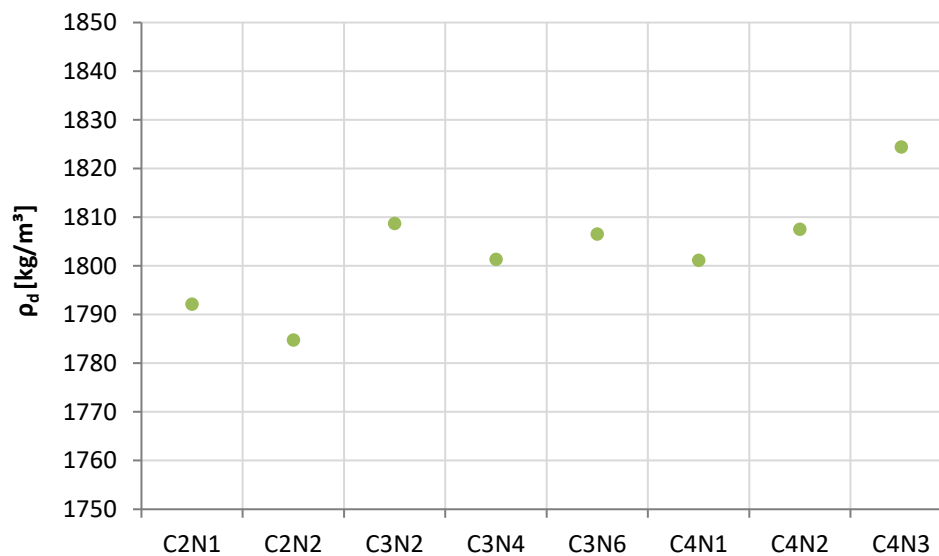


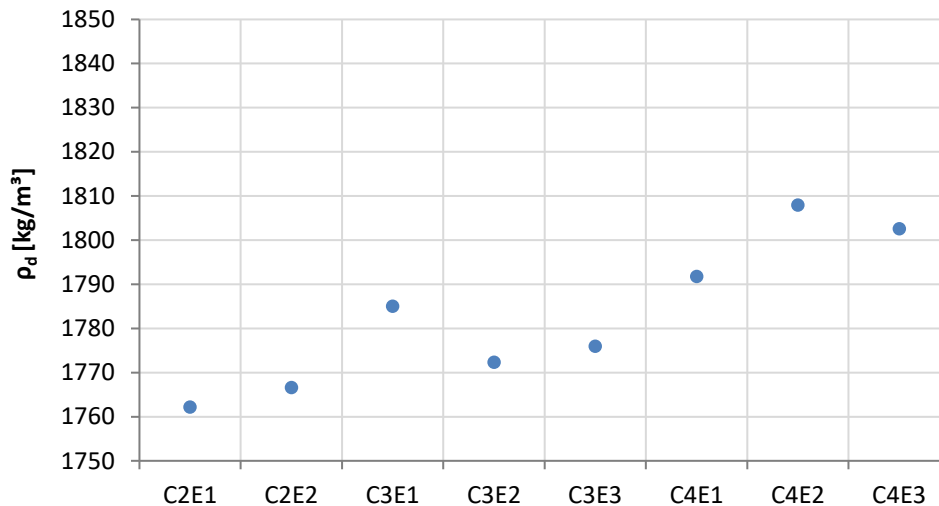
Figure 4.5 - Dry density of NOVA samples

As demonstrated, the samples fabricated at NOVA have a wide range of values concerning the dry density, with differences between the three different thickness. This can be better seen in Table 4.3, the obtained values for the samples with 2 cm thickness are lower comparing to the others. Samples with 3 and 4 cm of thickness also present a variation within the results; nevertheless, this variation is slightly lower, with a highest value of dry density for the 4 cm samples.

Table 4.3 – Dry density by thickness of NOVA samples

Thickness [cm]	ρ_d [kg/m ³]	
	Average	Standard deviation
2	1788.45	5.24
3	1805.52	3.78
4	1811.02	12.04

In Figure 4.6 the results of dry density obtained for ENTPE samples are presented. It can be seen an increase of dry density with increased thickness of the samples. The majority of the results within the same thickness are homogeneous. In fact, for the same thickness, a variation of less than 20 kg/m³ between the minimum and maximum values is considerably good.

**Figure 4.6** – Dry density of ENTPE samples

Now focusing on the differences of the values between the three thickness, according to the average results presented in Table 4.4, it can be seen a variation around 36 kg/m³ between samples of 2 and 4 cm thickness.

Table 4.4 – Dry density by thickness of ENTPE samples

Thickness [cm]	ρ_d [kg/m ³]	
	Average	Standard deviation
2	1764.34	3.12
3	1777.74	6.53
4	1800.69	8.24

Similarly, to the apparent density and thermal conductivity, the aim of these preliminary tests is given to ensure the similarities or differences between samples manufactured at different laboratories following the same procedure. Therefore, a comparison between NOVA and ENTPE samples, regarding their obtained dry density is showed in Figure 4.7.

Through the analysis of the results presented in Figure 4.7, the same behaviour can be understood for both types of samples. As previously discussed, 4 cm samples have the highest dry density, while those of 2 cm thickness have the lowest values. Regardless its thickness, NOVA samples showed higher values of dry density than the ENTPE samples, with less variation of results for the samples of 4 cm thick. The difference between the dry density values comparing the two samples types, namely those of 2 and 3 cm thickness is quite similar. Samples with a thickness of 2 cm have a difference of about 24 kg/m³, while those of 3 cm have a difference of 28 kg/m³, regarding their minimum and maximum value. As mentioned, this difference is much smaller for the thicker samples, having a difference of the dry density values obtained, between the samples produced in NOVA and ENTPE in the order of 10 kg/m³.

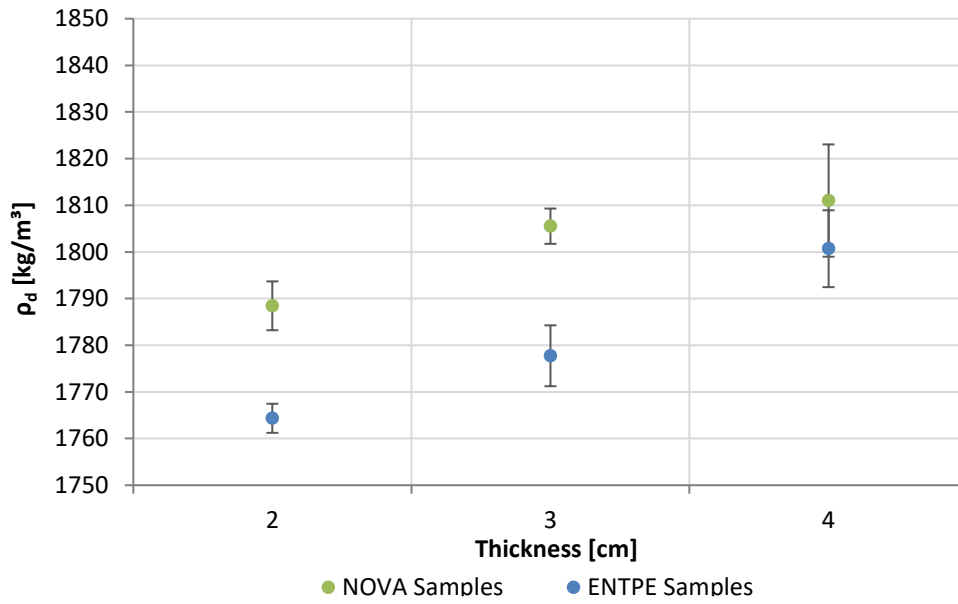


Figure 4.7 – Dry density of NOVA and ENTPE samples

4.1.3. Comparison between densities

The difference between the apparent density and dry density should be linked to the water content at 50% RH; so, a comparison between these two densities is presented.

A clear tendency can be found regarding the apparent density and dry density – see Figure 4.8. As a remark about Figure 4.8, for the determination of the average apparent density of NOVA samples, the data collected for the apparent density test was used but only for the samples tested for the determination of the dry density. The same behaviour is verified for both types of samples; NOVA samples have higher values of both densities, while ENTPE values are lower.

All in all, thicker samples show values of both densities higher than the samples with smaller thicknesses. Naturally, the dry density obtained for both types of samples is lower, since it is considered that the relative humidity inside the ventilated oven is close to 0% and that the samples are within the dry state, with its pores containing only gas (i.e. ideally, no liquid water can be found in this phase).

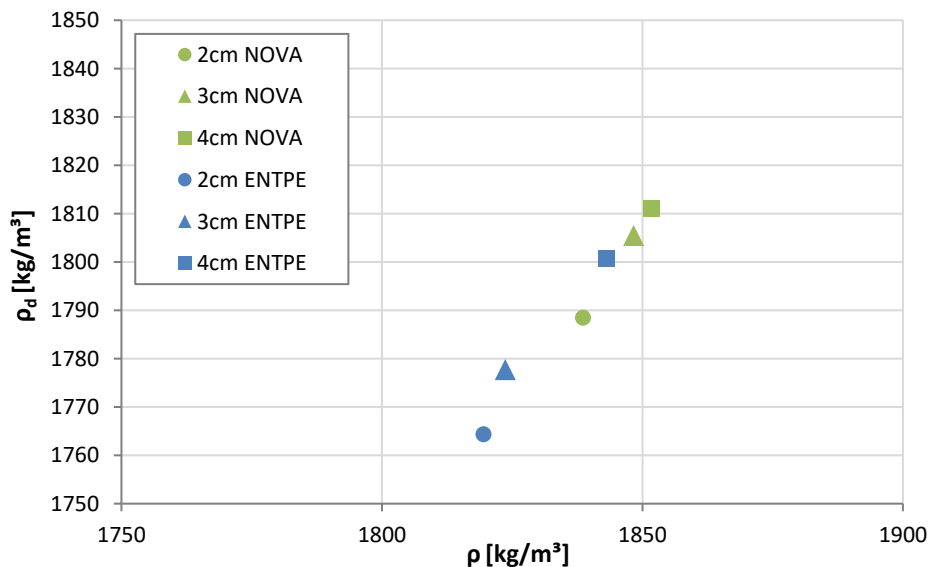


Figure 4.8 – Comparison between the apparent density and dry density of NOVA and ENTPE samples

4.2. Thermal conductivity

As explicit in Chapter 3, two procedures to measure the thermal conductivity were tested. The contact probe at NOVA and the hot wire at ENTPE. Although a comparison of the two methods used it is not possible, owing to different storage conditions of the specimens, samples from both laboratories can be compared within the same method.

Additionally, to the apparent density and dry density tests, a first evaluation of the samples made at the same laboratory was conducted for the thermal conductivity, either for both methods. After that, the comparison between samples made at different laboratories is presented.

4.2.1. Contact probe

Through the contact probe method, using the ISOMET 2104 Heat Transfer Analyser equipment the thermal conductivity measurements are obtained for each test sample based on its response to heat flow impulses. The results of the thermal conductivity performed at NOVA, for NOVA samples were plotted in Figure 4.9. These values are the result of the average value of three measurements for a single sample.

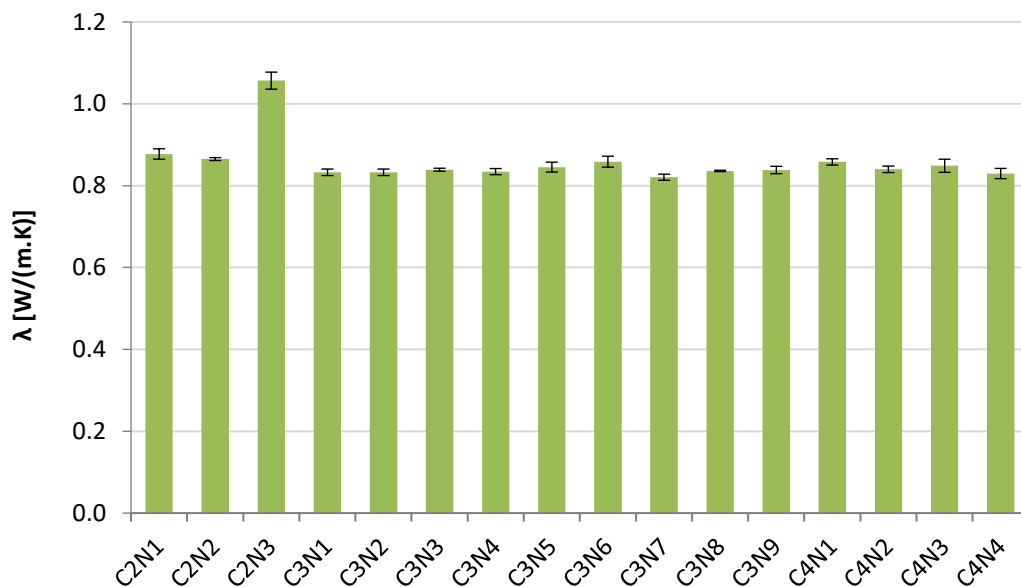


Figure 4.9 - Thermal conductivity measured by the contact probe method of NOVA samples

Regardless the specimen tested and thickness, better seen in Table 4.5, a thermal conductivity around 0.850 W/(m.K) may be observed, with a significant difference noticed for the specimen C2N3. As it can be seen, in comparison with the vast majority of the samples, C2N3 has a slightly different average value, in the order of 1.000 W/(m.K). This can be owing to the existence of a reduced number of pores or due to their smaller dimensions. The thermal conductivity of air is substantially smaller than the thermal conductivity of earth, being around 0.025 W/(m.K) (Santos & Matias, 2006). Besides it, sample C2N3 have a higher apparent density than the others samples manufactured at NOVA (see section 4.1), thus having a higher compactness resulting in a greater amount of solid material (i.e. earth) and less voids. Therefore, if smaller or less pores exist it can be deduced that there is less air within the sample resulting on a higher thermal conductivity of the material. It is of fundamental importance to take into account that when measuring the thermal conductivity of a certain sample, this measurement is a combination of earth, air and water (i.e. the material is not in the dried phase).

Table 4.5 – Thermal conductivity by thickness measured by the contact probe of NOVA samples

Thickness [cm]	λ [W/(m.K)]	
	Average	Standard deviation
2	0.933	0.107
3	0.838	0.010
4	0.844	0.012

As it is possible to see in Table 4.5, NOVA samples show a very small variation of thermal conductivity, concerning the samples of 3 and 4 cm thickness. However, the average for the 2 cm samples is much higher than the others, as it was expected by the previous individual results. If sample C2N3 is excluded, the measurement of thermal conductivity of NOVA samples with 2 cm thickness by the contact probe method gives $0.871 (\pm 0.009)$ W/(m.K), thus the average values get closer for the three thicknesses.

The same data analysis of the results, the average value and standard deviation of three measurements, for each ENTPE samples are presented in Figure 4.10 and the average value for the three different thickness in Table 4.6. Similarly, to NOVA samples, ENTPE samples showed the same behaviour concerning the values of thermal conductivity, with an average value around 0.820 W/(m.K).

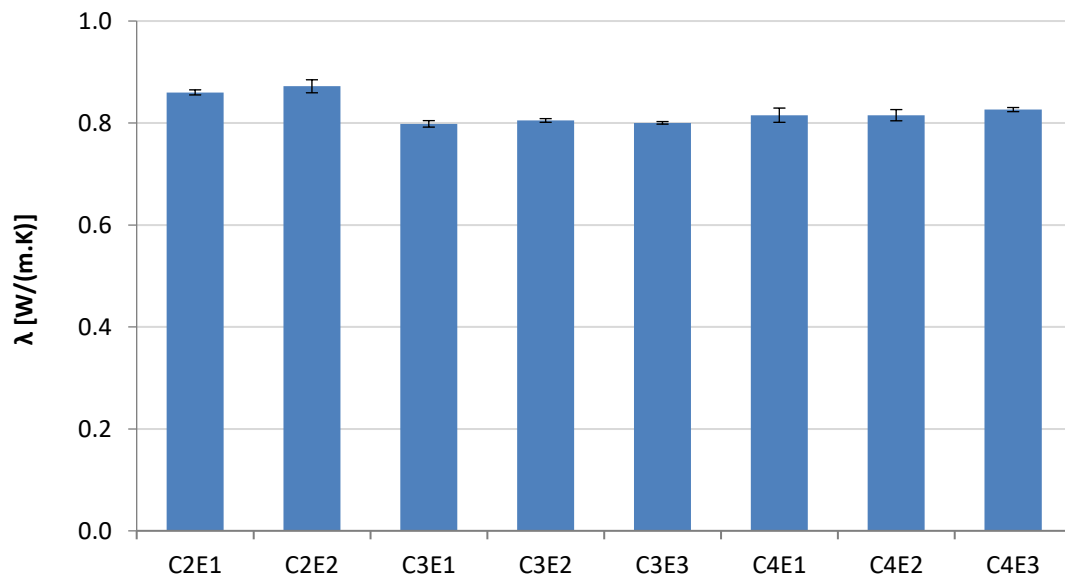

Figure 4.10 - Thermal conductivity measured by the contact probe method of ENTPE samples

Table 4.6 – Thermal conductivity by thickness measured by the contact probe of ENTPE samples

Thickness [cm]	λ [W/(m.K)]	
	Average	Standard deviation
2	0.866	0.008
3	0.801	0.003
4	0.819	0.006

Figure 4.11 presents the thermal conductivity values measured by the contact probe method for both types of samples, either for NOVA and ENTPE samples, excluding sample C2N3. In comparison with ENTPE samples, it is clearly visible that the samples manufactured at NOVA present higher values of thermal conductivity, with a range between 0.844 W/(m.K) and 0.871 W/(m.K). On the whole, this can be seen for the three different thicknesses, although with a great proximity for the 2 cm thickness samples.

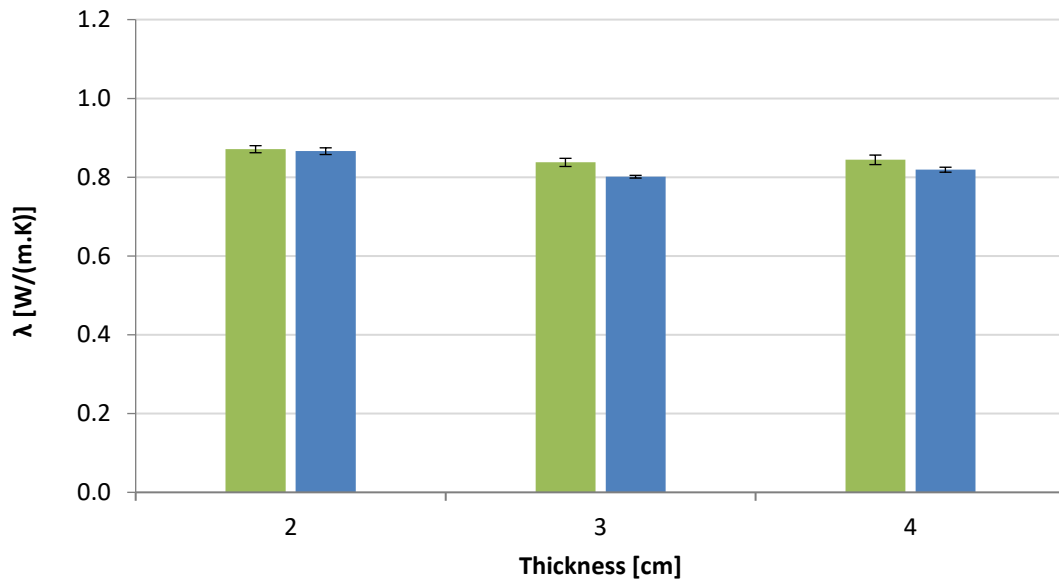


Figure 4.11 – Thermal conductivity measured by the contact probe of NOVA and ENTPE samples

In a study conducted by Zhang et al. (2018), several compressed earth bricks with different bulk densities were tested in terms of thermal conductivity, reaching values in a range of 0.52 to 0.93 W/(m.K) with the hot disk method. On top of that, Moevus et al. (2012), in a literature review of earthen materials properties, suggests values of about 0.50 to 1.70 W/(m.K) for compacted earth. Altogether, the values obtained for NOVA and ENTPE samples are within the values found in the literature for earth samples.

The experimental data collected from the apparent density and thermal conductivity measured by the contact probe method were plotted in Figure 4.12. A trend between the apparent density and thermal conductivity between NOVA and ENTPE samples can be observed, although not clearly. Regarding the comparison between samples within the same manufacture laboratory, it can be seen that samples with 2 cm thickness present the lower apparent densities and highest thermal conductivities, while the samples with 4 cm thickness have the highest apparent densities and the intermediate values of thermal conductivity. Focusing on the samples of 3 cm thickness, these present the lowest values of thermal conductivity and intermediate apparent densities.

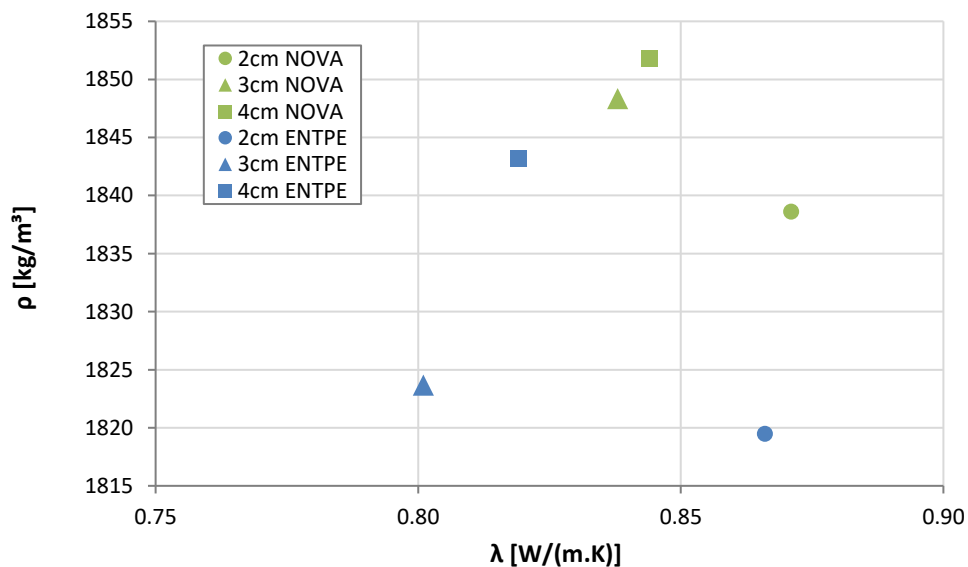


Figure 4.12 – Comparison between the thermal conductivity measured by the contact probe and the apparent density

4.2.2. Hot wire

Alternatively, to the contact probe method performed at NOVA, at ENTPE the method used for the measurement of the thermal conductivity was the hot wire. As previously explained (see section 3.2.2.2), the hot-wire method consists in placing the hot wire between the interface of the material. That is to say, to place the hot-wire between two samples, thus contacting with one surface of each sample. As a result, with this method it is not possible to measure the thermal conductivity of a single sample but it is, instead, measured the thermal conductivity of two samples.

By contrast with the contact probe, it is not possible to conduct a comparison between the samples within the same thickness, but specifically a comparison between different thicknesses.

In order to obtain the thermal conductivity, several samples were tested; three measurements were done for each two samples within the same thickness. Therefore, the values shown in this section are the result of the average of these measurements, that took place at ENTPE.

It must be noticed that the samples used for the measurement of the thermal conductivity with the hot-wire method are not exactly the same used in the contact probe method. To some extent, not all samples were moved from one laboratory to the other.

The results of the samples manufactured at NOVA and sent to ENTPE, by their thickness, are presented in Table 4.7. Regardless their thickness, NOVA samples present an insignificant variation of values for the samples of 2, 3 and 4 cm, respectively. Also, it can be noticed that the three average values are within the deviation standard of the others. The same behaviour can be seen for the ENTPE samples – see Table 4.8. Alongside with NOVA samples, samples with 2 cm thickness have a lower value of thermal conductivity, despite this difference not being significative.

Table 4.7 – Thermal conductivity measured by the hot wire of NOVA samples

Thickness [cm]	λ [W/(m.K)]	
	Average	Standard deviation
2	0.737	0.027
3	0.712	0.062
4	0.727	0.034

Table 4.8 – Thermal conductivity measured by the hot wire of ENTPE samples

Thickness [cm]	λ [W/(m.K)]	
	Average	Standard deviation
2	0.732	0.050
3	0.704	0.036
4	0.719	0.028

At last, the comparison between samples from both laboratories is presented in Figure 4.13. As verified for the samples from the same laboratory, when compared to those from the other one, the thermal conductivity results are very close. Although with no significant differences, NOVA samples have higher values for all thicknesses.

In brief, taking into account the values of thermal conductivity of earthen materials presented in Chapter 2 (see Table 2.1), namely for compacted earth and compressed earth bricks, which are the closest to the samples under study, it is possible, once again, to notice that NOVA and ENTPE samples are within the values found in the literature

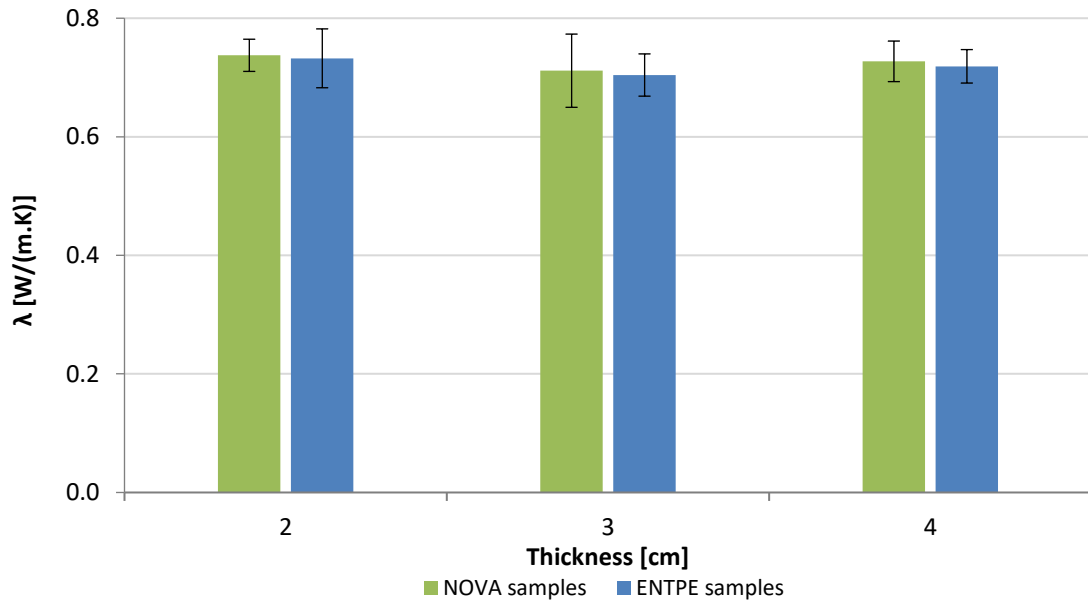


Figure 4.13 - Thermal conductivity measured by the hot-wire method of NOVA and ENTPE samples

A comparison between the apparent density and thermal conductivity measurements carried out through the hot wire method is presented in Figure 4.14. As previously achieved for the thermal conductivity measured by the contact probe, for the hot wire the same trend can be observed – see section 4.2.1.

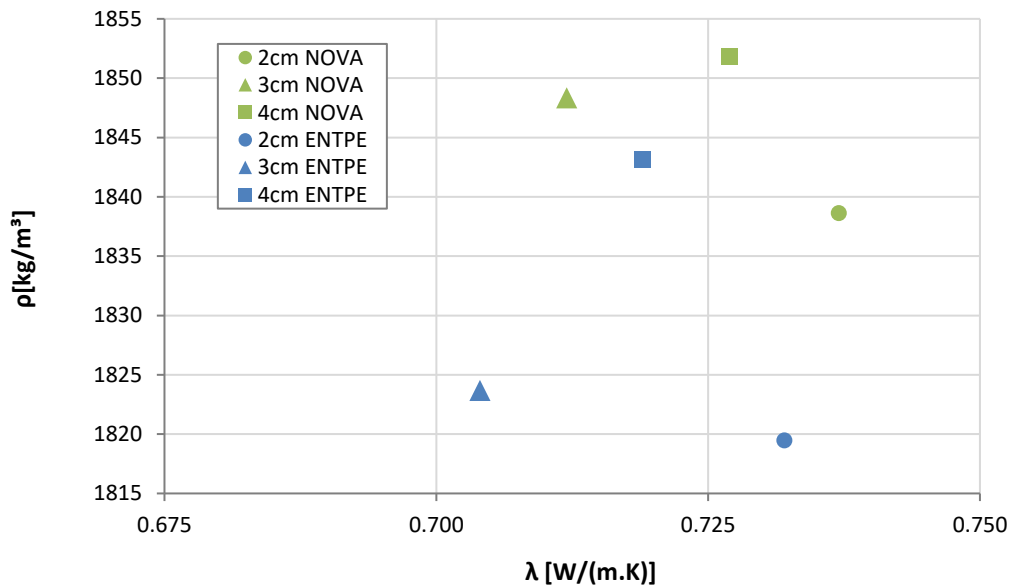


Figure 4.14 – Comparison between the thermal conductivity measured by the hot wire and the apparent density

4.3. Discussion

In this chapter, the results obtained from the three properties assessed for both types of samples are fundamental to better understand the implications on the similarity of these samples and its validation. Altogether, the samples manufactured at NOVA present higher values than those manufactured at ENTPE, in terms of apparent density, dry density and thermal conductivity.

By analysing the results of the apparent density of samples within the same laboratory, it can be concluded that the values are similar although with some variations. For both types of samples, those with 4 cm thickness have highest values opposing the 2 cm thickness samples with the lowest apparent densities. One should notice that sample C2N3 present a much higher apparent density than the others and, therefore, this sample should not be taking into account in the continuity of the present study. If the apparent density data collected for this sample is not used, the variation between samples manufactured at NOVA is drastically reduced. As expected, if variations between samples within the same laboratory exist, there are also variations when comparing the samples from both laboratories, although small. It can be seen that the greater difference between the minimum and maximum value of NOVA and ENTPE samples is between the samples of 3 cm, discarding sample C2N3, with a value around 24 kg/m³, when using the average results for the three thicknesses. Overall, the most significative variation within samples manufactured at the same laboratory is about 34 kg/m³, by analysing samples individual results; this value is valid for both types of samples. Therefore, the difference between NOVA and ENTPE samples is within that previously obtained.

By contrast to the thermal conductivity, the apparent and dry densities obtained present a smaller variation when comparing samples within the same laboratory but also comparing samples from different laboratories – see Table 4.9. Once more, as referred, NOVA samples present higher values than ENTPE samples, for both thermal conductivity methods tested. It can be seen that when the hot wire method is used the variation of results between both types of samples is significantly reduced. Hence, taking into account that two different methods were used to measure the thermal conductivity, it can be concluded that in a thermal and density point of view NOVA and ENTPE samples have very similar characteristics.

Table 4.9 – Variation within the sample repeatability experiments

Samples	Apparent density (ρ)		Dry density (ρ_d)		Thermal conductivity (λ)			
					Contact probe		Hot wire	
	Variation [%]		Variation [%]		Variation [%]		Variation [%]	
C2N	0.78	0.72	0.65	1.00	2.07	3.20	1.73	1.73
C3N								
C4N								
C2E	0.69		1.03		4.05		1.95	
C3E								
C4E								

Although for earthen materials, a strong dependency of the thermal conductivity with the water content can be found, there does not appear to be a clear enough tendency between the thermal conductivity and the dry density (Fabbri et al., 2018). Nevertheless, it should be expected to obtained higher values of thermal conductivity with a higher dry density, but at this point, that it was not obtained, for both types of samples – see Figure 4.15.

On balance, the differences observed between samples manufactured at the same laboratory as well as manufactured at distinct laboratories remain satisfactory. Hence, NOVA and ENTPE samples are similar and can be evaluated together.

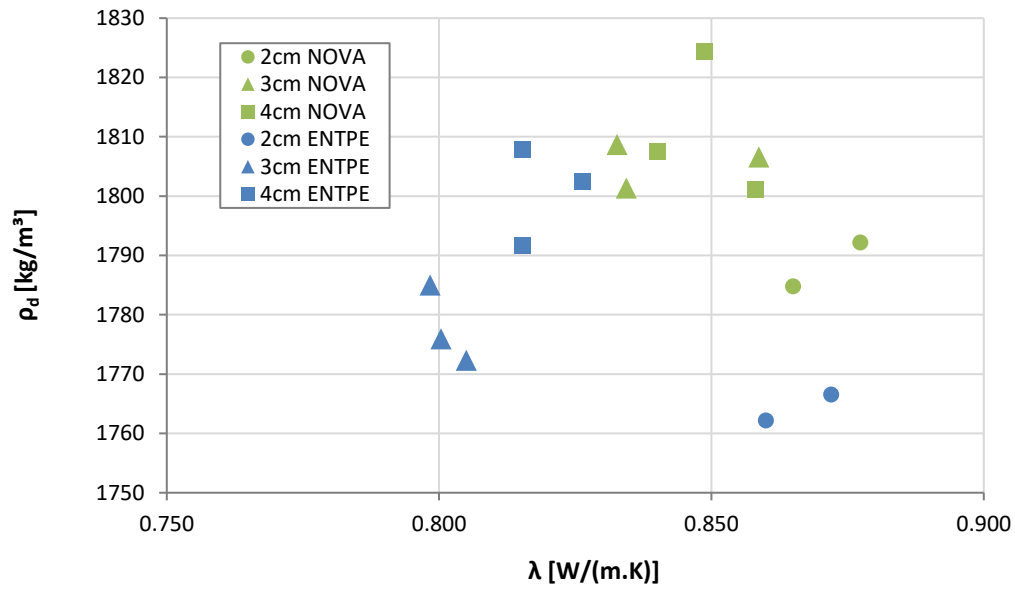


Figure 4.15 - Comparison between the thermal conductivity, obtained by the contact probe method, and dry density of NOVA and ENTPE samples

5. Assessment of the hygrothermal characteristics

The following Chapter presents the results and discussion of the tests used for the assessment of the hygrothermal of the compacted earth under study. In a first stage, the results obtained from the procedures tested for the determination of the water vapour permeability are presented followed by the results of the drying experiments, namely by those obtained by the sorption isotherms and the cycles of drying and wetting.

5.1. Water vapour permeability

As explained in Chapter 3 (see section 3.2.4), three methods were studied for the determination of the water vapour permeability of earthen materials, including the wet cup performed in plastic boxes, climatic chamber and gloves box. Although all of these procedures were tested in the LTDS at ENTPE, only the method using the climatic chamber was performed at the materials laboratory of the DEC at NOVA, mainly due to materials limitations, concerning the salts used for the aqueous saturated solutions.

Samples manufactured at both laboratories were tested thus comparing the difference of results within the same method. Nevertheless, the same NOVA samples were tested at both laboratories, whereas the ENTPE samples tested were not the same.

5.1.1. Plastic boxes

The first procedure used to assess the most accurate and repeatable method for the determination of the water vapour permeability, consisted in performing the wet cup test in plastic boxes equilibrated with saturated salt solutions. The collected data from this experimental test were plotted in Figure 5.1 and 5.2, for NOVA and ENTPE samples, respectively, thus representing the mass variation during the test over time. The 4 cm thickness samples showed a lower mass variation over time, opposing the 2 cm thick samples that showed a much higher mass variation during the test, as regards NOVA and ENTPE samples. These two types of samples showed the same behaviour, meaning mass variations over time in the same range of values with no significant differences, thus being considered together henceforth. It can clearly be seen for all that constant mass variation was reached within four days and afterwards it remains in the permanent stage.

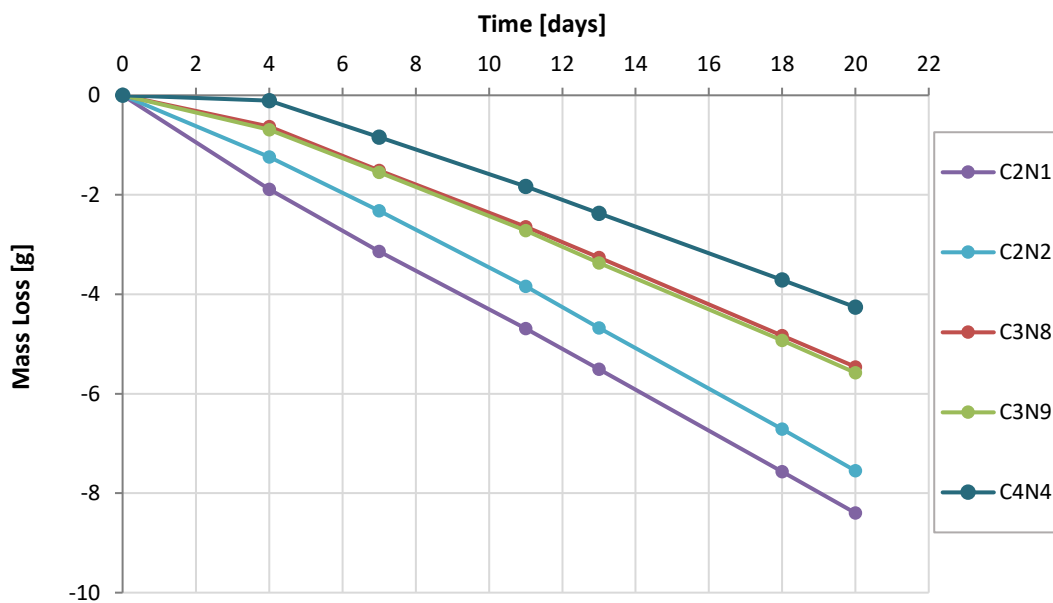


Figure 5.1 – Mass variation during the wet cup test performed in plastic boxes for NOVA samples

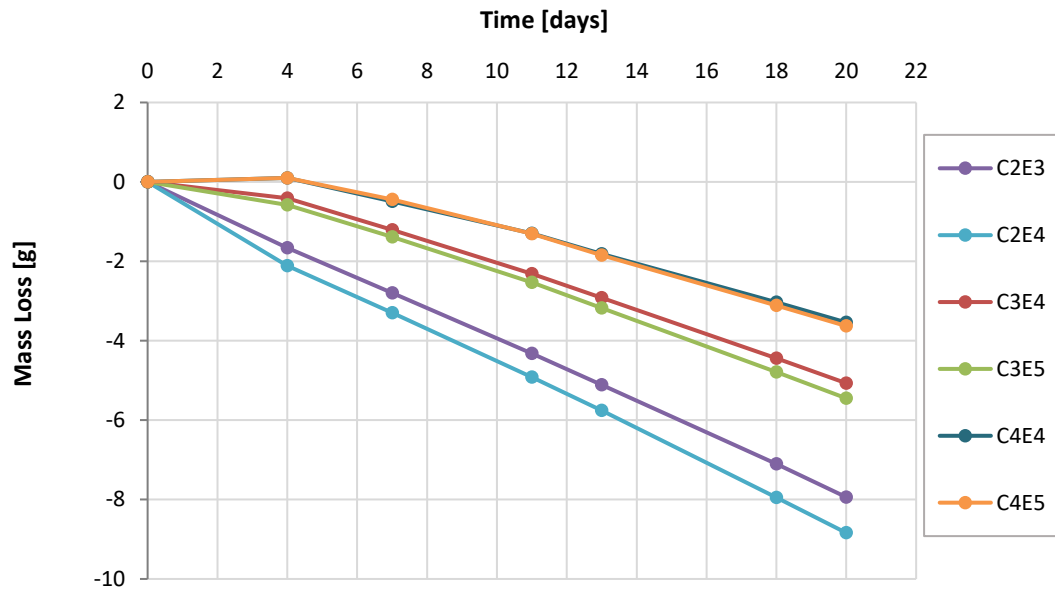


Figure 5.2 – Mass variation during the wet cup test performed in plastic boxes for ENTPE samples

The analysis and calculations of the experimental data collected were done, according to the standard EN ISO 12572 (CEN 2001) as mentioned in section 3.2.4 of Chapter 3, and its results are presented in Table 5.1.

Table 5.1 – Average values of water vapour permeability and water vapour resistance factor for NOVA and ENTPE samples obtained by the wet cup test performed in plastic boxes

Samples	Thickness [cm]	δ_p [kg/(s.m.Pa)]		μ [-]	
		Average	Standard deviation	Average	Standard deviation
NOVA	2	1.56E-11	4.05E-13	12.66	0.33
	3	1.78E-11	7.50E-13	11.09	0.47
	4	1.99E-11	-	9.91	-
ENTPE	2	1.58E-11	1.35E-12	12.48	1.06
	3	1.77E-11	1.19E-12	11.17	0.75
	4	1.86E-11	1.14E-12	10.59	0.65

Comparing the samples manufactured at different laboratories, it can be seen that those results are very similar, valid for the three thickness. On the contrary, when comparing samples of different thickness within the same manufacture laboratory, significant variations are observed. The 2 cm thickness samples showed higher values concerning the water vapour resistance factor, whereas the samples of 3 and 4 cm thick showed the middle and lower results, respectively. This clear tendency can be observed either for NOVA and ENTPE samples. The water resistance factor is an intrinsic characteristic of the material and since the same material is being tested, these differences must be explained. It can be directly affected by phenomena such as the difference in vapour pressures occurring at the surface of the material and within the inside and outside of the cup.

The results presented above are the values originated from the calculations without taking into account those phenomena. As a result, two types of corrections are needed to be done, to take into consideration the surface transfer resistances.

The first correction to be made, proposed by the standard EN ISO 12572 (CEN 2001), concerns the resistance of the air layer existent between the sample and the salt solution. With this correction, this resistance is taken into account, thus assuming that the vapour flow within the cup is only resultant by diffusion phenomena and not by convection. As implicit in Chapter 3 (section 3.2.4), this correction is referred in the present work as “ISO correction”. This correction is recommended for the cases in which the water vapour diffusion-equivalent air layer thickness is inferior to 0.2m, following equations 30 and 31 of Chapter 3. Therefore, the correction was applied and the results are presented in Table 5.2. The average corrected values are lower than the original values, and also reducing the difference of results for the three thicknesses within samples manufactured at the same laboratory. Nevertheless, this difference of results after the ISO correction is still significative, valid for both types of samples. For this reason, it is perfectly understandable that another correction is needed.

Table 5.2 – Average values of water vapour permeability and water vapour resistance factor for NOVA and ENTPE samples obtained by the wet cup test performed in plastic boxes after the ISO correction

Samples	Thickness [cm]	δ_p^{ISO} [kg/(s.m.Pa)]		μ^{ISO} [-]	
		Average	Standard deviation	Average	Standard deviation
NOVA	2	1.69E-11	4.78E-13	11.66	0.33
	3	1.89E-11	8.49E-13	10.42	0.47
	4	2.09E-11	-	9.41	-
ENTPE	2	1.72E-11	1.59E-12	11.48	1.06
	3	1.88E-11	1.34E-12	10.50	0.75
	4	1.96E-11	1.25E-12	10.09	0.65

Neither the water vapour permeability calculation or the correction proposed in the standard EN ISO 12752 (CEN 2001) take into account the dependency on the sample thickness. As somehow expected, and shown by Feng et al. (2015), the resistance of the surface of the material has an impact on the ratio of resistance. McGregor et al. (2017) proposes a correction, taking into consideration the surface film resistance to vapour flow; whereas the convective conditions at the surface of porous samples have a great influence on the measurement of water vapour permeability. Therefore, the surface film resistance needs to be considered, at both external surfaces of the sample tested (i.e. inside and outside the cup).

For the calculation of the water vapour permeability and water vapour resistance following the recommended in EN ISO 12752 (CEN 2001), it is considered that the material is exposed to the vapour pressure gradient (Δp_v), resultant by the chosen internal and external conditions (i.e. Δp_{v1} and Δp_{v2}). However, the material is subjected to a different vapour pressure gradient, the real one (Δp_v^*), which is stemmed by the real partial vapour pressure at the exposed surfaces of the material, p_{v1}^* and p_{v2}^* . This can be better understood by Figure 5.3 which represents the layout of the wet cup process, where g is the density of water vapour flow rate, β the apparent vapour surface transfer coefficient, d the samples thickness, d_a the air layer thickness and A the exposed surface. All the calculations within this correction are presented in Appendix D. The correction is thus applied following equation 32 which gives the water vapour permeability corrected by the β correction:

$$\delta_p^\beta = \frac{d}{\frac{s \cdot \Delta P_v}{G} - \left(\frac{d_a}{\delta_a} + \frac{1}{\beta} \right)} \quad (322)$$

Concerning the β value two approaches are possible, its determination through the results obtained by the test or to assume one of the several values existent in the literature. As it is known, the main focus of this study is to evaluate the best procedure to assess hygrothermal properties of earth, such as the water vapour permeability. For that reason, a detailed results analysis is fundamental, thus the surface film resistance was estimated following the method described by McGregor et al., (2017).

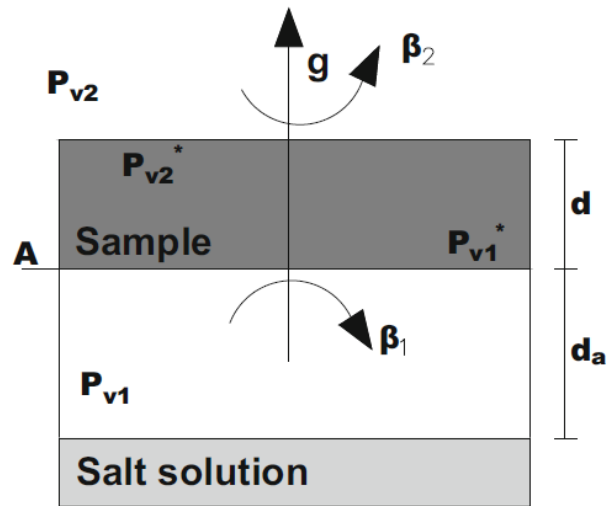


Figure 5.3 – Layout of the process during the wet cup test (McGregor et al., 2017)

Firstly, it is plotted, in function of the material thickness, the ratio of material thickness over the water vapour permeability previously obtained by the ISO correction – see Figure 5.4. The intercept of this linear regression gives the value of the surface film resistance, Z^S , whereas its inverse gives the surface transfer coefficient. The results of the surface transfer coefficient for the wet cup test performed in plastic boxes obtained by the method above described are presented in Table 5.3. Hence, the corrected water vapour permeability and water vapour resistance factor values obtained through the beta correction are shown in Table 5.4.

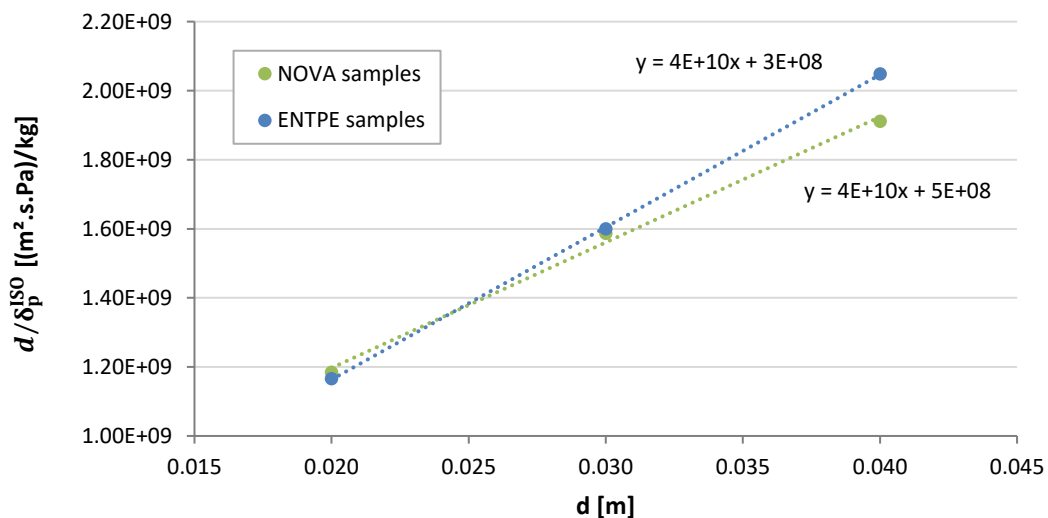


Figure 5.4 – d/δ_p^{ISO} as a function for the wet cup test performed in plastic boxes of NOVA and ENTPE samples

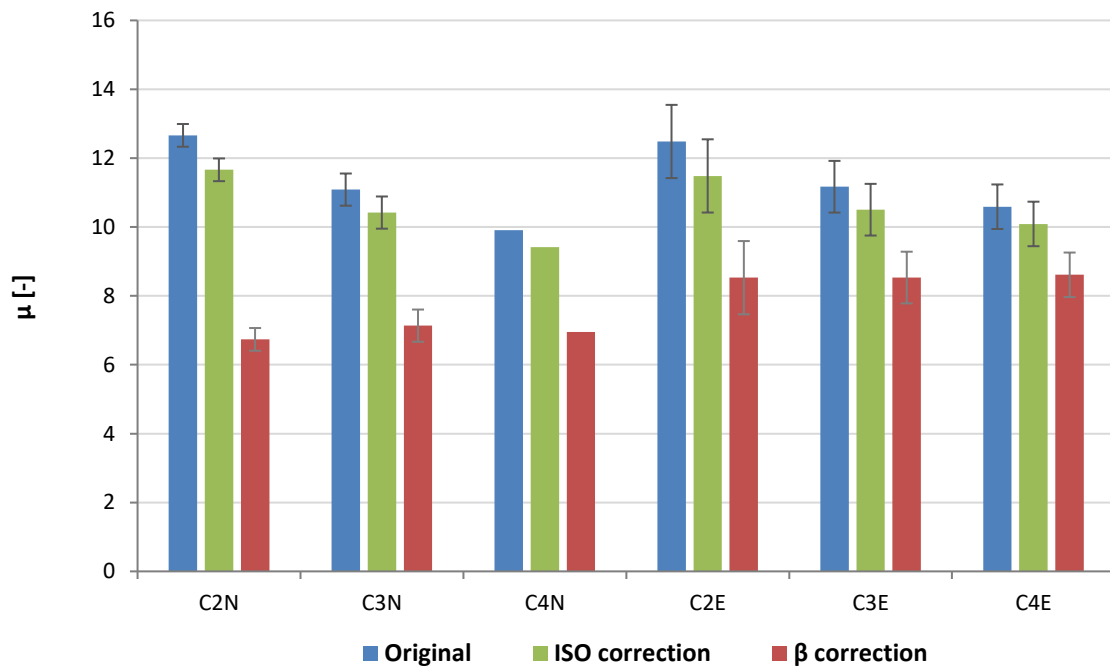
Table 5.3 – Surface vapour transfer resistance and apparent vapour surface transfer coefficient obtained according to the method proposed by McGregor et al. (2017) for the wet cup test performed in plastic boxes

Samples	Z^S	β
NOVA	5.00E+08	2.00E-09
ENTPE	3.00E+08	3.33E-09

Table 5.4 – Average values of water vapour permeability and water vapour resistance factor for NOVA and ENTPE samples obtained by the wet cup test performed in plastic boxes after the beta correction

Samples	Thickness [cm]	δ_p^β [kg/(s.m.Pa)]		μ^β [-]	
		Average	Standard deviation	Average	Standard deviation
NOVA	2	6.93E-11	1.43E-12	6.74	0.33
	3	2.77E-11	1.18E-12	7.14	0.47
	4	2.83E-11	-	6.95	-
ENTPE	2	2.33E-11	2.90E-12	8.53	1.06
	3	2.32E-11	2.04E-12	8.53	0.75
	4	2.29E-11	1.72E-12	8.61	0.65

By analysing Table 5.3, it can be seen some differences in the β values for samples manufactured at different laboratories. This can be due to the fact that the samples tested showed some differences in the rugosity of the surfaces, thus possibly influencing the surface vapour transfer resistance and consequently the β value. Also, only one sample of 4 cm thickness from NOVA was tested, not being representative enough. After the β correction, the water vapour resistance factor became lower for the three thickness, either for samples of NOVA and ENTPE. It is also important to notice that the water vapour resistance values are much more similar between samples of different thicknesses. Therefore, it can be seen the lower influence of the thickness in these results. This proximity of values is more significative for the ENTPE samples, which presented almost no variation between them. This can be better seen in Figure 5.5, which presents the original and corrected values of the water vapour resistance obtained by the wet cup test performed in plastic boxes.

**Figure 5.5** – Comparison between the water vapour resistance factor results obtained by the wet cup test performed in plastic boxes for NOVA and ENTPE samples

5.1.2. Climatic chamber

Once finished the wet cup performed in plastic boxes, the samples were immediately placed in the climatic chamber, without a period for conditioning. This can be explained by the fact that the samples were already in the permanent state, thus the period for the equilibrium with the exterior conditions (i.e. inside the climatic chamber) it should be faster. Also, in order to ensure that the aqueous salt solutions inside the cups remained saturated, preventing to remove the samples from the cups which may damage them.

The same methodology was applied for the data collected from the test performed inside the climatic chamber. In figure 5.6 it can be seen the mass variation during the test for both types of samples; the samples started its permanent state within one day inside the climatic chamber. Although the mass variation is not as linear as the one observed for the test performed inside the plastic boxes, the linear relationship for all samples is within a value of R^2 superior to 0.99. It should be noticed that during the test there was a problem with the fan of the climatic chamber, that is to say that the results obtained should be carefully analysed. However, in order to a better comparison between the three procedures, the results are still presented.

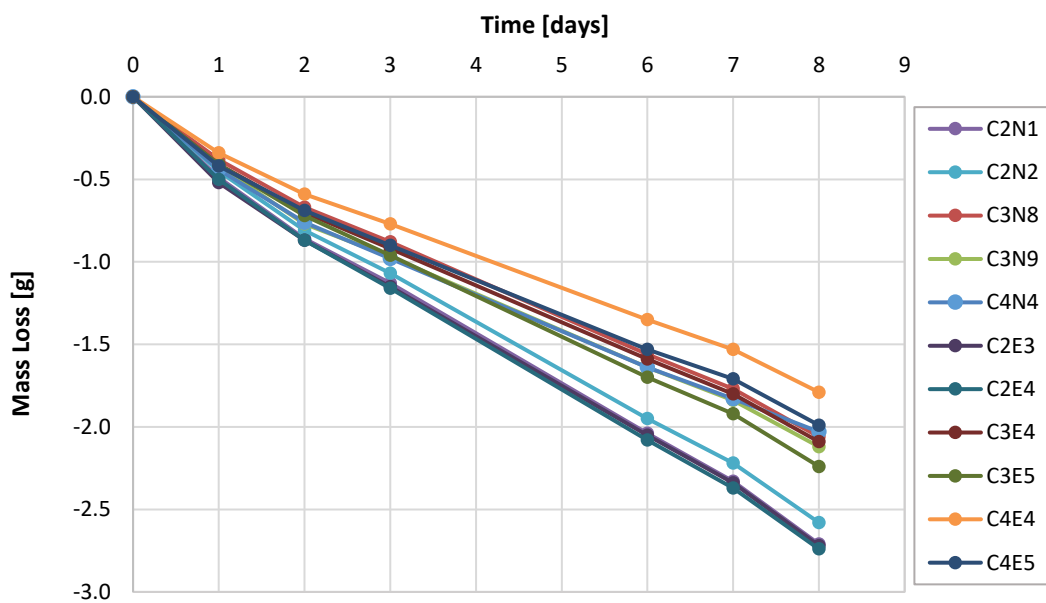


Figure 5.6 – Mass variation during the wet cup test performed in the climatic chamber at ENTPE for NOVA and ENTPE samples

The results of the original calculation and ISO correction for both types of samples are presented in Table 5.5 and 5.6.

Table 5.5 – Average values of water vapour permeability and water vapour resistance factor for NOVA and ENTPE samples obtained by the wet cup test performed in the climatic chamber at ENTPE

Samples	Thickness [cm]	δ_p [kg/(s.m.Pa)]		μ [-]	
		Average	Standard deviation	Average	Standard deviation
NOVA	2	1.07E-11	3.24E-13	18.37	0.56
	3	1.12E-11	2.27E-13	16.22	0.30
	4	1.53E-11	-	12.89	-
ENTPE	2	1.10E-11	1.06E-12	17.91	0.17
	3	1.28E-11	8.13E-13	15.38	0.97
	4	1.47E-11	8.00E-13	13.44	0.73

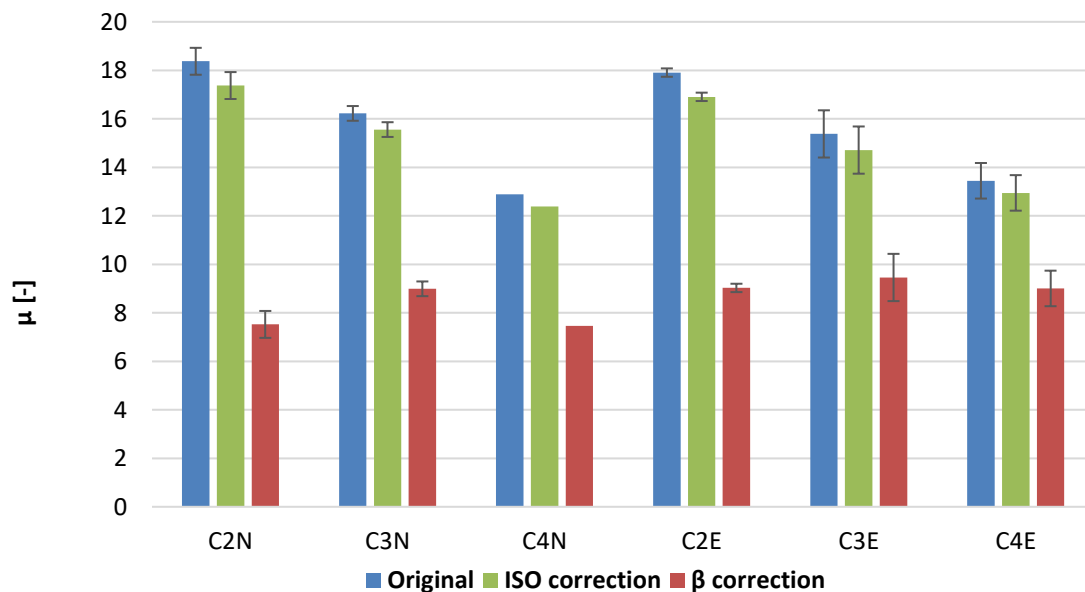
Table 5.6 – Average values of water vapour permeability and water vapour resistance factor for NOVA and ENTPE samples obtained by the wet cup test performed in the climatic chamber at ENTPE after the ISO correction

Samples	Thickness [cm]	δ_p^{ISO} [kg/(s.m.Pa)]		μ^{ISO} [-]	
		Average	Standard deviation	Average	Standard deviation
NOVA	2	1.13E-11	3.62E-13	17.37	0.56
	3	1.27E-11	2.47E-13	15.56	0.30
	4	1.59E-11	-	12.39	-
ENTPE	2	1.17E-11	1.19E-13	16.91	0.17
	3	1.34E-11	8.89E-13	14.71	0.97
	4	1.52E-11	8.63E-13	12.94	0.73

The β values obtained by the method suggested by McGregor et al. (2017) can be seen in Table 5.7. It is observed that these values are very similar between the two types of samples. The Figure containing d/δ_p^{ISO} as a function for the wet cup test performed in the climatic chamber at ENTPE for NOVA and ENTPE samples can be found in Appendix E.2. After the determination of these values, the β correction was applied and the obtained values are presented in Appendix E.2. The comparison between the original and corrected results of the water vapour resistance factor is presented in Figure 5.7; ENTPE samples showed water vapour resistance factor values more similar between its three thicknesses, compared to NOVA samples.

Table 5.7 – Surface vapour transfer resistance and apparent vapour surface transfer coefficient obtained according to the method proposed by McGregor et al. (2017) for the wet cup test performed in the climatic chamber at ENTPE

Samples	Z^s	β
NOVA	1.00E+09	1.00E-09
ENTPE	8.00E+08	1.25E-09

**Figure 5.7** – Comparison between the water vapour resistance factor results obtained by the wet cup test performed in the climatic chamber at ENTPE for NOVA and ENTPE samples

After the wet cup test performed with the three different procedures at ENTPE, the procedure in which the exterior conditions to the cup are maintained by a climatic chamber was repeated at NOVA, as previously explained.

The NOVA samples tested at ENTPE were again tested at NOVA; additionally, ENTPE samples were also tested but not the exact same tested at ENTPE. The samples were placed in a conditioning room at 20 ± 3 °C temperature and 50 ± 5 % relative humidity until constant mass was reached before the test.

In figure 5.8 it is represented the mass variation during the wet cup test performed in the climatic chamber at NOVA. The samples started their permanent stage within two days of test, maintaining it until the end of the test.

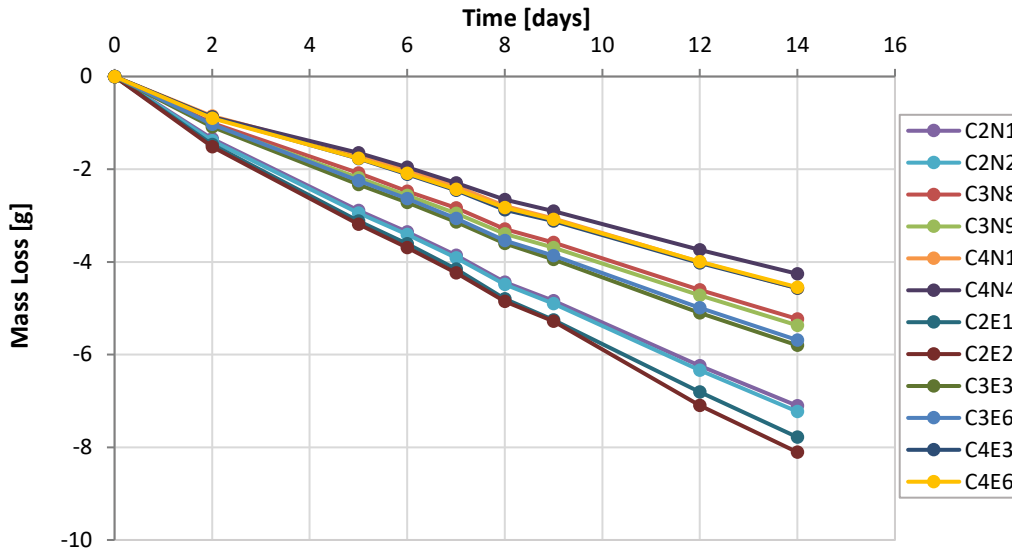


Figure 5.8 – Mass variation during the wet cup test performed in the climatic chamber at NOVA for NOVA and ENTPE samples

The results of the original calculation and ISO correction are presented in Table 5.8 and 5.9, respectively. It is clearly that the water vapour resistance is significantly much lower comparing to the results obtained by the same test performed at ENTPE.

For the determination of the real water vapour resistance factor, the β correction was applied, following the same method explained above. The values of the surface vapour transfer resistance and apparent vapour surface transfer coefficient resistance obtained by it are shown in Table 5.10. Once again, it can be seen a significant difference between these values of samples manufactured at different laboratories, with ENTPE samples presenting a higher value of β . In addition, the original calculation, ISO and β corrections results are presented in Figure 5.9.

Table 5.8 – Average values of water vapour permeability and water vapour resistance factor for NOVA and ENTPE samples obtained by the wet cup test performed in the climatic chamber at NOVA

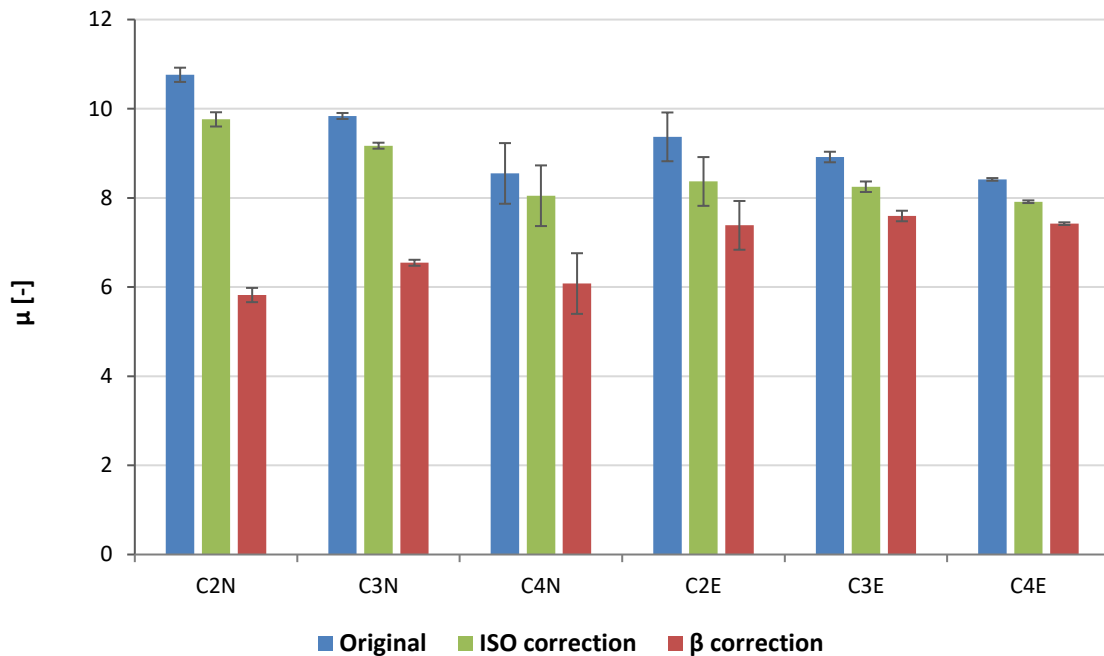
Samples	Thickness [cm]	δ_p [kg/(s.m.Pa)]		μ [-]	
		Average	Standard deviation	Average	Standard deviation
NOVA	2	1.83E-11	2.72E-12	10.76	0.16
	3	2.00E-11	1.36E-13	9.84	0.07
	4	2.13E-11	1.84E-12	8.55	0.68
ENTPE	2	2.11E-11	1.23E-12	9.37	0.55
	3	2.21E-11	2.92E-13	8.92	0.12
	4	2.34E-11	8.36E-14	8.41	0.03

Table 5.9 – Average values of water vapour permeability and water vapour resistance factor for NOVA and ENTPE samples obtained by the wet cup test performed in the climatic chamber at NOVA after the ISO correction

Samples	Thickness [cm]	δ_p^{ISO} [kg/(s.m.Pa)]		μ^{ISO} [-]	
		Average	Standard deviation	Average	Standard deviation
NOVA	2	2.02E-11	3.31E-13	9.76	0.16
	3	2.15E-11	1.57E-13	9.17	0.07
	4	2.46E-11	2.08E-12	8.05	0.68
ENTPE	2	2.36E-11	1.54E-12	8.37	0.55
	3	2.39E-11	3.42E-13	8.25	0.12
	4	2.49E-11	9.45E-14	7.91	0.03

Table 5.10 – Surface vapour transfer resistance and apparent vapour surface transfer coefficient obtained according to the method proposed by McGregor et al. (2017) for the wet cup test performed in the climatic chamber at NOVA

Samples	Z^s	β
NOVA	4.00E+08	2.50E-09
ENTPE	1.00E+08	1.00E-08

**Figure 5.9** – Comparison between the water vapour resistance factor results obtained by the wet cup test performed in the climatic chamber at NOVA for NOVA and ENTPE samples

By contrast with the water resistance factor obtained by the test conducted at ENTPE, the results obtained at NOVA are much lower in a range of 5.82 (0.68) to 6.54 (0.07) and 7.38 (0.55) to 7.59 (0.12) for NOVA and ENTPE samples, respectively. According to Vololonirina & Perrin (2016), the air velocity inside the climatic chamber has a clearly noticeable influence on the measured water resistance factor value. Therefore, keeping in mind that two different climatic chambers were used and that the air velocity inside them it is probably not the same, the difference of results can be due to this. Also, as mentioned, a problem with the fan of the climatic chamber used at ENTPE was recorded, thus affecting the air velocity inside it. It should be also noted that by monitoring the RH inside the chamber through a portable sensor, it was found that in the last three days of the test, the RH measured was not correct, consequently affecting the environmental conditions.

5.1.3. Gloves box

Lastly, the wet cup test was performed in the gloves box at ENTPE, immediately after the ending of the test in the climatic chamber. In Figure 5.10 it is shown the evolution of the mass variation over time during the period of the test. It can clearly be seen for all samples that constant mass variation was reached within the first days and afterwards it remains in the permanent stage.

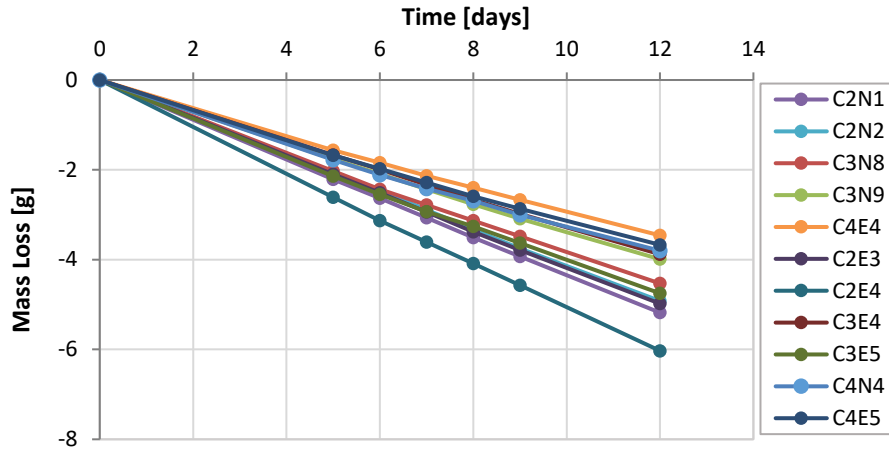


Figure 5.10 – Mass variation during the wet cup test performed in the gloves box for NOVA and ENTPE samples

The same methodology used for the previously two procedures was used for the last method. The results of the original calculation and ISO correction can be found in Table 5.11 and Table 5.12, respectively. As mentioned, for the determination of the real value of water vapour resistance factor the β correction was applied, hence, the supporting values of this correction are presented in Table 5.13.

Table 5.11 – Average values of water vapour permeability and water vapour resistance factor for NOVA and ENTPE samples obtained by the wet cup test performed in the gloves box

Samples	Thickness [cm]	δ_p [kg/(s.m.Pa)]		μ [-]	
		Average	Standard deviation	Average	Standard deviation
NOVA	2	1.46E-11	3.63E-13	13.54	0.34
	3	1.74E-11	1.27E-12	11.33	0.83
	4	1.96E-11	-	10.05	-
ENTPE	2	1.56E-11	1.79E-12	12.70	1.46
	3	1.78E-11	1.93E-12	11.14	1.21
	4	1.92E-11	5.92E-13	10.27	0.32

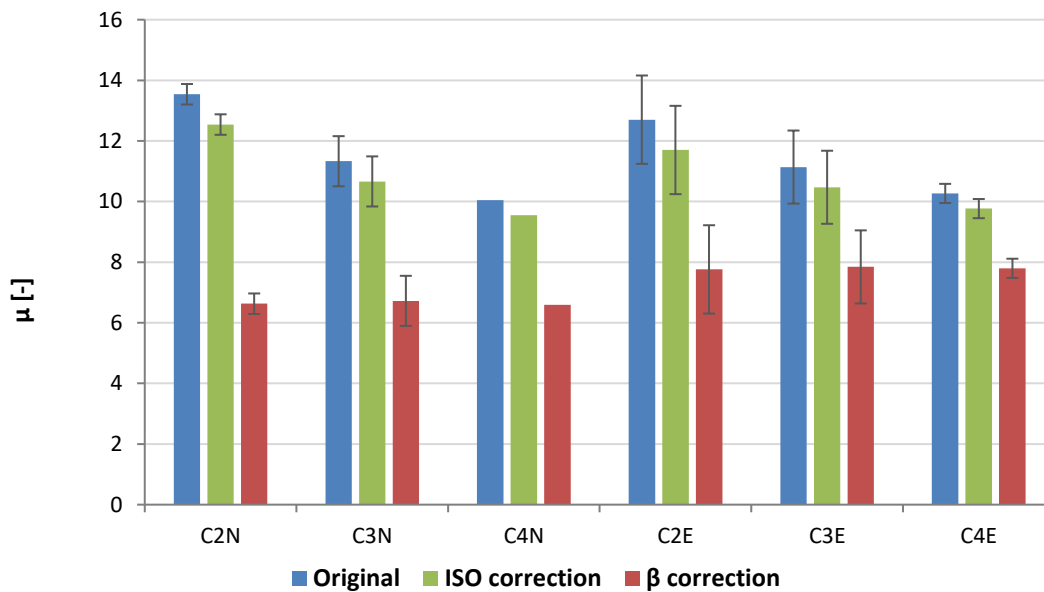
Table 5.12 – Average values of water vapour permeability and water vapour resistance factor for NOVA and ENTPE samples obtained by the wet cup test performed in the gloves box after the ISO correction

Samples	Thickness [cm]	δ_p^{ISO} [kg/(s.m.Pa)]		μ^{ISO} [-]	
		Average	Standard deviation	Average	Standard deviation
NOVA	2	1.57E-11	4.24E-13	12.54	0.34
	3	1.85E-11	1.44E-12	10.66	0.83
	4	2.06E-11	-	9.55	-
ENTPE	2	1.70E-11	2.11E-12	11.70	1.46
	3	1.89E-11	2.18E-12	10.47	1.21
	4	2.02E-11	6.54E-13	9.77	0.32

Table 5.13 – Surface vapour transfer resistance and apparent vapour surface transfer coefficient obtained according to the method proposed by McGregor et al. (2017) for the wet cup test performed in the gloves box

Samples	Z^s	β
NOVA	6.00E+08	1.67E-09
ENTPE	4.00E+08	2.50E-09

Figure 5.11 represents the comparison between the original and corrected values for the water vapour resistance for the wet cup performed in the gloves box. By analysing it, one can see that although with small differences between the values of the two types of samples, when comparing samples of different thicknesses within the same laboratory of fabrication, the values are very similar, with less influence of the samples thickness.

**Figure 5.11** – Comparison between the water vapour resistance factor results obtained by the wet cup test performed in the gloves box for NOVA and ENTPE samples

5.1.4. Comparison between the three procedures

In order to analyse which method of those tested can be the most accurate and repeatable for the determination of the water vapour permeability and therefore the water vapour resistance factor, a comparison is made in the current section. To some extent, this comparison is made either for the real water vapour resistance factor stemmed by the β correction but also for the previous corrected values obtained by the ISO correction, thus having a better understanding of the differences within the three procedures used.

It is clearly visible that the wet cup performed in the climatic chamber gives substantially higher values of water vapour resistance after ISO correction, for the three thickness of both types of samples, but if comparing NOVA and ENTPE samples they are very consistent – see Figure 5.12. As far as the differences between the three thicknesses are concerned, the β correction should be applied in order to obtain the real values of water vapour resistance factor, as previously mentioned. As a result, Figure 5.13 presents the comparison of water vapour resistance stemmed by the three methods of NOVA and ENTPE samples after this correction.

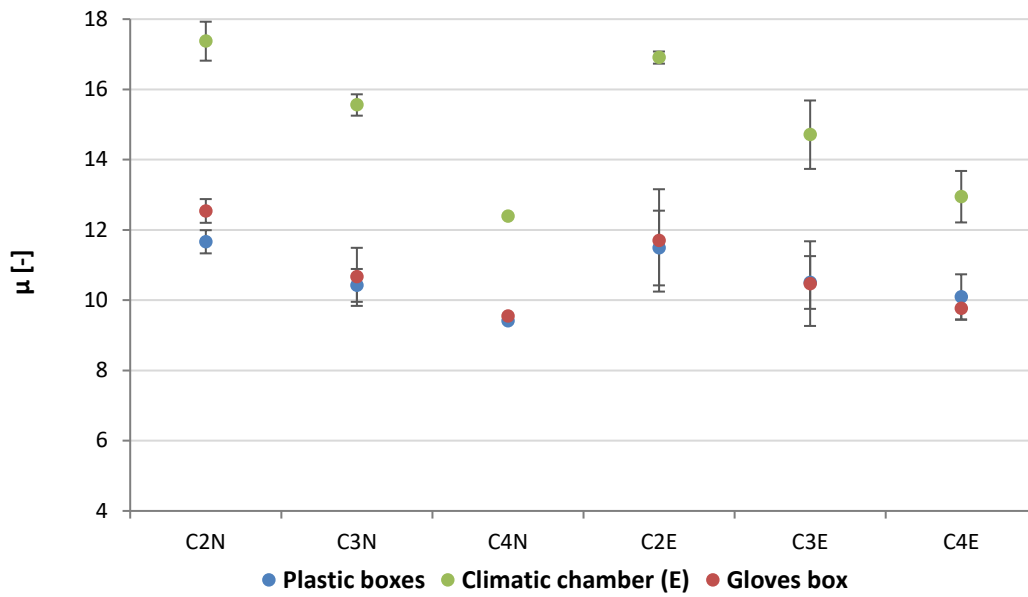


Figure 5.12 – Comparison between the water vapour resistance factor results obtained by the three procedures of the wet cup test performed at ENTPE after the ISO correction

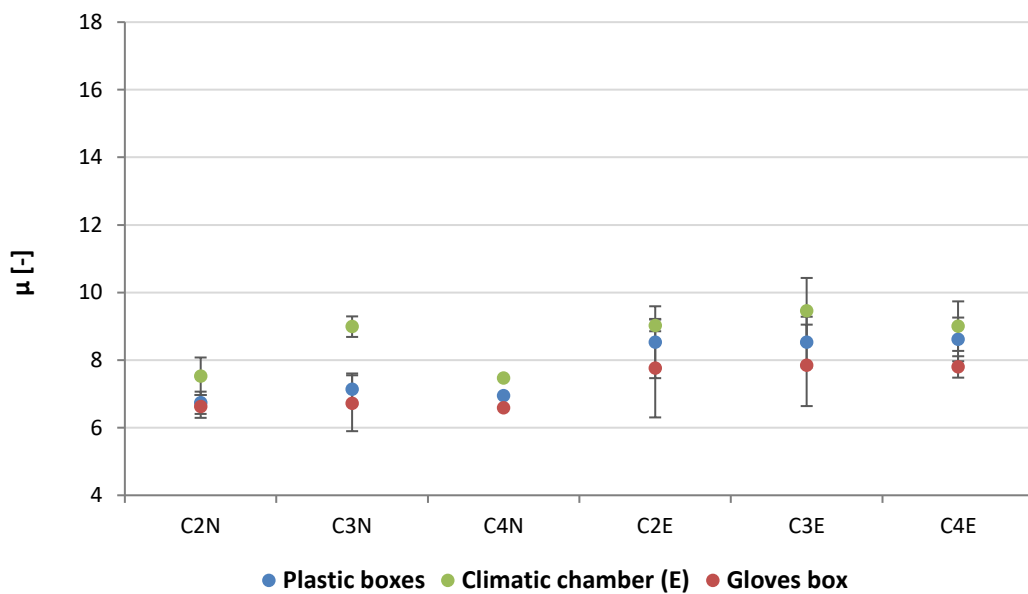


Figure 5.13 – Comparison between the water vapour resistance factor results obtained by the three procedures of the wet cup performed at ENTPE after the β correction

By analysing Figure 5.13, it can be seen that after β correction, the differences of water vapour resistance factor between those obtained by the wet cup carried out in the climatic chamber and the two other methods becomes significantly lower. However, the corrected results lessen the almost non existing divergence of values between the plastic boxes and gloves box procedures.

Regardless of the fundamental importance of comparing the water vapour resistance factor achieved by different test procedures, β values should also be the subject of the comparison study. By comparing the β values between NOVA and ENTPE samples, these showed a very significant difference, except for the climatic chamber method, which presents a much smaller dissimilarity – see Figure 5.14.

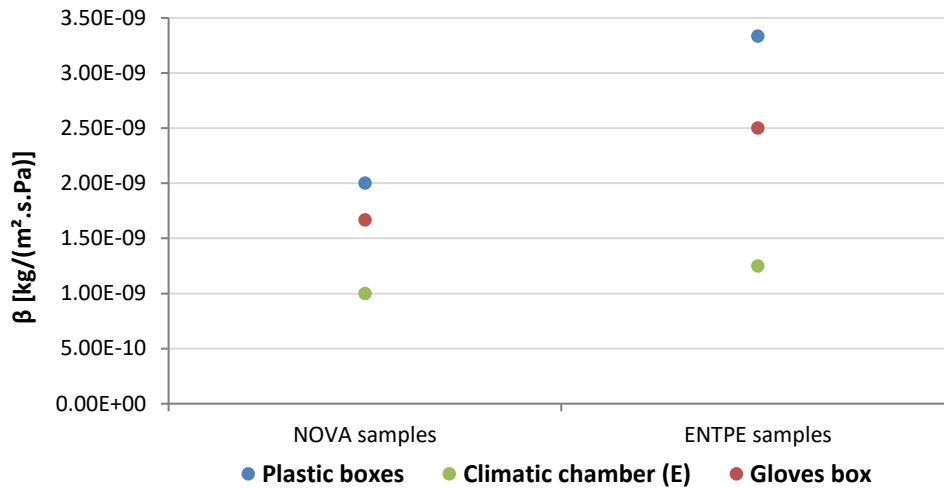


Figure 5.14 – Vapour surface transfer coefficient determined according to the method proposed by McGregor et al. (2017) for the three procedures of the wet cup test

It is noticeable that inside the plastic and gloves boxes used, without the use of forced convection equipment, the air velocity inside them is greatly reduced; opposing the apparatus inside the climate chamber, which through a fan generates considerable higher air velocities. As found by Vololonirina & Perrin (2016) and stated in section 5.1.2, the air velocity is an influence factor to the measurement of water resistance factor and also suggest that the surface transfer resistance, Z^s , should decrease with the air velocity thus, increasing the value of the surface transfer coefficient. Altogether, it was expected to achieved a variation within the water resistance factor measured by different procedures with different conditions concerning the air velocity. However, the results obtained for β are contradictory to those expected; although a variation is observed, the climatic chamber method gives lower values. This can be explained by the variations of the RH level recorded inside the chamber and also by the malfunction of the chamber's fan. All things considered, this test presented considerable limitations and it was performed once again at NOVA.

The vapour resistance factor measured by the wet cup test conducted following the climatic chamber procedure, either at ENTPE (E) and NOVA (N), after ISO and β correction are presented in Figure 5.15. A great divergence of values can be observed, the test performed at ENTPE gives higher values, with a great variation between results of the two corrections. By contrast, NOVA results, for both types of samples, are much lower with small differences between the corrected values.

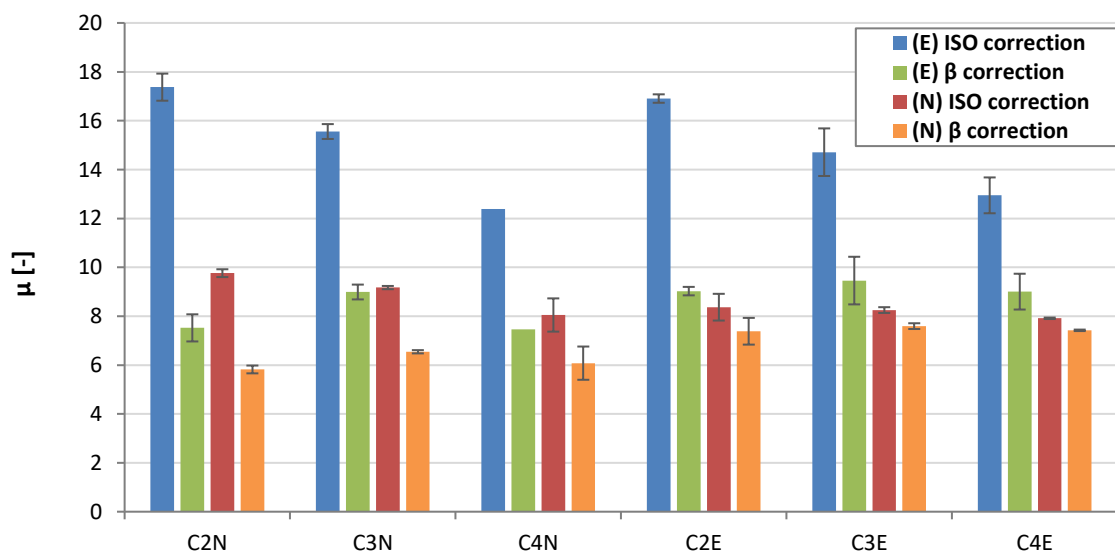


Figure 5.15 – Comparison between the water vapour resistance factor obtained by the climatic chamber procedure carried out at ENTPE and NOVA after ISO and β correction

A comparison between the plastic boxes and gloves box procedures performed at ENTPE and the climatic chamber procedure carried out at NOVA is presented in Figures 5.16 and 5.17, concerning the corrected results with the ISO correction and after β correction, respectively. By contrast to the climatic chamber approach carried out at ENTPE, the results obtained by the same approach but performed at NOVA present lower values of water resistance factor than the other two approaches, valid for both corrections. Equally to the obtained results with the ENTPE climatic chamber, it can be observed that after the β correction, the dissimilarity between this method, performed at NOVA, and the others, decreases whereas between the plastic boxes and gloves box has the opposite outcome.

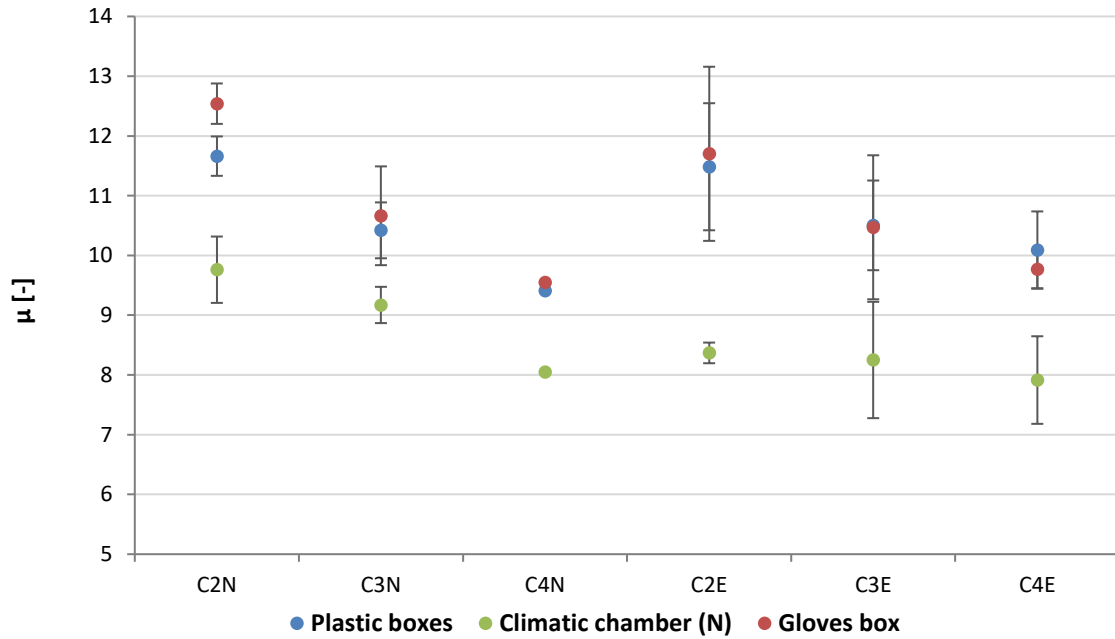


Figure 5.16 – Comparison between the water vapour resistance factor results obtained by the three procedures of the wet cup test, with the climatic chamber procedure performed at NOVA after the ISO correction

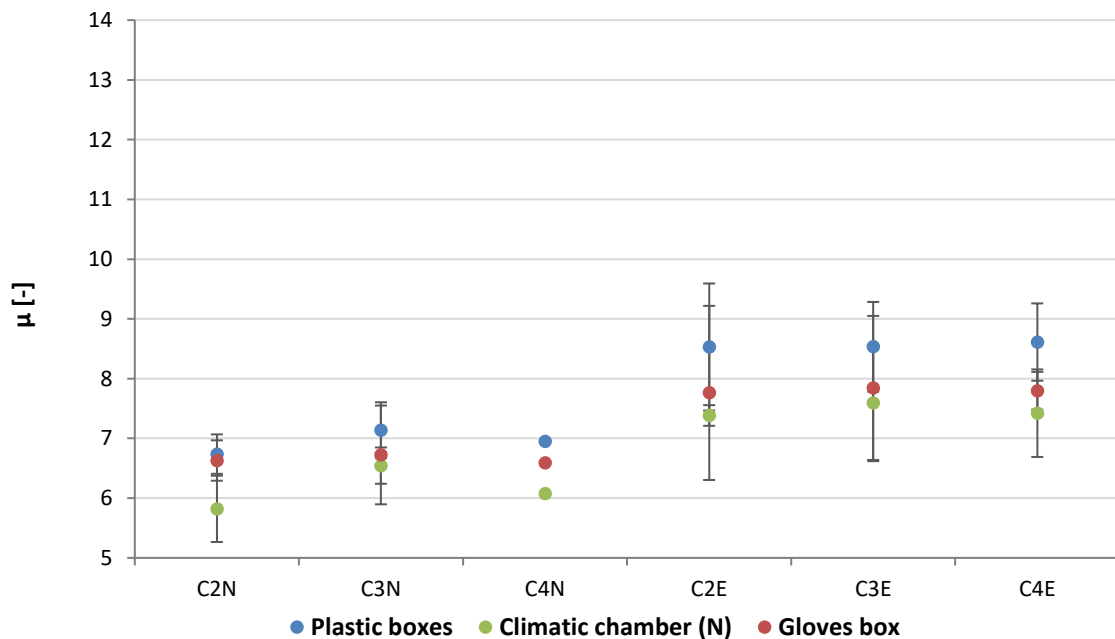


Figure 5.17 – Comparison between the water vapour resistance factor results obtained by the three procedures of the wet cup test, with the climatic chamber procedure performed at NOVA after the β correction

As well as expected, the climatic chamber approach gives higher values of vapour surface transfer coefficients than the alternative approaches – see Figure 5.18. It is mainly owing to the air velocity inside the climatic chamber which is supposed to be substantially superior than within the other methods. Nevertheless, a divergence of values is seen; for ENTPE samples, this vapour surface coefficient, stemmed by the climatic chamber method, is much higher by comparison to the plastic boxes and gloves box methods.

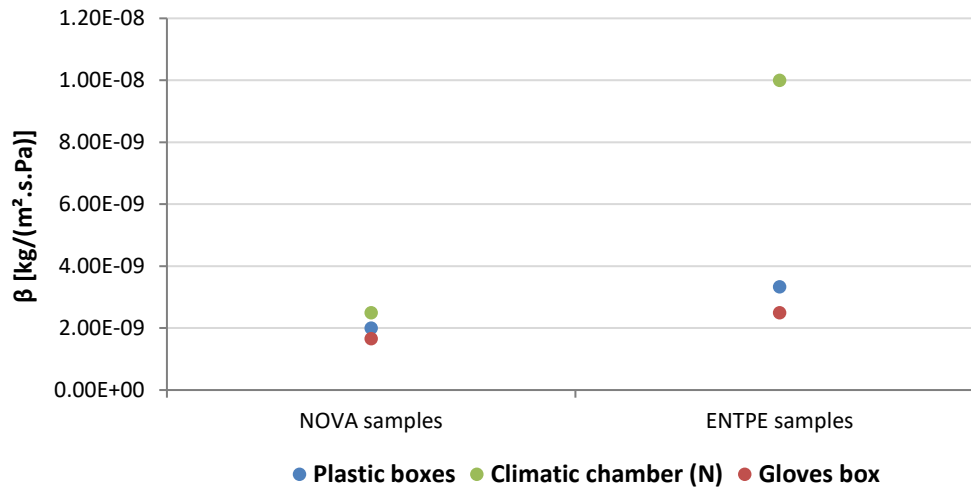


Figure 5.18 – Vapour surface transfer coefficient determined according to the method proposed by McGregor et al. (2017) for the three procedures of the wet cup test the three procedures of the wet cup test, with the climatic chamber procedure performed at NOVA

Additionally, Feng et al. (2015) conducted a study to evaluate the influence of the pre-conditioning method on the measurements of water vapour permeability; it was found that for highly hygroscopic materials, the pre-conditioning has a strong impact for the wet cup measurements. Additionally, as referred, the three wet cup tests that took place at ENTPE were carried out in a row, without a period for conditioning between test, thus this may lead to an influence on the values obtained.

In Table 5.14 the variation within each of the three procedures under study is presented. By its analysis, it can be clearly seen that for both types of samples the tendency is similar; the lowest value of variation for NOVA samples corresponds to the lowest value of variation for ENTPE samples, stemmed by the gloves box method, and so on. However, the variations found between the three methods is much lower for ENTPE samples, contrasting with those of NOVA samples.

Table 5.14 – Average values of the water vapour resistance factor obtained by the wet cup test performed with the three procedures after the β correction and its variation

Samples	μ^β Plastic boxes		μ^β Climatic chamber (N)		μ^β Gloves box	
	Average	Variation [%]	Average	Variation [%]	Average	Variation [%]
C2N	6.74	2.88	5.82	5.96	6.63	1.02
C3N	7.14		6.54		6.72	
C4N	6.95		6.08		6.59	
C2E	8.53	0.55	7.38	1.50	7.76	0.54
C3E	8.53		7.59		7.84	
C4E	8.61		7.42		7.80	

It is of fundamental importance to note that the results obtained, regardless the procedure used, are within the expected values for water vapour resistance factor of earthen materials; such as example, those found by: Cagnon et al. (2014), between 3 and 7 for extruded earth bricks; McGregor. (2014) for clay plasters and CEB with results in the order of 9 to 13 and 6 to 13, respectively; Faria et al. (2015), around 8 for earth plasters; or Liuzzi et al. (2013), with values around 8.8 to 11.1 for clay composites.

5.2. Drying experiments

As mentioned in Chapter 3, sorption isotherms and cycles of drying and wetting were performed in order to fulfil the assessment of the most accurate test protocol for the determination of the dry mass of earthen materials. Its results are presented and discussed in the current section.

5.2.1. Sorption isotherms

The sorption isotherms were determined by the desiccator approach which uses saturated salt solutions to obtain different RH levels, and using equation 15 of Chapter 2 – see section 3.2.5. Three different oven-dry temperatures were used, 50, 70 and 105°C; the dry mass of each tested specimen was obtained by placing each of these in each dry-oven temperature until constant mass was reached. Afterwards, three specimens of each oven-dry temperature were placed in the first level of RH and so on. Two cycles of sorption and desorption were performed; the first cycle consisted in placing the samples in levels of 23%, 59% and 85% of RH whereas the second in levels of 43%, 75% and 97%. Therefore, the determination of the sorption isotherms was obtained faster.

Once two cycles were used in order to achieve a single curve of sorption and other of desorption for each oven-dry temperature, the GAB model was used to combined them, following the procedure described by Bui et al. (2017). Also, through the two cycles only one point was obtained for the RH level of 85%; it is known that for earthen materials a hysteresis between the sorption and desorption curves exists – see section 2.3.1.

The sorption isotherms for each oven-drying temperature are represented in Figure 5.19, with dashed desorption curves for a better understanding of its representation. Despite the clear difference between the three isotherms curves, with higher water contents for oven-dry at 105°C, the same tendency is observed. At this point, the results are the expected with a “S” shape sorption and desorption curves – see section 2.3.

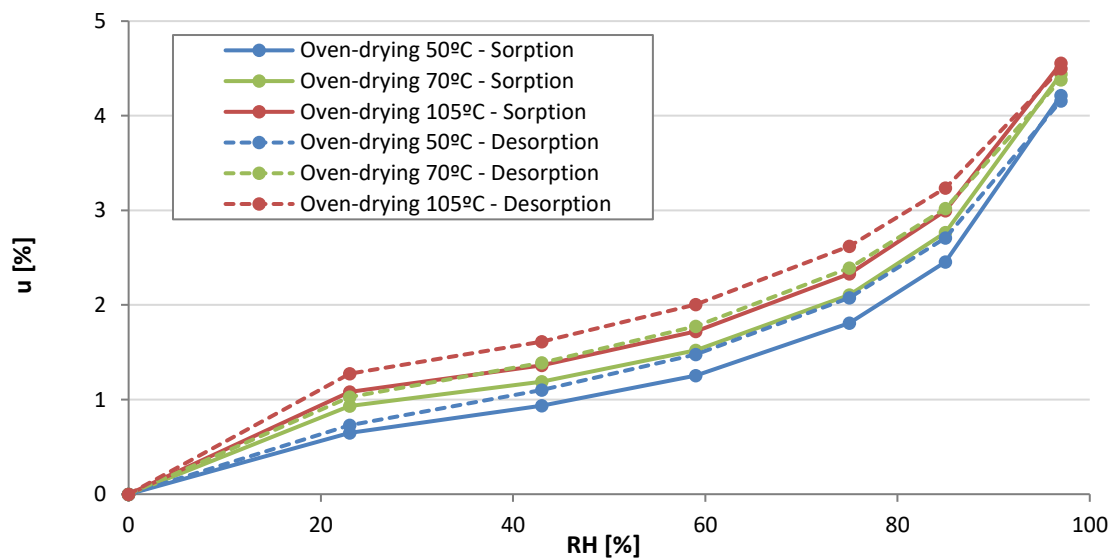


Figure 5.19 – Oven-drying temperature influence on the sorption isotherms

The sorption isotherms curves obtained (Figure 5.19) are within the range of maximum water contents found in the literature for earthen materials. Liuzzi et al. (2012) measured values of maximum water contents between 3.5% and 5% for several clay mixes. Additionally, by testing earth bricks and different types of compressed earth blocks using the DVS method, Cagnon et al. (2014) obtained results in the range of 4.5% and 6% and McGregor (2014) recorded values between 3% and 7%. Also, the hysteresis found in these curves is the expected for earth-based materials (i.e. small hysteresis), while for other type of material it can be significantly higher, as shown by Hansen (1986) who obtained and gathered sorption and desorption curves for several materials.

For instance, concerning expanded polystyrene and autoclaved aerated concrete, which presented maximum water contents of about 5 - 8% and 15 - 20%, the hysteresis observed is considerable higher with a difference between the maximum water content of the sorption curve and desorption curve of around 3% and 6%, respectively (Hansen, 1986).

In order to evaluate the effect of the three different oven-drying temperatures, six smaller specimens were dried at each temperature in January of 2019 and placed in a conditioning room with 20 ± 3 °C temperature and 50 ± 5 % relative humidity. Later on, in March of 2019, these specimens were tested for the sorption isotherm test without further drying. Therefore, the m_0 used for the determination of the water content was the equilibrium mass of the specimens with the conditioning room environment. The results stemmed by this process are represented in Figure 5.20. It can be seen that the influence of the three different oven-drying temperatures is lower after a long enough period of time.

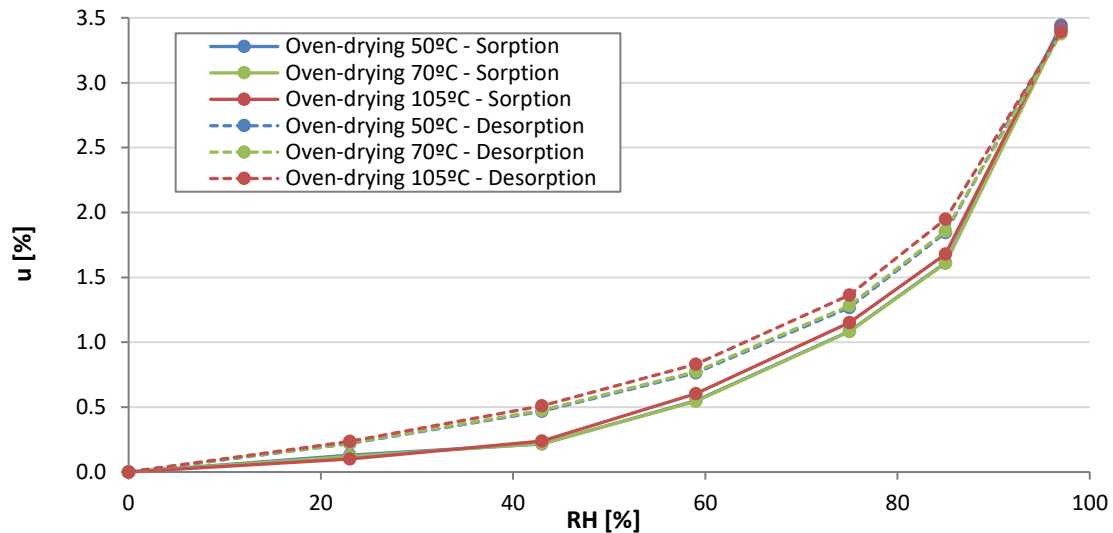


Figure 5.20 – Oven-drying temperatures and pre-conditioning influence on the sorption isotherms

A comparison with the sorption isotherms obtained by the DVS method for the same material is shown in Figure 5.21. By analysing it, it is possible to observe the same tendency between the sorption curves obtained by the desiccator method followed by the GAB model and the DVS method. This last curve is found to be between the sorption curves of those obtained by oven-drying temperatures of 50 and 70°C; in the DVS method, the material is dried by a dry air close to 0% of RH before the different steps of RH.

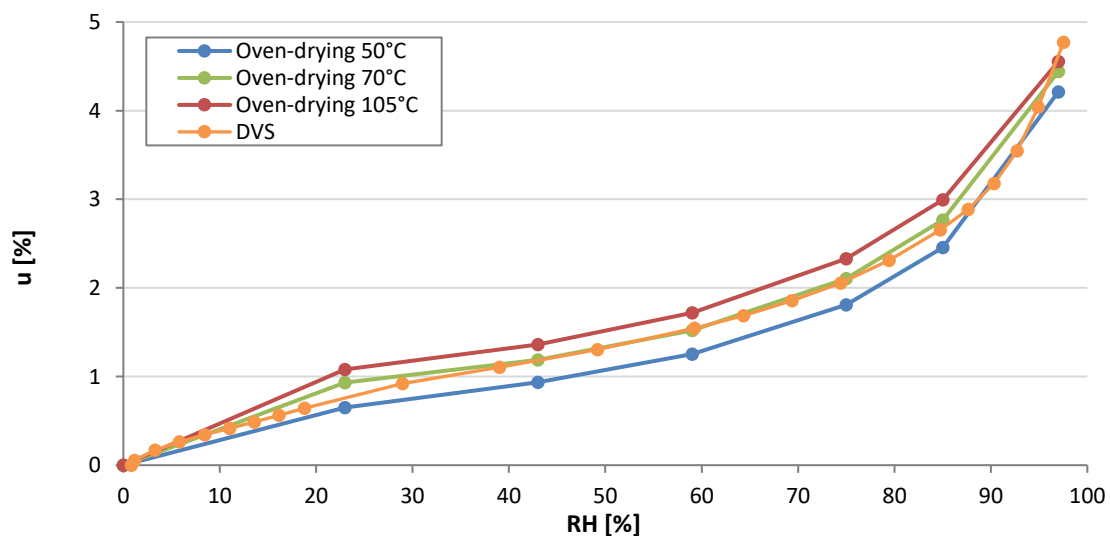


Figure 5.21 – Comparison between the sorption isotherms obtained by the desiccator method for the three oven-drying temperatures and by the DVS method

5.2.2. Cycles of drying-wetting

Four different dry-methods, two oven-dry temperatures and two RH levels, were studied through cycles of drying and wetting in order to compare its reproducibility and repeatability.

Samples of similar dimensions to those tested in sorption isotherms test were placed in a conditioning room with environmental conditions of 20 ± 3 °C temperature and 50 ± 5 % relative humidity until equilibrium, after which were dried at each drying-method. After the constant mass was reached for each drying-method (i.e. achieved the first dry mass), the samples were placed for about 15 days in plastic boxes acting like desiccators at 85% RH; this period of time was enough for samples to reach equilibrium with the wetting conditions. Afterwards, the samples were once again dried at its correspondent drying-method for 15 days and so on.

The results of the drying-wetting cycles, for each dry and wet mass in each cycle, in terms of water content, obtained through equation 15 of Chapter 2, compared to the first dry mass and first wet mass are presented in Figure 5.22.

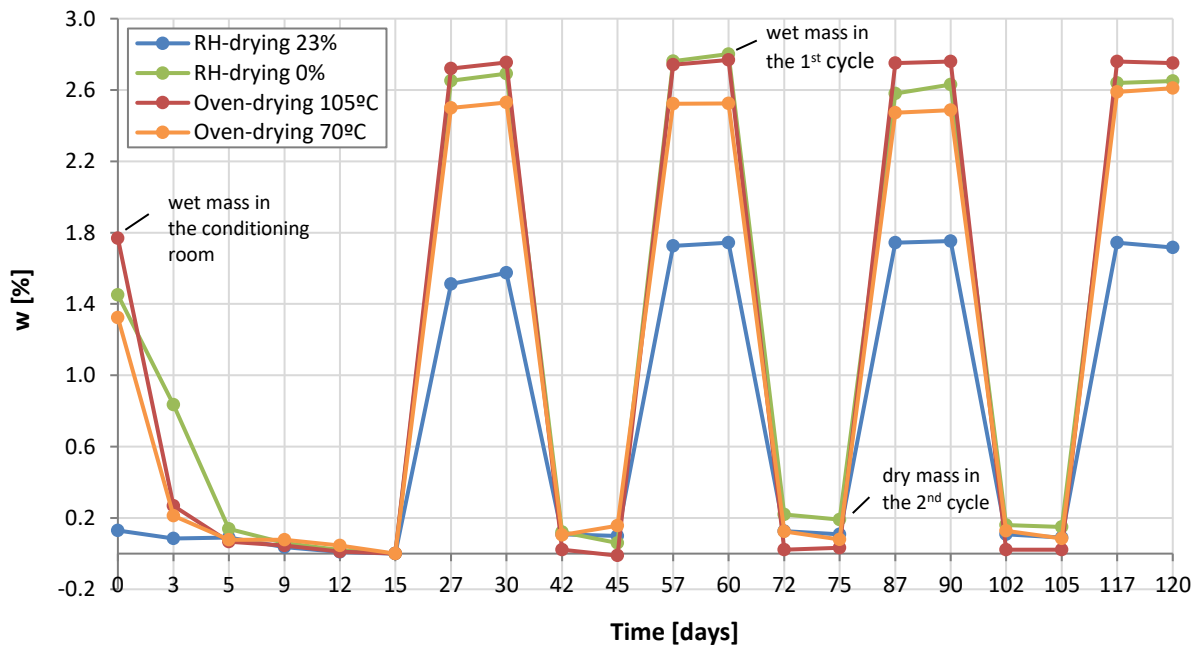


Figure 5.22 – Water content in dry and wet mass during the drying-wetting cycles

By analysing figure 5.22, it can be noticed that using oven-drying temperature of 105°C is an effective dry method to complete dry the samples since almost no hysteresis was found within the water content of the several cycles. Also, it can be understood that even after cycles of wetting, this temperature is capable of removing the totally of the water gained in the wetting period, returning to a water content near 0%. In contrast, the other drying-methods are not capable to return to the initial water content after the first drying, presenting some hysteresis between cycles. This is additionally illustrated in Figures 5.23 and 5.24, for the drying and wetting cycles, respectively. The called zero cycle consists in first drying and wetting, corresponding to 15 days and 30 days for the dry and wet cycles respectively.

According to Figure 5.23, all others methods besides the drying-method performed in a ventilated oven maintaining a temperature of 105°C have not lost all their water content between drying cycles. It is followed by the drying method at 23% RH; both methods at 0% RH and 70°C present values of mass differences in the same range of magnitude. The same tendency is found for the wetting cycles regarding the oven-drying at 105°C, followed by the oven-drying at 70°C with the lower variations between cycles – see Figure 5.24. A clear tendency cannot be found for the drying method of RH at 0%, since it showed a dispersion of results between the first and the following wetting cycles.

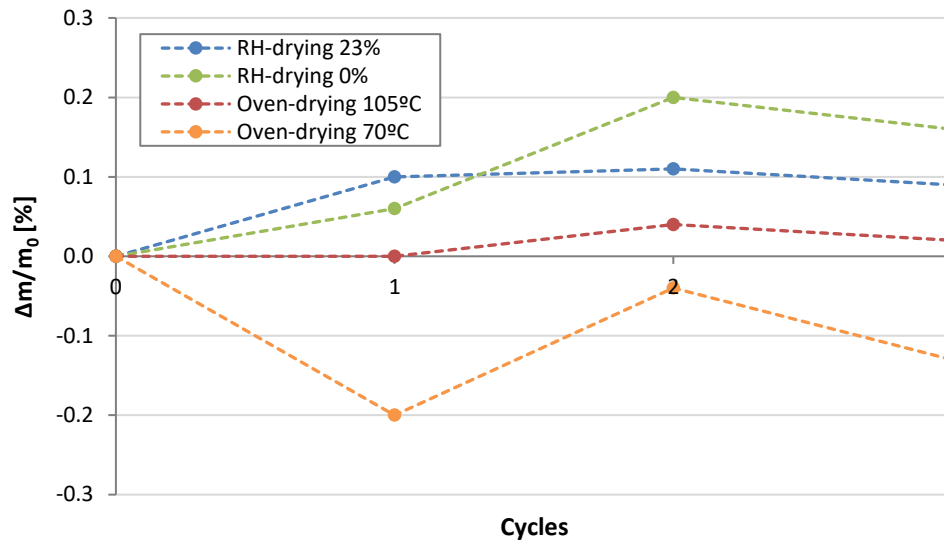


Figure 5.23 – Dry mass in each cycle for the different drying-methods

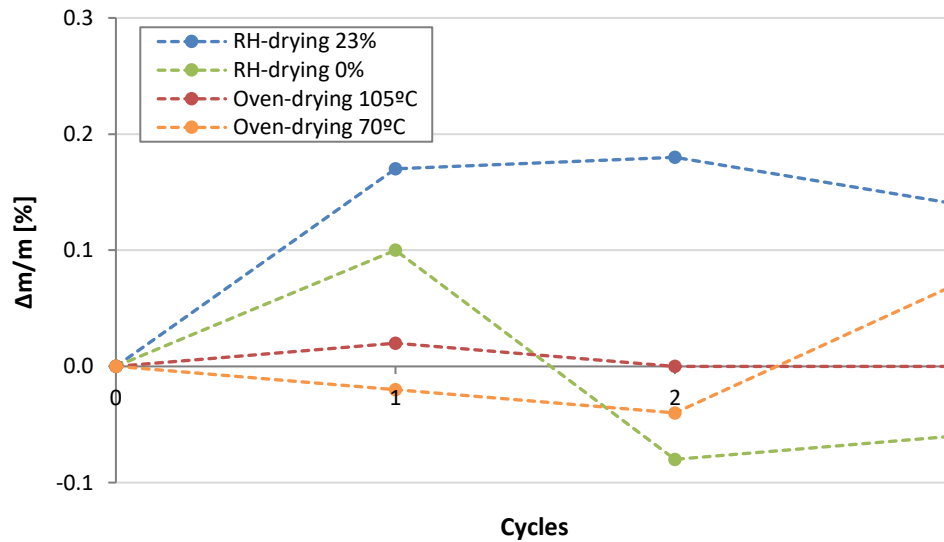


Figure 5.24 – Wet mass in each cycle for the different drying-methods

The determination of variations of the dry and wet mass was achieved following equations 33 and 34, respectively.

$$\frac{\Delta m}{m_0} = \frac{m_{0i} - m_0}{m_0} ; i = [0,3] \quad (333)$$

$$\frac{\Delta m}{m} = \frac{m_i - m}{m} ; i = [0,3] \quad (344)$$

where m_{0i} is the dry mass of the cycle i , m_0 the reference dry mass of each drying-method (i.e. the first dry mass obtained at 15 days), m_i the wet mass of the cycle i and m the reference wet mass of each type of cycle (i.e. the first wet mass achieved at 30 days).

5.3. Discussion

In the current chapter, several procedures were performed with the aim to achieve the most accurate, repeatable and reproducible protocol for the determination of the water vapour resistance factor and dry mass of earthen materials.

The effect of reproducing the wet cup test with three distinct methods lead to a difference of values obtained for the vapour resistance factor. A small variation between the results achieved by the plastic boxes and gloves box methods was found, opposing that between these and the climatic chamber method, either performed at NOVA or at ENTPE. This variation increases with the β corrected values for the plastic boxes and gloves box protocol whereas approaches the climatic chamber results to the remaining methods. Overall, the β correction does lead to a decrease of discrepancy between the three methods.

Contrary to expected, the climatic chamber protocol performed at ENTPE gave lower surface transfer coefficients than the two other methods. It can be mainly due to malfunctions detected to the climatic chamber fan and the RH levels inside it. On the contrary, the surface transfer coefficients are higher while achieved by the climatic chamber protocol carried out at NOVA, thus confirming the predicted tendency. It might be owing to variations of the air velocities existent inside the plastic boxes, climatic chamber and gloves box; higher air velocities predict higher values of surface transfer coefficient. In addition, within the climatic chambers there are some variations of the air velocity and the samples are not in the same exact position.

Although presenting differences, may be as well due to different pre-conditioning of samples between test, all of the water vapour resistance factors obtained are within with those found in the literature. Without further experimental data, namely reproducing the same protocols at different laboratories, it can be seen a lower variation between the μ factors for the gloves box protocol, valid for both types of samples.

The sorption isotherms obtained from the experimental data and modelling through the GAB model, at three different oven-drying temperatures, presented differences concerning the amount of water adsorbed, with the oven-drying temperature at 105°C recording the highest water contents. With reference to the fact that at 105°C the RH found inside the ventilated oven is near 0%, the samples are considered to be completely dried thus adsorbing a great amount of water vapour than the samples dried at 50 and 70°C.

Drying the earth under study at three different oven-drying temperatures and submit it to the same conditions for a period long enough has a neglected effect concerning the amount of water adsorbed. Samples dried at 105°C showed values of water contents, obtained by the sorption isotherms, very similar to those dried at 50°C and 70°C. This might suggest that drying compacted earth at 105°C does not have a great impact in its hygroscopic capacity, thus not damaging its microstructure, essential for the adsorption process, and allows the material to return to its initial stage (i.e. before drying).

The sorption and desorption curves obtained by drying the samples at the three different oven-drying temperatures were found to be within the results exhibited in the literature, with a maximum water content range of 3% to 5%. Several studies, focused on earthen materials, have measured these maximum water contents in ranges of 3.5% to 5% (Liuzzi et al., 2012), 4.5% to 6% (Cagnon et al., 2014), and 3% to 7% (McGregor, 2014).

This hypothesis can be confirmed by the cycles of drying and wetting, in which the oven-drying at 105°C samples showed a neglect water contents differences between cycles, as well as differences of dry and wet masses. On the contrary, drying methods of RH-drying at 0% and oven-drying at 70°C did not presented a clear tendency between its loss of water content in the drying and wetting cycles. This might probably due to the fact that it is highly difficult to maintain the same dry-air pressure within the plastic box and that inside the ventilated oven at 70°C the RH is not near 0%, presenting some fluctuations between the day and night time and during weather seasons. Therefore, these two drying-methods are not considered repeatable or reproducible, in contrast to the oven-drying method at 105°C.

6. Conclusions

6.1. Summary

Firstly, a comparison between the similarities of samples manufactured at different laboratories following the same protocol was conducted. Afterwards, three different procedures for the determination of the water vapour permeability and water vapour resistance factor were tested. At the same time, drying experiments were performed, allowing an analysis of the most repeatable and reproducibly method in order to obtain the dry mass of earthen materials.

Results obtained from the comparison between samples manufactured at different laboratories showed that these are similar regarding the apparent density, dry density and thermal conductivity, although presenting more significant variations concerning their thermal conductivity.

Samples manufactured at ENPTE presented lower apparent density and dry density, and thus lower values of thermal conductivity than NOVA samples. Nevertheless, a clear tendency between the dry density and thermal conductivity was not found.

The determination of the water vapour permeability and water vapour resistance factor stemmed by three different protocols for the water vapour diffusion test, with the wet cup, stated that it is highly sensitive to any modifications within the test conditions. The plastic boxes and gloves box procedures lead to very similar vapour resistance factors, whereas the climatic chamber procedure gave a wide discrepancy of results when compared to those methods. It was found the effect of applying the β correction in the drastic decrease of dissimilarities between the water resistance factors obtained by the three procedures under study.

For different wet cup protocols, the surface transfer coefficient obtained showed a heterogeneity of results. Additionally, although with a slight difference, samples manufactured at different laboratories presented distinct surface transfer coefficients. These variations are found to be influenced by the air velocities at the exposed surface of the material and by the conditioning environment before the test. Hereupon, the test conditions must be constantly monitored and be the most similar in order to obtain close results.

Through sorption isotherms experiments, regarding several drying-methods, no significant differences between samples of compacted earth oven-dried at 50, 70 and 105°C were found when submitted to the same conditions of temperature and relative humidity for a period of time long enough.

For the earth samples under study, the cycles of drying and wetting confirmed that oven-drying at 105°C is an accurate, repeatable and reproducible drying method, which allows the material to return to its initial state from a hygroscopic point of view, for this particular type of earth. A neglect variation of water contents in dry and wet masses was found for this drying-method, whereas for oven-drying temperature of 70°C and 0% RH the variations in mass and thus of water contents observed are considerably higher. That is to say that oven-drying at 70°C and RH-drying at 0% are drying-methods with poor accuracy, repeatability and reproducibility.

6.2. Future work

With a view to further develop the research presented in this dissertation, an additionally work should be performed and integrated with the achieved outcomes. Further studies can confirm the accuracy of the results found and be a support of their improvement. Some will hopefully be performed in the near future within the RILEM TC 274 Round Robin Tests in laboratories all over the world.

The results of the present research work will soon be disseminated. They will also be integrated with the ones of other laboratories in order to propose a draft for a standard for testing compressed earth building products. The author wishes to be able to continue this research within a PhD thesis.

Samples fabrication and transportation protocols:

The fabrication of samples between different laboratories with the same material must be evaluate in order to define an accurate protocol, thus improving the process and avoiding variations. On top of that, the transportation means of samples from one laboratory to others must be evaluated.

Procedure to obtain the dry mass:

More tests to assess the effect of the oven-drying method at 105°C in the microstructure of earthen materials should be conducted, either for a hygroscopic point of view but also assessing the modifications on its mineralogy and microstructure.

In addition, the evolution of the dry and wet mechanical characteristics should be measured during the cycles of drying and wetting, specifically by non-destructive testing such as the dynamic modulus of elasticity and ultrasound pulse velocity.

Enlarge of the experimental data and its reproducibility:

On balance, the tests performed should be repeated, namely the water vapour diffusion tests through round robin-tests. The same samples or samples with a neglect discrepancy of characteristics should be tested in different laboratories with the three protocols used. Tests within climatic chambers should be performed with the same air velocity. Between tests of different methods, the pre-conditioning methods should be respected and followed.

In order to increase the accuracy of the experimental data achieved, all the sorption isotherms, only tested in one cycle, and the cycles of drying-wetting should be repeated with a further number of cycles, in a minimum of two laboratories.

Also, other types of earth should be scope of the same study, namely with different mineralogical compositions, clay contents and particle size distribution. The effect of the addition of low binder contents can also be assessed.

Finally, other samples of earthen construction products should be tested, namely reproducing not only compacted earth blocks (the case of the present study) but also other earthen building techniques such as rammed earth, adobe, extruded earth and earth plasters, to validate the methodology.

References

- Al Haffar, N. (2017). Optimization of earth stabilization for building construction applications Optimization of earth stabilization for building construction applications. MSc Thesis. Université Grenoble Alpes, Saint-Martin-d'Hères
- Al horr, Y., Arif, M., Katafygiotou, M., Mazroei, A., Kaushik, A., & Elsarrag, E. (2016). Impact of indoor environmental quality on occupant well-being and comfort: A review of the literature. *International Journal of Sustainable Built Environment*, 5(1), 1–11. <https://doi.org/10.1016/j.ijbsbe.2016.03.006>
- Allinson, D., & Hall, M. (2010). Hygrothermal analysis of a stabilised rammed earth test building in the UK. *Energy and Buildings*, 42(6), 845–852. <https://doi.org/10.1016/j.enbuild.2009.12.005>
- Anderson, J. E., Wulfhorst, G., & Lang, W. (2015). Energy analysis of the built environment - A review and outlook. *Renewable and Sustainable Energy Reviews*, 44, 149–158. <https://doi.org/10.1016/j.rser.2014.12.027>
- Antunes, A., Faria, P., Silva, V., & Brás, A. (2019). Rice husk-earth based composites: A novel bio-based panel for buildings refurbishment. *Construction and Building Materials*, 221, 99–108. <https://doi.org/10.1016/j.conbuildmat.2019.06.074>
- Arundel, A. V., Sterling, E. M., Biggin, J. H., & Sterling, T. D. (1986). Indirect health effects of relative humidity in indoor environments. *Environmental Health Perspectives*, 65(3), 351–361. <https://doi.org/10.2307/3430203>
- Bui, Q. B., Morel, J. C., Hans, S., & Walker, P. (2014). Effect of moisture content on the mechanical characteristics of rammed earth. *Construction and Building Materials*, 54, 163–169. <https://doi.org/10.1016/j.conbuildmat.2013.12.067>
- Bui, R., Labat, M., & Aubert, J.-E. (2017). Comparison of the Saturated Salt Solution and the Dynamic Vapor Sorption techniques based on the measured sorption isotherm of barley straw. *Construction and Building Materials*, 141, 140–151. <https://doi.org/10.1016/j.conbuildmat.2017.03.005>
- Cagnon, H., Aubert, J. E., Coutand, M., & Magniont, C. (2014). Hygrothermal properties of earth bricks. *Energy and Buildings*, 80, 208–217. <https://doi.org/10.1016/j.enbuild.2014.05.024>
- Cellura, M., Guarino, F., Longo, S., & Mistretta, M. (2014). Energy life-cycle approach in Net zero energy buildings balance: Operation and embodied energy of an Italian case study. *Energy and Buildings*, 72, 371–381. <https://doi.org/10.1016/j.enbuild.2013.12.046>
- Chabriac, P. A., Fabbri, A., Morel, J. C., Laurent, J. P., & Blanc-Gonnet, J. (2014). A procedure to measure the in-situ hygrothermal behavior of earth walls. *Materials*, 7(4), 3002–3020. <https://doi.org/10.3390/ma7043002>
- Champiré, F., Fabbri, A., Morel, J. C., Wong, H., & McGregor, F. (2016). Impact of relative humidity on the mechanical behavior of compacted earth as a building material. *Construction and Building Materials*, 110, 70–78. <https://doi.org/10.1016/j.conbuildmat.2016.01.027>
- Chastas, P., Theodosiou, T., Kontoleon, K. J., & Bikas, D. (2018). Normalising and assessing carbon emissions in the building sector: A review on the embodied CO2 emissions of residential buildings. *Building and Environment*, 130, 212–226. <https://doi.org/10.1016/j.buildenv.2017.12.032>
- Costa, I. (2017). Sorption properties of biobased and raw earth materials: investigation of temperature and dry mass measurements. MSc thesis. Faculdade de Ciências e Tecnologia - Universidade Nova de Lisboa, Monte da Caparica
- Davis, W. R. (1978). Determination of the Thermal Conductivity of Refractory Insulating Materials by the Hot-Wire Method, Thermal Transmission Measurements of Insulating. ASTM STP 660, R. P. Tye, Ed., America Society for Testing Materials, 1978, pp. 186-199

- DIN 18945 (2012). Earth blocks - Terms and definitions, requirements, test methods (in German). Berlin, German: Deutsches Institut Fur Normung
- Dixit, Manish K. (2017). Life cycle embodied energy analysis of residential buildings: A review of literature to investigate embodied energy parameters. *Renewable and Sustainable Energy Reviews*, 79, 390–413. <https://doi.org/10.1016/j.rser.2017.05.051>
- Dixit, Manish K. (2019). Life cycle recurrent embodied energy calculation of buildings: A review. *Journal of Cleaner Production*, 209, 731–754. <https://doi.org/10.1016/j.jclepro.2018.10.230>
- Dixit, Manish Kumar, Fernández-Solís, J. L., Lavy, S., & Culp, C. H. (2010). Identification of parameters for embodied energy measurement: A literature review. *Energy and Buildings*, 42(8), 1238–1247. <https://doi.org/10.1016/j.enbuild.2010.02.016>
- Dubois, S., McGregor, F., Lebeau, F., Evrard, A., & Heath, A. (2014). An inverse modelling approach to estimate the hygric parameters of clay-based masonry during a moisture buffer value test. *Building and Environment*, 81, 192–203. <https://doi.org/10.1016/j.buildenv.2014.06.018>
- El Fgaier, F., Lafhaj, Z., Brachelet, F., Antczak, E., & Chapiseau, C. (2015). Thermal performance of unfired clay bricks used in construction in the north of France: Case study. *Case Studies in Construction Materials*, 3, 102–111. <https://doi.org/10.1016/j.cscm.2015.09.001>
- Fabbri, A., Morel, J.-C., & Gallipoli, D. (2018). Assessing the performance of earth building materials: a review of recent developments. *RILEM Technical Letters*, 3, 46–58. <https://doi.org/10.21809/rilemtechlett.2018.71>
- Fabbri, A., Soudani, L., McGregor, F., Morel, J.C. (2019). Analysis of the water absorption test to assess the intrinsic permeability of earthen materials. *Construction and Building Materials*, 199, 154–162. <https://doi.org/10.1016/j.conbuildmat.2018.12.014>
- Faria, P., dos Santos, T., & Aubert, J.-E. (2015). Experimental Characterization of an Earth Eco-Efficient Plastering Mortar. *Journal of Materials in Civil Engineering*, 28(english). [https://doi.org/10.1061/\(ASCE\)MT.1943-5533.0001363](https://doi.org/10.1061/(ASCE)MT.1943-5533.0001363).
- Feng, C., & Janssen, H. (2016). Hygric properties of porous building materials (II): Analysis of temperature influence. *Building and Environment*, 99, 107–118. <https://doi.org/10.1016/j.buildenv.2016.01.016>
- Feng, C., Meng, Q., Feng, Y., & Janssen, H. (2015). Influence of pre-conditioning methods on the cup test results. *Energy Procedia*, 78, 1383–1388. <https://doi.org/10.1016/j.egypro.2015.11.158>
- Gomes, M. I., Faria, P., & Gonçalves, T. D. (2018). Earth-based mortars for repair and protection of rammed earth walls. Stabilization with mineral binders and fibers. *Journal of Cleaner Production*, 172, 2401–2414. <https://doi.org/10.1016/j.jclepro.2017.11.170>
- Gomes, M. I., Faria, P., & Gonçalves, T. D. (2019). Rammed earth walls repair by earth-based mortars: the adequacy to assess effectiveness. *Construction and Building Materials*, 205, 213–231. <https://doi.org/10.1016/j.conbuildmat.2019.01.222>
- Gummerson, R. J., Hall, C., & Hoff, W. D. (1980). Water movement in porous building materials-II. Hydraulic suction and sorptivity of brick and other masonry materials. *Building and Environment*, 15(2), 101–108. [https://doi.org/10.1016/0360-1323\(80\)90015-3](https://doi.org/10.1016/0360-1323(80)90015-3)
- Habert, G., Castillo, E., Vincens, E., & Morel, J. C. (2012). Power: A new paradigm for energy use in sustainable construction. *Ecological Indicators*, 23, 109–115. <https://doi.org/10.1016/j.ecolind.2012.03.016>
- Hall, M., & Allinson, D. (2009). Analysis of the hygrothermal functional properties of stabilised rammed earth materials. *Building and Environment*, 44(9), 1935–1942. <https://doi.org/10.1016/j.buildenv.2009.01.007>
- Henriques, F. M. A. (2016). Comportamento Higrotérmico de Edifícios. Faculdade de Ciências e Tecnologia - Universidade Nova de Lisboa, Monte de Caparica.

- ISO-12571. (2013). Hygrothermal performance of building materials and products. Determination of hygroscopic sorption properties. Geneva, Switzerland: International Organization for Standardization.
- ISO-12572. (2001). Determination of water vapour transmission properties. Geneva, Switzerland: International Organization for Standardization.
- Klepeis, N. E., Nelson, W. C., Ott, W. R., Robinson, J. P., Tsang, A. M., Switzer, P., ... Engelmann, W. H. (2001). The National Human Activity Pattern Survey (NHAPS): A resource for assessing exposure to environmental pollutants. *Journal of Exposure Analysis and Environmental Epidemiology*, *11*(3), 231–252. <https://doi.org/10.1038/sj.jea.7500165>
- Krus, M., & Kießl, K. (1998). Determination of the moisture storage characteristics of porous capillary active materials. *Materials and Structures*, *31*
- Kunzel, H. (1995). *Simultaneous Heat and Moisture Transport in Building Components*.
- Kwiatkowski, J., Woloszyn, M., & Roux, J. J. (2009). Modelling of hysteresis influence on mass transfer in building materials. *Building and Environment*, *44*(3), 633–642. <https://doi.org/10.1016/j.buildenv.2008.05.006>
- Labat, M., Magniont, C., Oudhof, N., & Aubert, J. E. (2016). From the experimental characterization of the hygrothermal properties of straw-clay mixtures to the numerical assessment of their buffering potential. *Building and Environment*, *97*, 69–81. <https://doi.org/10.1016/j.buildenv.2015.12.004>
- Laborel-Préneron, A., Magniont, C., & Aubert, J. E. (2018). Hygrothermal properties of unfired earth bricks: Effect of barley straw, hemp shiv and corn cob addition. *Energy and Buildings*, *178*, 265–278. <https://doi.org/10.1016/j.enbuild.2018.08.021>
- Lima, J., Faria, P., & Santos Siva, A. (2020). Earth plasters: the influence of clay mineralogy in the plasters properties. *International Journal of Architectural Heritage*. <https://doi.org/10.1080/15583058.2020.1727064>
- Liuzzi, S., Hall, M. R., Stefanizzi, P., & Casey, S. P. (2013). Hygrothermal behaviour and relative humidity buffering of unfired and hydrated lime-stabilised clay composites in a Mediterranean climate. *Building and Environment*, *61*, 82–92. <https://doi.org/10.1016/j.buildenv.2012.12.006>
- Duriez, M., Vieux-Champagne, F., Trad, R., Maillard, P., & Aubert, J-E. (2020). A methodology for the mix design of earth bedding mortar. *Materials and Structures*, *53*(16). <https://doi.org/10.1617/s11527-020-1413-9>
- McGregor, F., Fabbri, A., Ferreira, J., Simões, T., Faria, P., & Morel, J. C. (2017). Procedure to determine the impact of the surface film resistance on the hygric properties of composite clay/fibre plasters. *Materials and Structures*, *50*(4). <https://doi.org/10.1617/s11527-017-1061-3>
- McGregor, F., Heath, A., Fodde, E., & Shea, A. (2014). Conditions affecting the moisture buffering measurement performed on compressed earth blocks. *Building and Environment*, *75*, 11–18. <https://doi.org/10.1016/j.buildenv.2014.01.009>
- McGregor, F., Heath, A., Maskell, D., Fabbri, A., & Morel, J. C. (2016). A review on the buffering capacity of earth building materials. *Proceedings of Institution of Civil Engineers: Construction Materials*, *169*(5), 241–251. <https://doi.org/10.1680/jcoma.15.00035>
- McGregor, F., Heath, A., Shea, A., & Lawrence, M. (2014). The moisture buffering capacity of unfired clay masonry. *Building and Environment*, *82*, 599–607. <https://doi.org/10.1016/j.buildenv.2014.09.027>
- Medjelekh, D., Ulmet, L., Gouny, F., Fouchal, F., Nait-Ali, B., Maillard, P., & Dubois, F. (2016). Characterization of the coupled hygrothermal behavior of unfired clay masonries: Numerical and experimental aspects. *Building and Environment*, *110*, 89–103. <https://doi.org/10.1016/j.buildenv.2016.09.037>

- Melià, P., Ruggieri, G., Sabbadini, S., & Dotelli, G. (2014). Environmental impacts of natural and conventional building materials: A case study on earth plasters. *Journal of Cleaner Production*, *80*, 179–186. <https://doi.org/10.1016/j.jclepro.2014.05.073>
- Moevus, M., Anger, R., & Fontaine, L. (2012). Hygro-thermo-mechanical properties of earthen materials for construction : a literature review. *Terra* 2012, 1–10.
- Monteiro, H., Fernández, J. E., & Freire, F. (2016). Comparative life-cycle energy analysis of a new and an existing house: The significance of occupant's habits, building systems and embodied energy. *Sustainable Cities and Society*, *26*, 507–518. <https://doi.org/10.1016/j.scs.2016.06.002>
- Morel, J. C., Mesbah, A., Oggero, M., & Walker, P. (2001). Building houses with local materials: Means to drastically reduce the environmental impact of construction. *Building and Environment*, *36*(10), 1119–1126. [https://doi.org/10.1016/S0360-1323\(00\)00054-8](https://doi.org/10.1016/S0360-1323(00)00054-8)
- Parracha, J. L., Lima, J., Freire, M. T., & Faria, P. (2019). Vernacular Earthen Buildings from Leiria, Portugal: Material characterization. *International Journal of Architectural Heritage*. <https://doi.org/10.1080/15583058.2019.1668986>
- Praseeda, K. I., Reddy, B. V. V., & Mani, M. (2016). Embodied and operational energy of urban residential buildings in India. *Energy and Buildings*, *110*, 211–219. <https://doi.org/10.1016/j.enbuild.2015.09.072>
- Remki, B., Abahri, K., Belarbi, R., & Bensaïbi, M. (2017). Hydric and structural approaches for earth based materials characterization. *Energy Procedia*, *139*, 417–423. <https://doi.org/10.1016/j.egypro.2017.11.231>
- Roels, S., Talukdar, P., James, C., & Simonson, C. J. (2010). Reliability of material data measurements for hygroscopic buffering. *International Journal of Heat and Mass Transfer*, *53*(23–24), 5355–5363. <https://doi.org/10.1016/j.ijheatmasstransfer.2010.07.020>
- Rouquerol, J., Avnir, D., Fairbridge, C., Everett, D., Haynes, J., Pernicone, N., ... Unger, K. (1994). Recommendations for the characterization of porous solids, *66*(8), 1739-1758.
- Rudy, B., Matthieu, L., & Jean-Emmanuel, A. (2017). Comparison of the Saturated Salt Solution and the Dynamic Vapor Sorption techniques based on the measured sorption isotherm of barley straw. *Construction and Building Materials*, *141*, 140–151. <https://doi.org/10.1016/j.conbuildmat.2017.03.005>
- Rupp, R. F., Vásquez, N. G., & Lamberts, R. (2015). A review of human thermal comfort in the built environment. *Energy and Buildings*, *105*, 178–205. <https://doi.org/10.1016/j.enbuild.2015.07.047>
- Saidi, M., Cherif, A. S., Zeghmami, B., & Sediki, E. (2018). Stabilization effects on the thermal conductivity and sorption behavior of earth bricks. *Construction and Building Materials*, *167*, 566–577. <https://doi.org/10.1016/j.conbuildmat.2018.02.063>
- Santos, C.; Matias, L. (2014). Coeficientes de Transmissão Térmica de Elementos da Envolvente dos edifícios. ITE 50. Lisboa: LNEC. ISBN 978-972-49-2065-8
- Santos, T., Faria, P., & Silva, V. (2019). Can an earth plaster be efficient when applied on different masonries? *Journal of Building Engineering*, *23*, 314–323. <https://doi.org/10.1016/j.jobbe.2019.02.011>
- Santos, T., Nunes, L., & Faria, P. (2018). Production of eco-efficient earth-based plasters: Influence of composition on physical performance and bio-susceptibility. *Journal of Cleaner Production*, *167*, 55–67. <https://doi.org/10.1016/j.jclepro.2017.08.131>
- Soudani, L., Fabbri, A., Morel, J. C., Woloszyn, M., Chabriac, P. A., Wong, H., & Grillet, A. C. (2016). Assessment of the validity of some common assumptions in hygrothermal modeling of earth based materials. *Energy and Buildings*, *116*, 498–511. <https://doi.org/10.1016/j.enbuild.2016.01.025>

-
- Stephan, A., Crawford, R. H., & De Myttenaere, K. (2012). Towards a comprehensive life cycle energy analysis framework for residential buildings. *Energy and Buildings*, *55*, 592–600. <https://doi.org/10.1016/j.enbuild.2012.09.008>
- Tham, K. W. (2016). Indoor air quality and its effects on humans—A review of challenges and developments in the last 30 years. *Energy and Buildings*, *130*, 637–650. <https://doi.org/10.1016/j.enbuild.2016.08.071>
- Vololonirina, O., & Perrin, B. (2016). Inquiries into the measurement of vapour permeability of permeable materials. *Construction and Building Materials*, *102*, 338–348. <https://doi.org/10.1016/j.conbuildmat.2015.10.126>
- Whitaker, S. (1976). *Advances in Heat Transfer*, Vol. 12
- W.H.O. (2009). *Guidelines for indoor air quality: dampness and mould*. Copenhagen: World Health Organisation/Regional Office for Europe. ISBN 978 92 890 4168 3
- Zhang, L., Yang, L., Jelle, B. P., Wang, Y., & Gustavsen, A. (2018). Hygrothermal properties of compressed earthen bricks. *Construction and Building Materials*, *162*, 576–583. <https://doi.org/10.1016/j.conbuildmat.2017.11.163>

Appendix

I. Sample repeatability experiments

A. Apparent density

Table A.1 – Samples mass and dimensions used for the determination of apparent density

Sample	meq [g]	Dimensions [mm]					
		Diameter			Thickness		
C2N1	300.313	100.65	100.61	100.64	20.46	20.49	20.47
C2N2	300.660	100.36	100.35	100.38	20.77	20.7	20.73
C2N3	328.207	100.74	100.73	100.69	21.16	21.14	21.18
C3N1	450.612	100.75	100.68	100.73	30.47	30.41	30.4
C3N2	449.583	100.51	100.49	100.52	30.52	30.51	30.54
C3N3	452.066	100.66	100.69	100.67	30.81	30.65	30.76
C3N4	451.646	100.48	100.46	100.45	30.61	30.62	30.61
C3N5	451.909	100.5	100.45	100.47	31.17	31.1	31.14
C3N6	450.380	100.38	100.33	100.36	30.91	30.73	30.88
C3N7	451.189	100.59	100.58	100.55	31.07	31.06	31.09
C3N8	451.771	100.65	100.64	100.66	30.52	30.49	30.51
C3N9	451.738	100.44	100.47	100.46	31.09	31.04	31.05
C4N1	600.962	100.53	100.55	100.32	41	41.02	41.03
C4N2	601.492	100.51	100.5	100.53	40.92	40.84	40.88
C4N3	602.538	100.54	100.53	100.48	40.97	40.99	40.98
C4N4	602.861	100.55	100.56	100.58	40.96	40.92	40.9
C2E1	294.520	100.43	100.46	100.45	20.41	20.4	20.42
C2E2	293.790	100.42	100.44	100.41	20.42	20.38	20.41
C3E1	442.213	100.95	100.93	100.96	30.15	30.16	30.15
C3E2	439.171	100.18	100.21	100.19	30.52	30.54	30.56
C3E3	440.379	100.68	100.67	100.65	30.49	30.51	30.47
C4E1	588.098	100.45	100.41	100.42	40.24	40.21	40.22
C4E2	589.287	100.41	100.41	100.43	40.52	40.57	40.59
C4E3	588.627	100.43	100.43	100.42	40.11	40.22	40.23

Table A.2 – Apparent density of NOVA and ENTPE samples

Sample	meq [kg]	Volume [m ³]	ρ [kg/m ³]	ρ [kg/m ³]	
				Average	Std dev.
C2N1	0.300313	0.000163	1844.22	1874.66	62.68
C2N2	0.300660	0.000164	1833.02		
C2N3	0.328207	0.000169	1946.76		
C3N1	0.450612	0.000242	1858.78	1847.19	14.31
C3N2	0.449583	0.000242	1856.51		
C3N3	0.452066	0.000245	1847.48		
C3N4	0.451646	0.000243	1861.15		
C3N5	0.451909	0.000247	1830.57		
C3N6	0.450380	0.000244	1846.22		
C3N7	0.451189	0.000247	1827.74		
C3N8	0.451771	0.000243	1861.25		
C3N9	0.451738	0.000246	1835.01		
C4N1	0.600962	0.000325	1848.22	1852.49	2.95
C4N2	0.601492	0.000324	1854.31		
C4N3	0.602538	0.000325	1852.88		
C4N4	0.602861	0.000325	1854.56		
C2E1	0.294520	0.000162	1821.01	1819.47	2.17
C2E2	0.293790	0.000162	1817.93		
C3E1	0.442213	0.000241	1832.41	1823.67	9.85
C3E2	0.439171	0.000241	1823.88		
C3E3	0.440379	0.000243	1814.71		
C4E1	0.588098	0.000319	1845.80	1843.16	7.65
C4E2	0.589287	0.000321	1834.54		
C4E3	0.588627	0.000318	1849.14		

B. Dry density

Table A.3 – Dimensions of NOVA samples measured through a digital calliper for the dry density determination

Sample	Dimensions [mm]											
	Diameter						Thickness					
C2N1	100.15	100.24	100.22	100.37	100.35	100.14	20.54	20.64	20.66	20.73	20.48	20.44
C2N2	100.37	100.10	100.22	100.39	100.44	100.11	20.75	20.66	20.64	20.75	20.74	20.52
C3N2	100.60	100.58	100.53	100.54	100.55	100.63	30.54	30.85	30.39	30.37	30.61	30.77
C3N4	100.67	100.73	100.70	100.62	100.59	100.64	30.77	30.94	30.93	30.72	30.70	30.76
C3N6	100.61	100.59	100.52	100.49	100.65	100.67	30.62	30.50	30.77	30.63	30.74	30.48
C4N1	100.60	100.63	100.34	100.48	100.32	100.36	41.23	41.04	41.10	41.06	41.10	41.08
C4N2	100.43	100.69	100.71	100.65	100.57	100.60	40.80	40.93	40.95	40.93	40.96	40.84
C4N3	100.71	100.46	100.40	100.62	100.72	100.44	40.69	40.49	40.54	40.54	40.66	40.75

Table A.4 – Dimensions of ENTPE samples measured through a digital calliper for the dry density determination

Sample	Dimensions [mm]											
	Diameter						Thickness					
C2E1	100.40	100.27	100.37	100.38	100.25	100.42	20.61	20.59	20.47	20.74	20.68	20.73
C2E2	100.19	100.48	100.42	100.37	100.40	100.27	20.47	20.72	20.53	20.40	20.59	20.60
C3E1	100.47	100.68	100.42	100.67	100.73	100.66	30.55	30.26	30.71	30.65	30.56	30.31
C3E2	100.89	100.47	100.50	100.82	100.62	100.91	30.36	30.26	30.55	30.47	30.55	30.53
C3E3	100.61	100.76	100.59	100.63	100.65	100.64	30.47	30.49	30.40	30.29	30.50	30.65
C4E1	100.97	100.74	100.81	100.93	100.75	100.84	40.26	40.34	40.30	40.28	40.17	40.14
C4E2	100.80	100.52	100.64	100.79	100.49	100.77	40.12	40.07	40.12	40.09	40.14	40.02
C4E3	100.46	100.93	100.57	100.42	100.84	100.46	39.93	40.21	40.28	40.19	40.16	40.05

Table A.5 – Dry density of NOVA and ENTPE samples

Sample	m_0 [g]	Volume [m ³]	ρ_d [kg/m ³]	ρ_d [kg/m ³]	
				Average	Std dev.
C2N1	291.12	0.00016	1792.16	1788.45	5.24
C2N2	291.41	0.00016	1784.75		
C3N2	439.50	0.00024	1808.68	1805.52	3.78
C3N4	441.55	0.00025	1801.33		
C3N6	439.63	0.00024	1806.55		
C4N1	586.73	0.00033	1801.13	1811.02	12.04
C4N2	587.73	0.00033	1807.50		
C4N3	588.44	0.00032	1824.42		
C2E1	287.60	0.00016	1762.13	1764.34	3.12
C2E2	287.17	0.00016	1766.54		
C3E1	432.87	0.00024	1784.98	1777.74	6.53
C3E2	429.87	0.00024	1772.31		
C3E3	430.47	0.00024	1775.94		
C4E1	575.93	0.00032	1791.70	1800.69	8.24
C4E2	576.92	0.00032	1807.87		
C4E3	575.20	0.00032	1802.51		

C. Thermal conductivity

C.1. Contact probe

Table A.6 – Thermal conductivity obtained by the contact probe method

Sample	λ [W/(m.k)]				
	Read 1	Read 2	Read 3	Average	Std dev.
C2N1	0.875	0.866	0.891	0.877	0.013
C2N2	0.862	0.869	0.864	0.865	0.004
C2N3	1.050	1.04	1.08	1.057	0.021
C3N1	0.832	0.825	0.841	0.833	0.008
C3N2	0.832	0.825	0.841	0.833	0.008
C3N3	0.838	0.843	0.836	0.839	0.004
C3N4	0.830	0.843	0.83	0.834	0.008
C3N5	0.857	0.833	0.846	0.845	0.012
C3N6	0.853	0.874	0.849	0.859	0.013
C3N7	0.815	0.818	0.829	0.821	0.007
C3N8	0.835	0.838	0.835	0.836	0.002
C3N9	0.828	0.842	0.845	0.838	0.009
C4N1	0.866	0.857	0.851	0.858	0.008
C4N2	0.848	0.84	0.832	0.840	0.008
C4N3	0.865	0.848	0.833	0.849	0.016
C4N4	0.842	0.83	0.817	0.830	0.013
C2E1	0.865	0.855	0.86	0.860	0.005
C2E2	0.886	0.869	0.861	0.872	0.013
C3E1	0.802	0.791	0.802	0.798	0.006
C3E2	0.809	0.802	0.804	0.805	0.004
C3E3	0.803	0.8	0.798	0.800	0.003
C4E1	0.816	0.801	0.829	0.815	0.014
C4E2	0.816	0.804	0.826	0.815	0.011
C4E3	0.831	0.824	0.824	0.826	0.004

Table A.7 – Average values of thermal conductivity obtained by the contact probe method

Group	λ [W/(m.k)]	
	Average	Std dev.
C2N	0.933	0.107
C3N	0.838	0.01
C4N	0.844	0.012
C2E	0.866	0.008
C3E	0.801	0.003
C4E	0.819	0.006

C.2. Hot wire

Table A.8 – Thermal conductivity obtained by the hot wire method

Sample	λ [W/(m.k)]				
	Read 1	Read 2	Read 3	Average	Std dev.
C2N	0.730	0.759	0.723	0.737	0.027
C3N	0.700	0.703	0.722	0.712	0.062
C4N	0.710	0.728	0.753	0.726	0.034
C2E	0.728	0.779	0.689	0.732	0.050
C3E	0.727	0.692	0.695	0.704	0.036
C4E	0.718	0.731	0.704	0.719	0.028

II. Water vapour diffusion test

D. β correction

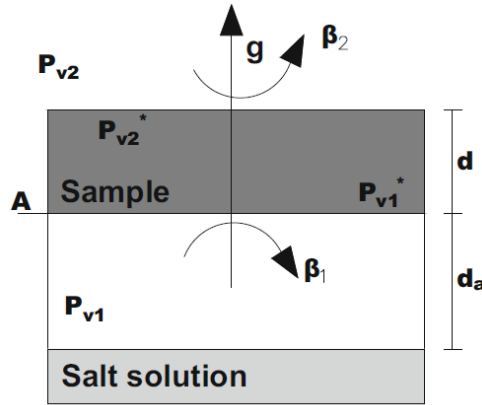


Figure A.0.1 – Layout of the process during the wet cup test

$$\frac{\Delta m}{\Delta t} = G = A \cdot \delta_p \cdot \frac{\Delta P_v^*}{d}$$

$$\frac{G}{A} = \beta_2 (P_{v2} - P_{v2}^*) = \beta_1 (P_{v1}^* - P_{v1})$$

$$\Delta P_v^* = \Delta P_v - \frac{G}{A \cdot \beta_2} - \frac{G}{A \cdot \beta_1}$$

$$\delta_p^\beta = \frac{G \cdot d}{A \cdot \Delta P_v - G \left(\frac{1}{\beta_2} + \frac{1}{\beta_1} \right)} = \frac{G \cdot d}{A \cdot \Delta P_v - \frac{G}{\beta}}$$

$$\delta_p^\beta = \frac{d}{\frac{d}{\delta_p^{agc}} + \frac{1}{\beta}}$$

E. Results

E.1. Plastic boxes

Table A.9 – Values of water vapour permeability and water vapour resistance factor obtained by the wet cup test performed in plastic boxes

Sample	G [kg/s]	g [kg/(s.m ²)]	W [kg/(s.m ² .Pa)]	δp [kg/(s.m.Pa)]	μ [-]	δp ISO [kg/(s.m.Pa)]	μ ISO [-]
C4N4	3.06E-09	3.89E-07	4.97E-10	1.99E-11	9.91	2.09E-11	9.41
C3N8	3.54E-09	4.50E-07	5.75E-10	1.73E-11	11.42	1.83E-11	10.75
C3N9	3.60E-09	4.58E-07	6.11E-10	1.83E-11	10.76	1.95E-11	10.09
C2N1	4.70E-09	5.98E-07	7.64E-10	1.53E-11	12.90	1.66E-11	11.90
C2N2	4.67E-09	5.95E-07	7.93E-10	1.59E-11	12.43	1.72E-11	11.43
C4E	2.74E-09	3.49E-07	4.46E-10	1.78E-11	11.05	1.87E-11	10.55
C4E	2.87E-09	3.65E-07	4.86E-10	1.94E-11	10.13	2.05E-11	9.63
C3E	3.45E-09	4.40E-07	5.61E-10	1.68E-11	11.70	1.79E-11	11.03
C3E	3.64E-09	4.63E-07	6.17E-10	1.85E-11	10.64	1.98E-11	9.97
C2E	4.58E-09	5.83E-07	7.44E-10	1.49E-11	13.24	1.61E-11	12.24
C2E	4.95E-09	6.30E-07	8.40E-10	1.68E-11	11.73	1.84E-11	10.73

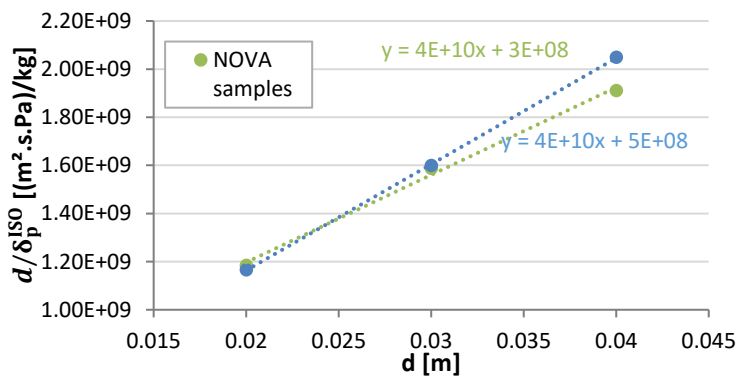


Figure A.0.2 – d/δ_p^{ISO} as a function for the wet cup test performed in plastic boxes

Table A.10 – Values of δ^{β} and μ^{β} obtained by the wet cup test performed in plastic boxes

Sample	1/β	δp β [kg/(s.m.Pa)]	μ β [-]
C4N4	5.00E+08	2.83E-11	6.95E+00
C3N8		2.64E-11	7.47E+00
C3N9		2.89E-11	6.81E+00
C2N1		2.83E-11	6.97E+00
C2N2		3.03E-11	6.50E+00
C4E	3.00E+08	2.17E-11	9.07E+00
C4E		2.42E-11	8.15E+00
C3E		2.17E-11	9.06E+00
C3E		2.46E-11	8.00E+00
C2E		2.12E-11	9.28E+00
C2E		2.53E-11	7.78E+00

E.2. Climatic chamber at ENTPE

Table A.11 – Values of water vapour permeability and water vapour resistance factor obtained by the wet cup test performed in the climatic chamber at ENTPE

Sample	G [kg/s]	g [kg/(s.m ²)]	W [kg/(s.m ² .Pa)]	δp [kg/(s.m.Pa)]	μ [-]	δp ISO [kg/(s.m.Pa)]	μ ISO [-]
C4N4	2.46E-09	3.14E-07	3.82E-10	1.53E-11	12.89	1.59E-11	12.39
C3N8	2.64E-09	3.37E-07	4.10E-10	1.23E-11	16.01	1.28E-11	15.34
C3N9	2.57E-09	3.28E-07	3.99E-10	1.20E-11	16.44	1.25E-11	15.77
C2N1	3.53E-09	4.50E-07	5.48E-10	1.10E-11	17.98	1.16E-11	16.98
C2N2	3.38E-09	4.31E-07	5.25E-10	1.05E-11	18.76	1.11E-11	17.76
C4E	2.27E-09	2.89E-07	3.53E-10	1.41E-11	13.96	1.46E-11	13.46
C4E	2.46E-09	3.13E-07	3.81E-10	1.52E-11	12.93	1.59E-11	12.43
C3E	2.63E-09	3.35E-07	4.09E-10	1.23E-11	16.07	1.28E-11	15.40
C3E	2.88E-09	3.67E-07	4.47E-10	1.34E-11	14.69	1.40E-11	14.02
C2E	3.52E-09	4.48E-07	5.46E-10	1.09E-11	18.03	1.16E-11	17.03
C2E	3.57E-09	4.55E-07	5.54E-10	1.11E-11	17.78	1.17E-11	16.78

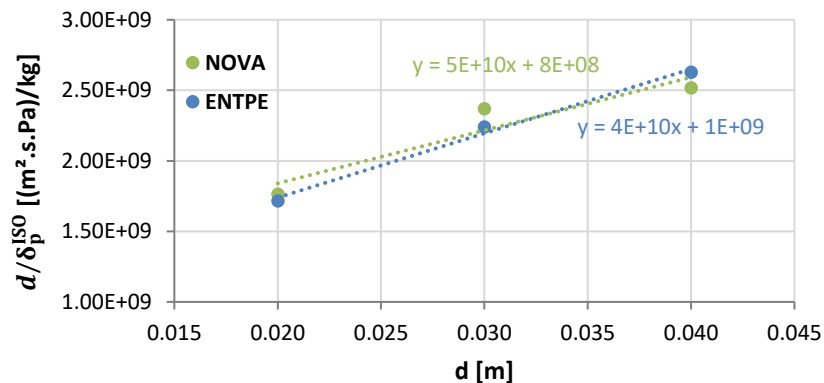


Figure A.0.3 – d/δ_p^{ISO} as a function for the wet cup test performed in the climatic chamber at ENTPE

Table A.12 – Values of δ^β and μ^β obtained by the wet cup test performed in climatic chamber at ENTPE

Sample	1/β	δp β [kg/(s.m.Pa)]	μ β [-]
C4N4	1.00E+09	2.64E-11	7.47E+00
C3N8		2.25E-11	8.77E+00
C3N9		2.14E-11	9.20E+00
C2N1		2.76E-11	7.13E+00
C2N2		2.49E-11	7.91E+00
C4E	8.00E+09	2.07E-11	9.52E+00
C4E		2.32E-11	8.49E+00
C3E		1.94E-11	1.01E+01
C3E		2.25E-11	8.77E+00
C2E		2.15E-11	9.15E+00
C2E		2.21E-11	8.90E+00

E.3. Climatic chamber at NOVA

Table A.13 – Values of water vapour permeability and water vapour resistance factor obtained by the wet cup test performed in the climatic chamber at NOVA

Sample	G [kg/s]	g [kg/(s.m ²)]	W [kg/(s.m ² .Pa)]	δ_p [kg/(s.m.Pa)]	μ [-]	δ_p ISO [kg/(s.m.Pa)]	μ ISO [-]
C4N1	3.59E-09	4.57E-07	6.10E-10	2.44E-11	8.07	2.60E-11	7.57
C4N4	3.20E-09	4.08E-07	5.45E-10	2.18E-11	9.03	2.31E-11	8.53
C3N8	3.90E-09	4.97E-07	6.64E-10	1.99E-11	9.88	2.14E-11	9.22
C3N9	3.94E-09	5.02E-07	6.71E-10	2.01E-11	9.79	2.16E-11	9.12
C2N1	5.32E-09	6.78E-07	9.06E-10	1.81E-11	10.87	2.00E-11	9.87
C2N2	5.44E-09	6.92E-07	9.25E-10	1.85E-11	10.65	2.04E-11	9.65
C4E3	3.45E-09	4.39E-07	5.87E-10	2.35E-11	8.39	2.50E-11	7.89
C4E6	3.43E-09	4.37E-07	5.84E-10	2.34E-11	8.44	2.48E-11	7.94
C3E4	4.29E-09	5.46E-07	7.30E-10	2.19E-11	9.00	2.36E-11	8.33
C3E7	4.37E-09	5.56E-07	7.43E-10	2.23E-11	8.83	2.41E-11	8.17
C2E1	5.93E-09	7.55E-07	1.01E-09	2.02E-11	9.76	2.25E-11	8.76
C2E2	6.44E-09	8.20E-07	1.10E-09	2.19E-11	8.98	2.47E-11	7.98

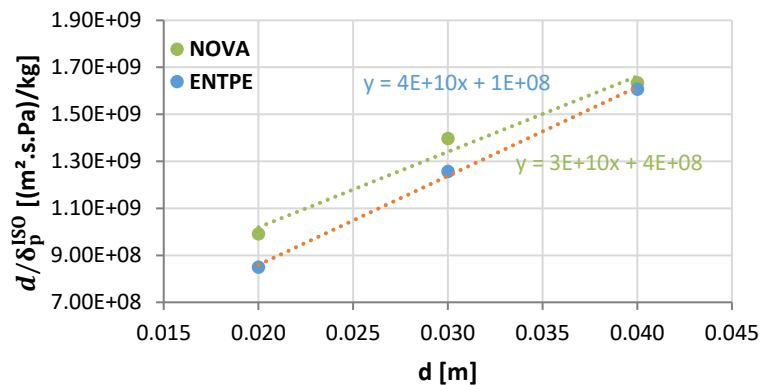


Figure A.0.4 – d/δ_p^{ISO} as a function for the wet cup test performed in the climatic chamber at NOVA

Table A.14 – Values of δ_p^β and μ^β obtained by the wet cup test performed in climatic chamber at NOVA

Sample	$1/\beta$	δ_p^β [kg/(s.m.Pa)]	μ^β [-]
C4N4	6.00E+08	2.99E-11	6.59E+00
C3N8		3.21E-11	6.14E+00
C3N9		2.70E-11	7.31E+00
C2N1		3.08E-11	6.39E+00
C2N2		2.87E-11	6.87E+00
C4E	4.00E+08	2.46E-11	8.02E+00
C4E		2.60E-11	7.57E+00
C3E		2.27E-11	8.70E+00
C3E		2.82E-11	6.99E+00
C2E		2.24E-11	8.79E+00
C2E		2.93E-11	6.73E+00

E.4. Gloves box

Table A.15 – Values of water vapour permeability and water vapour resistance factor obtained by the wet cup test performed in the gloves box

Sample	G [kg/s]	g [kg/(s.m ²)]	W [kg/(s.m ² .Pa)]	δp [kg/(s.m.Pa)]	μ [-]	δp ISO [kg/(s.m.Pa)]	μ ISO [-]
C4N4	3.25E-09	4.14E-07	4.90E-10	1.96E-11	10.05	2.06E-11	9.55
C3N8	4.05E-09	5.16E-07	6.11E-10	1.83E-11	10.75	1.95E-11	10.08
C3N9	3.65E-09	4.65E-07	5.51E-10	1.65E-11	11.91	1.75E-11	11.25
C2N1	4.91E-09	6.25E-07	7.41E-10	1.48E-11	13.30	1.60E-11	12.30
C2N2	4.74E-09	6.03E-07	7.15E-10	1.43E-11	13.78	1.54E-11	12.78
C4E	3.11E-09	3.96E-07	4.69E-10	1.88E-11	10.49	1.97E-11	9.99
C4E	3.25E-09	4.14E-07	4.90E-10	1.96E-11	10.04	2.06E-11	9.54
C3E	3.63E-09	4.62E-07	5.48E-10	1.64E-11	11.99	1.74E-11	11.32
C3E	4.23E-09	5.39E-07	6.38E-10	1.92E-11	10.29	2.05E-11	9.62
C2E	4.76E-09	6.05E-07	7.17E-10	1.43E-11	13.73	1.55E-11	12.73
C2E	5.59E-09	7.12E-07	8.44E-10	1.69E-11	11.67	1.85E-11	10.67

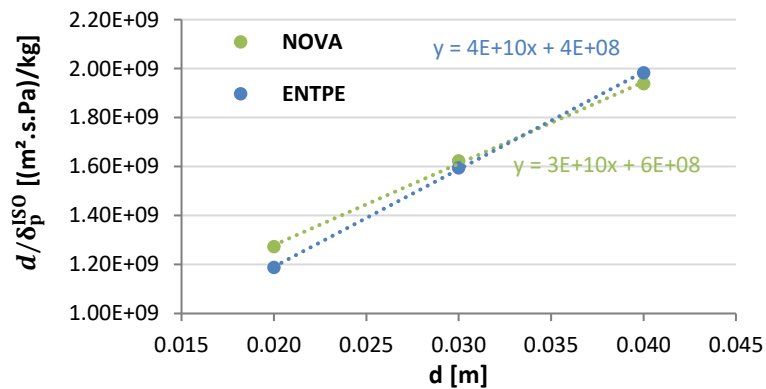


Figure A.0.5 – $d/\delta p^{ISO}$ as a function for the wet cup test performed in the gloves box

Table A.16 – Values of δp^β and μ^β obtained by the wet cup test performed in the gloves box

Sample	$1/\beta$	δp^β [kg/(s.m.Pa)]	μ^β [-]
C4N1	4.00E+08	3.52E-11	5.60E+00
C4N4		3.00E-11	6.56E+00
C3N8		2.99E-11	6.59E+00
C3N9		3.03E-11	6.50E+00
C2N1		3.32E-11	5.93E+00
C2N2		3.45E-11	5.71E+00
C4E3	1.00E+08	2.66E-11	7.40E+00
C4E6		2.65E-11	7.44E+00
C3E4		2.57E-11	7.68E+00
C3E7		2.62E-11	7.51E+00
C2E1		2.54E-11	7.77E+00
C2E2		2.82E-11	7.00E+00

III. Drying experiments

F. Sorption isotherms

Table A.17 – Water contents obtained through the sorption for the first cycle of RH levels

Sample		RH [%]	meq [g]	w [%]
C3N1.1	69.4666	23	69.8807	0.14
		59	70.3609	0.55
		85	71.1029	1.61
C3N1.3	90.0320	23	90.5832	0.13
		59	68.5946	0.55
		85	92.1684	1.61
C3N1.5	67.7211	23	68.1315	0.13
		59	71.5869	0.54
		85	69.3229	1.62
C3N3.1	67.6599	23	68.2700	0.13
		59	68.7290	0.55
		85	69.4565	1.61
C3N3.3	70.4764	23	71.1152	0.12
		59	71.5869	0.54
		85	72.3417	1.60
C3N3.5	71.9223	23	72.5856	0.12
		59	73.0697	0.54
		85	73.8438	1.61
C3N7.1	66.6786	23	67.4247	0.10
		59	67.9043	0.61
		85	68.6344	1.69
C3N7.3	62.9947	23	63.6988	0.10
		59	64.1446	0.60
		85	64.8249	1.67
C3N7.5	66.3041	23	67.0437	0.10
		59	67.5151	0.60
		85	68.2368	1.68

Table A.18 – Water contents obtained through the desorption for the first cycle of RH levels

Sample	meq [g]	RH [%]	meq RH [g]	w [%]
C3N1.1	69.4666	85	71.1029	1.61
		59	70.5126	0.76
		23	69.8939	0.12
C3N1.3	90.0320	85	92.1684	1.61
		59	91.4056	0.77
		23	90.6021	0.11
C3N1.5	67.7211	85	69.3229	1.62
		59	68.7622	0.80
		23	68.1502	0.10
C3N3.1	67.6599	85	69.4565	1.61
		59	68.8882	0.78
		23	68.2976	0.08
C3N3.3	70.4764	85	72.3417	1.60
		59	71.7559	0.78
		23	71.1408	0.09
C3N3.5	71.9223	85	73.8438	1.61
		59	73.2505	0.79
		23	72.6130	0.08
C3N7.1	66.6786	85	68.6344	1.69
		59	68.0779	0.87
		23	67.4920	0.00
C3N7.3	62.9947	85	64.8249	1.67
		59	64.3072	0.86
		23	63.7580	0.01
C3N7.5	66.3041	85	68.2368	1.68
		59	67.6959	0.87
		23	67.1132	0.00

Table A.19 – Water contents obtained through the sorption for the second cycle of RH levels

Sample	meq [g]	RH [%]	meq RH [g]	w [%]
C3N1.2	73.4128	43	73.5709	0.22
		75	74.2052	1.08
		97	75.9078	3.40
C3N1.4	59.2157	43	59.3451	0.22
		75	59.8604	1.09
		97	61.2636	3.46
C3N1.6	56.2699	43	56.3910	0.22
		75	56.8788	1.08
		97	58.2226	3.47
C3N3.2	60.0169	43	60.1450	0.21
		75	60.6638	1.08
		97	62.0666	3.42
C3N3.4	70.7263	43	70.8814	0.22
		75	71.4930	1.08
		97	73.1319	3.40
C3N3.6	75.9076	43	76.0750	0.22
		75	76.7287	1.08
		97	78.4994	3.41
C3N7.2	67.6786	43	67.8392	0.24
		75	68.4593	1.15
		97	70.0243	3.47
C3N7.4	66.5461	43	66.6955	0.22
		75	67.3030	1.14
		97	68.8166	3.41
C3N7.6	84.3587	43	84.5718	0.25
		75	85.3365	1.16
		97	87.2418	3.42

Table A.20 – Water contents obtained through the desorption for the second cycle of RH levels

Sample	meq [g]	RH [%]	meq RH [g]	w [%]
C3N1.2	73.4128	97	75.9078	3.40
		75	74.5384	1.53
		43	73.7179	0.42
C3N1.4	59.2157	97	61.2636	3.46
		75	60.1390	1.56
		43	59.4755	0.44
C3N1.6	56.2699	97	58.2226	3.47
		75	57.1471	1.56
		43	56.5182	0.44
C3N3.2	60.0169	97	62.0666	3.42
		75	60.9624	1.58
		43	60.2918	0.46
C3N3.4	70.7263	97	73.1319	3.40
		75	71.8412	1.58
		43	71.0541	0.46
C3N3.6	75.9076	97	78.4994	3.41
		75	77.1032	1.58
		43	76.2604	0.46
C3N7.2	67.6786	97	70.0243	3.47
		75	68.8103	1.67
		43	68.0655	0.57
C3N7.4	66.5461	97	68.8166	3.41
		75	67.6341	1.63
		43	66.9102	0.55
C3N7.6	84.3587	97	87.2418	3.42
		75	85.7401	1.64
		43	84.8176	0.54

G. Drying-wetting cycles

G.1. Cycle 23% -> 85%

Table A.21 – Water content in dry and wet mass during the drying-wetting cycles for the cycle dried at 23%

	Days	Mass [g]	mo [g]	w [%]
1st Drying	0	55.98	55.91	0.13
	3	55.96		0.09
	5	55.96		0.09
	9	55.93		0.04
	12	55.92		0.01
	15	55.91		0.00
1st Wetting	27	56.76	-	1.51
	30	56.79		1.57
2nd Drying	42	55.97	55.97	0.11
	45	55.97		0.10
2nd Wetting	57	56.88	-	1.73
	60	56.89		1.74
3rd Drying	72	55.98	55.97	0.13
	75	55.97		0.11
3rd Wetting	87	56.89	-	1.74
	90	56.89		1.75
4th Drying	102	55.97	55.96	0.11
	105	55.96		0.09
4th Wetting	117	56.89	-	1.74
	120	56.87		1.72

Table A.22 – Dry mass in each cycle for the different drying-methods for the cycle dried at 23%

Cycles	mo [g]	Δmo [g]	$\Delta mo/m$ [g]
0	55.91	0.00	0.00
1	55.97	0.06	0.10
2	55.97	0.06	0.11
3	55.96	0.05	0.09

G.2. Cycle 0% -> 85%

Table A.23 – Water content in dry and wet mass during the drying-wetting cycles for the cycle dried at 0%

	Days	Mass [g]	mo [g]	w [%]
1st Drying	0	51.06	50.33	1.45
	3	50.75		0.83
	5	50.40		0.14
	9	50.36		0.06
	12	50.34		0.02
	15	50.33		0.00
1st Wetting	27	51.67	-	2.65
	30	51.69		2.69
2nd Drying	42	50.38	50.36	0.12
	45	50.36		0.06
2nd Wetting	57	51.72	-	2.76
	60	51.74		2.80
3rd Drying	72	50.34	50.34	0.22
	75	50.34		0.19
3rd Wetting	87	51.73	-	2.58
	90	51.75		2.63
4th Drying	102	50.38	50.37	0.16
	105	50.37		0.15
4th Wetting	117	51.71	-	2.64
	120	51.72		2.65

Table A.24 – Dry mass in each cycle for the different drying-methods for the cycle dried at 0%

Cycles	mo [g]	Δmo [g]	$\Delta mo/m$ [g]
0	50.33	0.00	0.00
1	50.36	0.03	0.06
2	50.43	0.10	0.20
3	50.41	0.08	0.16

G.3. Cycle 105°C -> 85%

Table A.25 – Water content in dry and wet mass during the drying-wetting cycles for the cycle dried at 105°C

	Days	Mass [g]	mo [g]	w [%]
1st Drying	0	45.46	44.67	1.77
	3	44.79		0.27
	5	44.70		0.07
	9	44.69		0.04
	12	44.68		0.01
	15	44.67		0.00
1st Wetting	27	45.89	-	2.72
	30	45.90	-	2.75
2nd Drying	42	44.68	44.67	0.02
	45	44.67		-0.01
2nd Wetting	57	45.90	-	2.74
	60	45.91		2.77
3rd Drying	72	44.68	44.69	0.02
	75	44.69		0.03
3rd Wetting	87	45.86	-	2.75
	90	45.86		2.76
4th Drying	102	44.68	44.68	0.02
	105	44.68		0.02
4th Wetting	117	45.79	-	2.76
	120	45.81		2.75

Table A.26 – Dry mass in each cycle for the different drying-methods for the cycle dried at 105°C

Cycles	mo [g]	Δmo [g]	$\Delta mo/m$ [g]
0	44.67	0.00	0.00
1	44.67	0.00	0.00
2	44.69	0.02	0.04
3	44.68	0.01	0.02

G.4. Cycle 70°C -> 85%

Table A.27 – Water content in dry and wet mass during the drying-wetting cycles for the cycle dried at 70°C

	Days	Mass [g]	mo [g]	w [%]
1st Drying	0	45.31	44.81	1.32
	3	44.81		0.21
	5	44.75		0.08
	9	44.80		0.08
	12	44.82		0.04
	15	44.81		0.00
1st Wetting	27	45.95	-	2.50
	30	45.97		2.53
2nd Drying	42	44.69	44.67	0.10
	45	44.67		0.16
2nd Wetting	57	45.92	-	2.52
	60	45.92		2.53
3rd Drying	72	44.72	44.69	0.12
	75	44.69		0.08
3rd Wetting	87	45.90	-	2.47
	90	45.90		2.49
4th Drying	102	44.72	44.68	0.13
	105	44.68		0.08
4th Wetting	117	45.79	-	2.59
	120	45.81		2.61

Table A.28 – Dry mass in each cycle for the different drying-methods for the cycle dried at 70°C

Cycles	mo [g]	Δmo [g]	$\Delta mo/m$ [g]
0	44.81	0.00	0.00
1	44.72	-0.09	-0.20
2	44.79	-0.02	-0.04
3	44.75	-0.06	-0.13